CHAPTER 5

KINETICS OF COPPER DEPOSITION IN THE PRESENCE OF GUAR AND ACTIVATED POLYACRYLAMIDE USING CYCLIC VOLTAMMETRY AND ELECTROCHEMICAL IMPEDANCE SPECTROSCOPY

5.1 Introduction

The previous two Chapters have shown that polyacrylamide prepared in 16-fold diluted electrolyte at 50^{o}C for two hours under stirring most likely forms a block copolymer with up to 10% hydrolysis and a molecular weight less than 15 million Dalton. This polyacrylamide structure was named "activated polyacrylamide" (APAM). It has also been shown in the previous Chapters that APAM produces copper deposits with a lower surface roughness than polyacrylamide prepared in water or full-strength electrolyte. Moreover, APAM produced smoother copper deposits than either Guarfloc66 (Guar) the 40-year-old industry-standard organic additive or polyacrylic acid. The aim in this section is to investigate the interface between either stainless steel or copper metal and copper electrolyte in the presence and absence of both Guar and APAM using both Cyclic Voltammetry (CV) and Electrochemical Impedance Spectroscopy (EIS).

Electrochemical techniques are unique for in-situ investigation of electrochemical interfaces during deposition or dissolution of metals. The electrical quantities measured permit kinetic studies of elementary phenomena such as single-electron steps of the reaction mechanism and the presence of intermediates, often

unstable, may therefore also be inferred[1-4]. Cyclic Voltammetry and Electrochemical Impedance Spectroscopy were selected to extract kinetic parameters for copper electrodeposition in the presence of a mass transport rate-determining step and organic additives.

The interest in Electrochemical Impedance Spectroscopy to determine the double-layer capacitance, to characterize the electrode processes and to unravel the kinetics of electrochemical systems has enormously increased in recent years[5, 6]. The application of this technique in metals electrodeposition in the presence of additives has also increased in recent years since adsorption phenomena strongly influence the electrochemical impedance structure[7].

The principle of EIS is to measure the impedance, usually at fixed potential during a frequency scan, to study the kinetics of processes at the metal electrolyte interface and to distinguish between the various mechanisms that regulate charge-transfer. EIS involves high-precision measurements over wide time ranges (10^4 to 10^{-6} s or 10^{-4} to 10^6 Hz), which makes it suitable for the study of two one-electron steps with the stabilization of the intermediate step in copper deposition discussed in Section 2.4. This method analyses the response of the electrochemical system to a small-amplitude alternating current signal perturbation.

The results of EIS testwork can be interpreted using either or both the complex-plane plot, also known as the Nyquist plot, and Bode plot. The complex-plane plot presents the real and imaginary impedances as a function of frequency and the Bode plot presents the dependence of the phase angle on frequency. Analysis of the system response therefore may contain information about the chemical and electronic structure of the metal electrode/cupric ions-sulfuric acid electrolyte with either APAM or Guar at the interface as the impedance is measured as a function of the frequency of the AC source.

A number of studies have been recently conducted to understand the effect of organic additives on copper deposition. The effect of chloride ions on the current-voltage polarization behaviour of polyethylene glycol [PEG: $(CH_2\text{-}O\text{-}CH_2)_n$] indicates that, in the presence of either cupric ions (0.3M) or sulfuric acid (2.2M), PEG polarizes

or inhibits the electrode more strongly in the presence of chloride ions than in its absence[8, 9]. In separate studies, Moffat et al.[8, 10-12] presented the effect of the competitive interaction of 3-mercapto-1-propane-sulfonic acid (MPSA) with PEG and chloride ions in the copper electrolyte bath on the current voltage polarization as well as on the superconformal deposition of a smooth and "bright" copper deposit. While PEG and chloride ions reduce the deposition rate or provide the inhibition/polarization process, MPSA or some derivative thereof is associated with acceleration/depolarization processes.

A surface-enhanced Raman (SERS) study on the polarization effect of PEG during copper deposition indicates that the presence of chloride ions enhance the *adsorption* of PEG to the copper electrode surface[13]. It suggests the formation of PEG-Cu-Cl complex in which there are only two possible types of oxygen atoms the Cu(I) could bind with (i) an ether O in the CH_2-O-CH_2 chain and (ii) a hydroxyl oxygen O at the CH_2-O-H end. Therefore, Feng et al.[13] suggested two structural models involving a Cu atom with two oxygen atoms of PEG and one chloride ligand and (ii) with one ether oxygen and one hydroxyl oxygen atom of PEG and one chloride ligand.

The kinetics of copper electrodeposition from an acidified copper sulphate (0.25M) – sulfuric acid (1.8M) electrolyte containing PEG, bis(3-sulfo-propyl) disulfide (SPS: $Na_2[SO_3(CH_2)_3S]_2$) and chloride ions also indicated that there is a competitive interaction between PEG and SPS using EIS[8, 14]. PEG and chloride ions interact with cuprous ions to form a passivating film inhibiting the metal deposition[15]. SPS accelerates the formation of cuprous complexes near the surface of the electrode such as cuprous thiolate $[Cu(I)(S(CH_2)_3SO_3H_{ad}]$ as reported from current-potential curves using a rotating Pt-disk-glassy carbon (GC)-ring electrode[15].

The effect of glue, thiourea and chloride ions on copper electrodeposition was also studied using EIS at a copper-metal rotating disk electrode (RDE)[16, 17]. It was concluded that thiourea decreases the charge-transfer resistance that was increased by the presence of glue and chloride ions.

In summary, the presence of PEG and chloride ions or glue and chloride ions in a sulfuric acid – cupric ion electrolyte polarizes the current-potential relationship. In other words, these additives increase the charge-transfer resistance. The addition to the electrolyte of MPSA, SPS or thiourea, all of which contain the thiol group, depolarizes the electrode thus compensating from the inhibition processes caused by PEG and chloride ions or glue and chloride ions. The formation of PEG-cuprous ion and MPSA- or SPS-cuprous ion complexes are proposed for surface coverage purposes[8, 14] but the actual adsorption mechanisms of these organic additives have not been discussed in detail. Despite the variety of mechanisms proposed for the smoothening effect of additives[18], a consensus exists that adsorption of the additive near the surface of the substrate plays the determining role[19, 20].

5.1.1 Equivalent Circuit for Electrochemical Systems – Copper Deposition

An electrochemical cell can be considered as an impedance to the passage of a small sinusoidal amplitude current at the exact amplitude and phase angle as the source and therefore its performance can be represented by an equivalent circuit of resistors and capacitors in parallel[1, 3]. The main objective of EIS studies is to find the frequency dependencies of resistances and pseudo-capacitances in the equivalent circuit and to transform these functions into an improved knowledge of the chemical data.

Bard et al.[1] states that it is highly unlikely the faradaic process can be represented by a simple circuit in series comprising a single resistor, R and a single capacitor, C_d, whose values are independent of frequency, but as a general impedance, Z_f. Therefore parallel elements were introduced into the equivalent circuit to account for the total current through the working electrode as the sum of the distinct contributions from the faradaic processes, i_f, and double layer charging, i_c. The double-layer capacitance, sometimes referred to as constant phase element (CPE), represented in equivalent circuits by C_{dl} or C_d, is nearly a pure capacitance[1] and is generally associated with space charge polarization regions, specific adsorption[1], surface coverages[21] and electrocrystallization[4].

As the current passes through the electrolyte, a resistance, Rs, is inserted into the equivalent circuit as a series element. In contrast to Rs and C_d, which are nearly ideal circuit elements independent of frequency, the components of the faradaic impedance are non-ideal or dependent on the frequency (ω). As a result, the faradaic impedance consists of a pure resistance, R_{ct}, the charge-transfer resistance, also known as polarization resistance, and the Warburg impedance, Z_W, described by Bard et al.[1] as "the kind of resistance to mass transfer" or diffusion impedance.

The equivalent circuit most often referred to in the literature for electrochemical interfaces is depicted in Figure 5-56[4, 22-27]. This equivalent circuit that consists *only* of resistors and capacitors is used to describe the two single-electron transfer steps[21]. This selection appears to be valid for Langmuir isotherms and other similar isotherms such as the Frumkin isotherm. This equivalent circuit was also used for copper deposition in the presence[24] and absence[25] of organic additives.

Diffusion creates impedance in the low frequency range, known as the Warburg impedance. This impedance depends on the frequency of the potential perturbation. At high frequencies, the Warburg impedance drops out because the time scale is so short that diffusion cannot manifest itself as a factor affecting the current.

At very high frequencies, the equivalent circuit is represented by Figure 5.56 - R1, R2 and C2 only since R2 and C2 lead to a time constant, τ_D=R2*C2, the dielectric relaxation time of the electrode material. The value of τ_D gives the smallest time constant of interest in EIS experiments. The condition $\omega_{max}*\tau_D \ll 1$ is satisfied for the highest angular frequency applied, ω_{max}; since τ_D is often so small, e.g., 10^{-7}s. Therefore, the impedance plane curve is not observed. As the peak frequency, ω_p conforms in the vicinity of $\omega_p*\tau_D=1$ and therefore $\omega_{max}*\tau_D \gg 1$ it is only then that almost the full curve of the impedance plane can be observed[4].

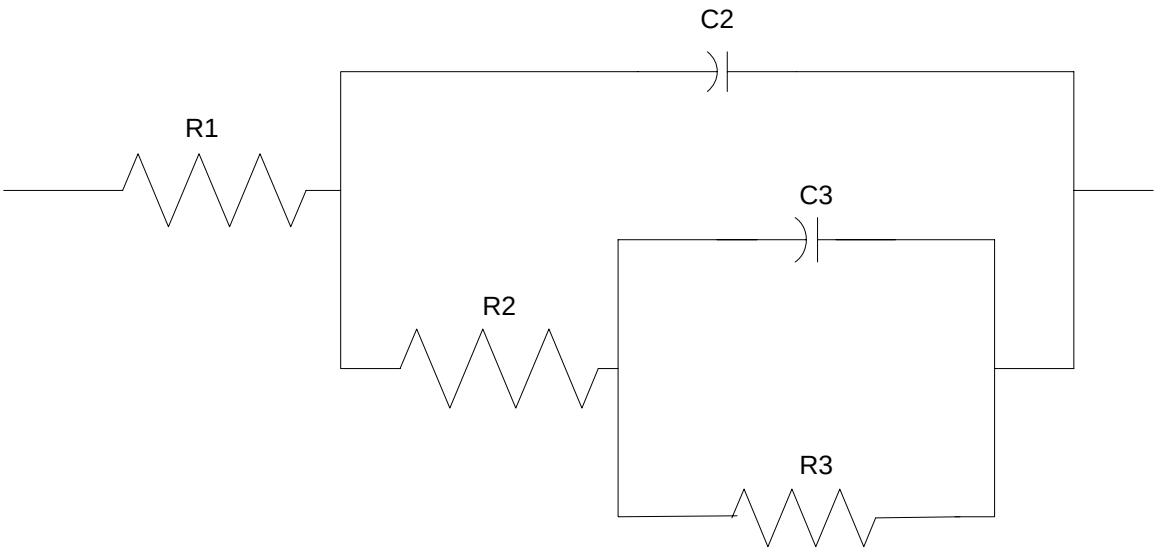

Figure 5-56: Parameters Definition in LEVM Equivalent Circuit B[28]
Legend: R1 = P(1), Electrolyte Resistance; R2 = P(4), Charge-Transfer Resistance; C3 = P(5), Double-Layer Capacitance and R3 = P(26) and C3 = P(27) are part of the Diffusion-Related Elements, the Warburg Impedance[4]. P(i) represents the parameters selected in LEVM.

The results of EIS testwork will be presented in the complex-plane plot, also known the Nyquist plot, where the imaginary and real impedance are depicted as a function of frequency. A plot of Z_{Im} vs. Z_{Re} should give a circular plot centered at Z_{Re} = R1+R2/2 and Z_{Im}=0 having a radius of R2/2 where R2 is the charge-transfer resistance, R_{ct}. The imaginary component to the impedance plotted from Figure 5-56 comes solely from the double-layer capacitance.

Figure 5-57 shows the complex-plane plot for an electrochemical system[1, 29]. The regions of kinetic and mass-transfer control are found at high and low frequencies, respectively.

The sine-wave for parallel circuits is described using the complex plane for an electrochemical cell. The total impedance characterizing the linear response of the system as a function of the oscillation frequency is given by[3, 14, 29, 30]

$$Z(\omega) = Rs + \frac{1}{\frac{1}{Z_F(\omega)} + j\omega C_{dl}} \qquad (5\text{-}24)$$

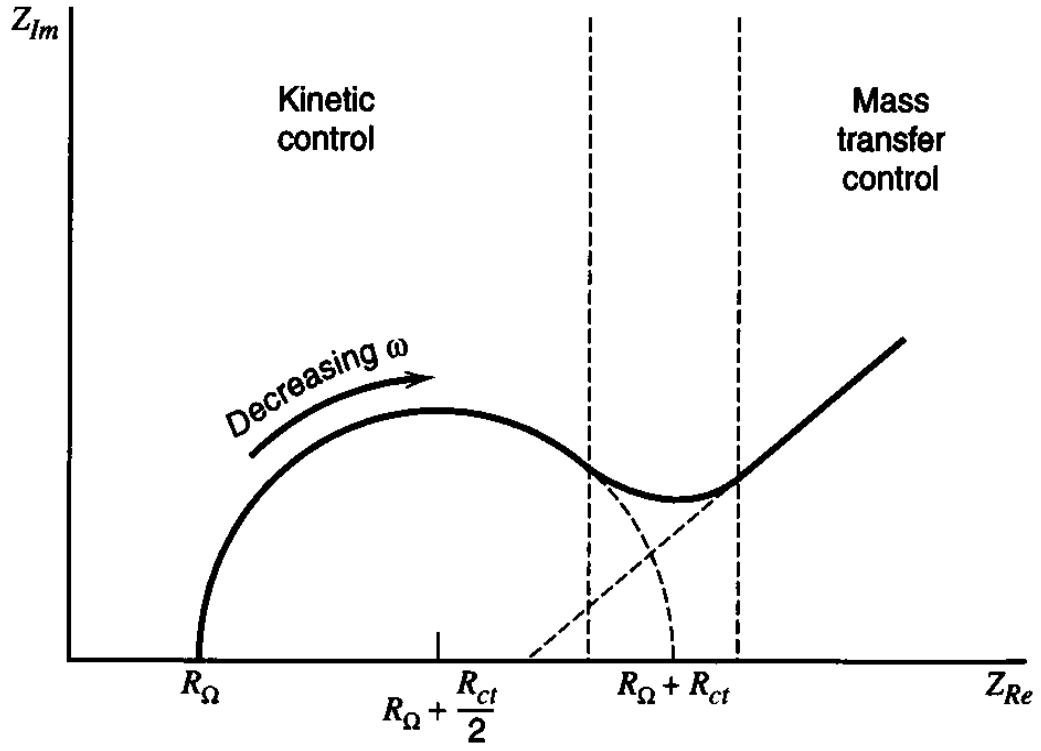

Figure 5-57: Complex-Plane Plot for an Electrochemical System

Z_{Re}, real impedance; **Z_{Im}**, imaginary impedance; **R_Ω,** electrolyte resistance (**R_s**); **R_{ct}**, charge-transfer resistance or polarization resistance and **ω**, frequency.

where Rs (or RΩ in Figure 5-57) represents the ohmic resistance of the electrolyte between the electrode surface and the reference electrode, and C_{dl} the double-layer capacitance and

$$Z_F(\omega) = \frac{\Delta V}{\Delta i_F} \qquad (5\text{-}25)$$

represents the complex faradaic impedance and it is often replaced by the charge-transfer resistance, R_{ct} for the high frequency region depicted in Figure 5-57. It is widely known that the current that flows is partly due to charging the double-layer capacity and to the faradaic reaction when the potential of the electrode is varied.

The equivalent circuit presented in Figure 5-56 will be used to conduct measurement modelling[31-34] of *all* experimental data in the presence and absence of

Guar and APAM using the commercially available software LEVM[28] and ZSimpWin™[35, 36]. LEVM and ZSimpWin™ (Princeton Applied Research) use the Levenberg-Marquardt algorithm to conduct the minimization procedure to find the set of parameters in the equivalent circuit.

5.1.2 Measurement Modelling of Electrochemical Impedance Spectroscopy Data

It is often suggested to derive the impedance as a function of the kinetic parameters for a given mechanism, and therefore data analysis should proceed from the measured impedance spectrum directly to the kinetic parameters of the postulated mechanism[21, 31]. The mechanism for copper deposition was given in Section 2.4.

The impedance measurement is valid provided that the criteria of linearity, causality, stability and finiteness are satisfied[3, 4]:

(i) The linearity of the system is defined when sum of individual input signals is equal to the sum of individual responses. Linearization of differential equations determines the impedance since electrochemical systems are usually highly nonlinear. This criteria holds with the application of a small AC amplitude such as $\Delta E < 8/n$ mV[3] peak-to-peak, where n is the number of electrons exchanged in the reaction.

(ii) A system is causal if the response of the system is entirely due to the applied perturbation,

(iii) A stable system remains invariant unless it is excited by an external source.

(iv) Finally, the real and imaginary components of the impedance must be finite valued over the entire frequency range $0 < \omega < \infty$.

Once the data is obtained, a measurement model can be conducted in which a complex nonlinear least-squares (CNLS) program is used to fit the real and imaginary parts, or the magnitude and phase angle of the experimental data to a given model. In general, the sum of squares is minimized using the following equation:

$$S(P) = \sum_{i=1}^{N} \left[w_i' \left(Z_i' - Z_{i,calc}' \right)^2 + w_i'' \left(Z_i'' - Z_{i,calc}'' \right)^2 \right] \qquad (5\text{-}26)$$

Where Z_i' and Z_i'' are the real and imaginary parts of the experimental impedances, respectively at frequency ω_i; $Z_{i,calc}'$ and $Z_{i,calc}''$ are the values calculated from the given model and w_i' and w_i'' are the statistical weights of the data. (P) represents the parameters selected in LEVM. The minimization is carried out using the iterative Marquardt-Levenberg algorithm[3, 4]. Thus the electrochemical impedance data can be directly correlated with an idealized model circuit of discrete electrical components[1, 4, 31, 37].

The EIS data in this thesis were obtained using a rotating cylinder electrode. However, a small number of tests were also conducted using a RDE to validate the RCE results. The non-uniformity of current distribution for the rotating disk electrode for finite values of the dimensionless exchange current density is widely known as is the uniformity of the current distribution for the rotating cylinder electrode[38]. Numerical calculations presented by Durbha et al.[39] demonstrated that the non-uniform current distribution observed below the mass-transfer-limited current has a significant effect on the impedance response of the rotating disc electrode when the electrode kinetics are fast and therefore the physical parameters obtained by regression models will be incorrect[39, 40].

The hydrodynamics for the RDE are well understood and hence surface concentration can be computed. The surface concentration of cupric ions on the RCE can also be calculated as described by Newman[38] and elsewhere[3, 41] and in Equation 2-11. Since planar electrodes, used in copper electrowinning and electrorefining, also have uniform current distribution[38], and since RCE's also show uniform current distribution, RCE was also used for the work described in this Chapter.

The effect of Guar and APAM will be compared in the high frequency loop only since the high frequency loop reflects the kinetic control region of a process[1]. The commercial software packages LEVM and ZSimpWin™ were used to the EIS modelling. ZSimpWin™ is often also known as the Boukamp software package in

honour of its author[35]. The statistical analysis presented in this work was conducted using LEVM. However, if poor fitting was obtained with LEVM; ZsimpWin™ was used to obtain the initial parameter values. These initial values were then used in LEVM for further iteration. ZSimpWin™ was easier to use than LEVM but the documentation for LEVM appears to be more comprehensive[4, 28].

5.2 Experimental

The electrochemical cell was a 500 mL long-necked glass beaker with a four-port lid made of Perspex depicted in Figure 5-58. A circular retaining wall, made also of Perspex, with an internal diameter similar to the external to the mouth of the beaker diameter was sealed on the bottom face of this four-port lid to immobilize it from any lateral movement. A PVC bush centred the working electrode within the electrochemical cell. This bush had an external diameter similar to the central-port diameter and internal diameter similar to the diameter of the shaft. Therefore the beaker was always centralized through the shaft and the distance between the electrodes were always kept constant.

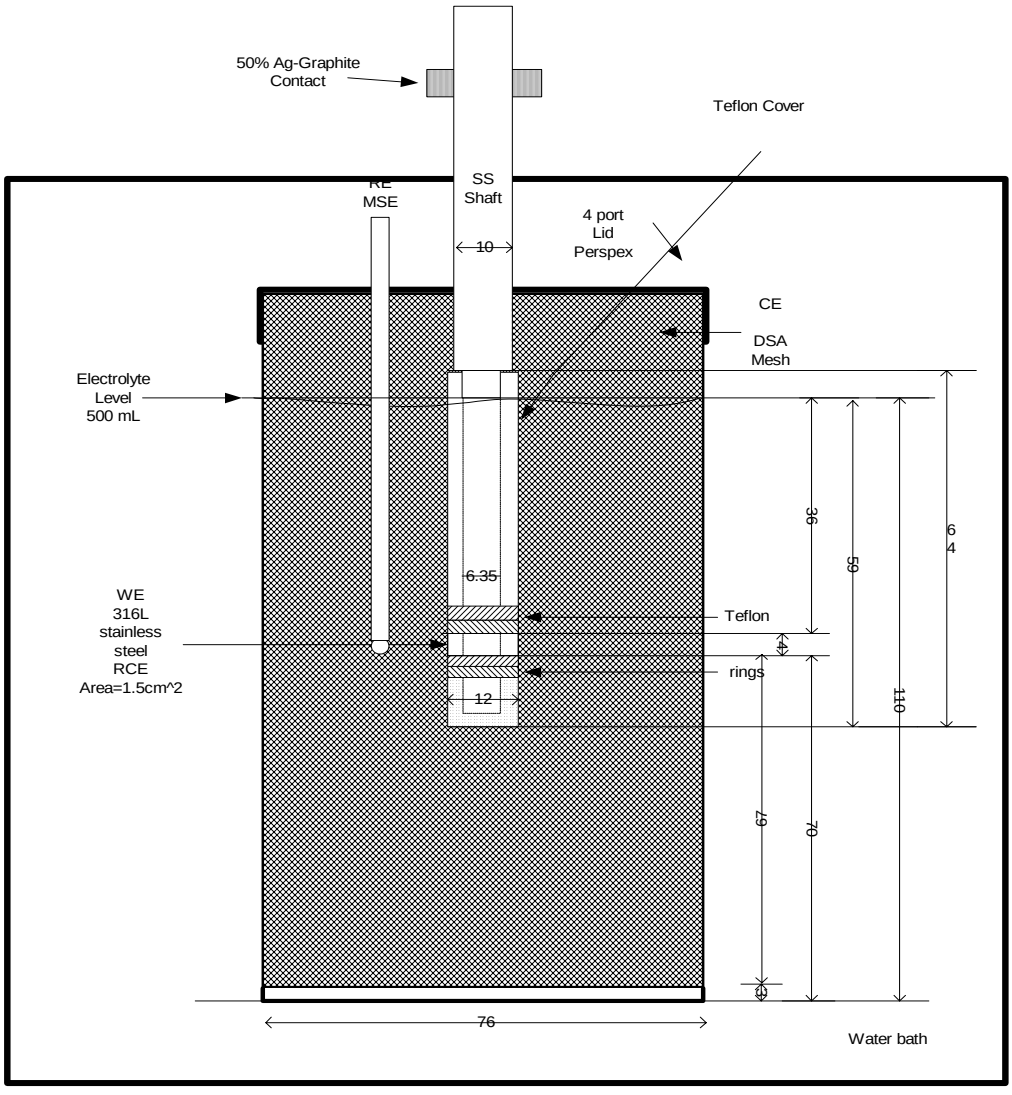

Figure 5-58: Rotating Cylinder Electrode Configuration used for CV and EIS

The cell was immersed in a water bath at either 45°C±0.5°C or 65±0.5°C. Evaporation was made up with water at about 1.4mL (45°C) and 7mL (65°C) per hour, respectively. The working electrode (WE) was a 316L stainless steel rotating cylinder electrode (RCE) sourced from Pine Instruments (QC3 series – ACQ012CY316). However, the original WE surface area was reduced to a $2cm^2$ surface area to conduct CV tests and to $1.5cm^2$ to conduct EIS tests. The smaller surface area produced less induction at the high frequency end where the frequency count starts. A mercurous-mercuric sulfate electrode (MSE, 651 mV vs. NHE) in saturated potassium sulfate from Radiometer Analytical was used as a reference electrode.

The counter electrode was prepared from dimensionally stable anode (DSA, a titanium-based substrate coated with ruthenium dioxide or iridium dioxide), sourced from Eltech Systems Corp. DSA is the standard anode for generating chlorine in the chlor-alkali, chlorate and hypochlorite industries where it has very long lifetimes. The DSA surrounded the internal wall of the 500mL long-necked beaker. The working electrode was initially polished with 1μm and 0.25μm diamond paste (Struers). After every test it was polished with the latter only, washed with distilled water and acetone, rinsed in an electrolyte solution and rinsed again with distilled water. Table 5-22 shows the experimental conditions for CV and EIS experiments.

The aim of the experimental design was to approximate the diffusion layer thickness of a commercial scale electrowinning plant as suggested in a computational fluid dynamic study by Filzwierser et al.[42]. The rotation speed of the RCE at 25rpm and at temperatures from 25°C to 65°C gives a Reynolds number ($Re=\omega d^2/2\nu$) from 48 to 527. At this rpm and temperature range the Taylor (Ta) number varies from 932 to 1804. It is reported that the critical Reynolds number is 200 for the RCE[43] and therefore radial and axial motion is superimposed on the tangential flow across the electrolyte[38, 44]. This can been seen in Figure 5-59. The Reynolds and Taylor numbers therefore appear to indicate that the flow regime at 25 rpm and 45°C - 65°C is laminar with vortexes. Deposition conditions such as electrolyte composition, temperature and current density also simulate commercial scale conditions.

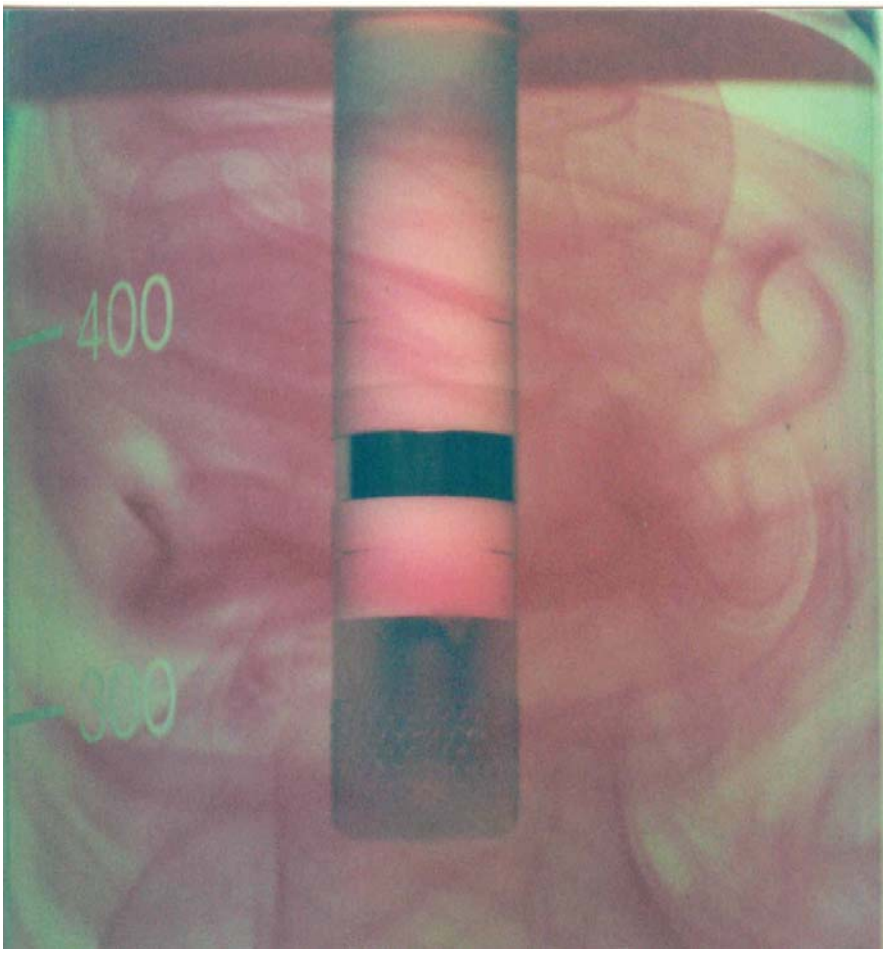

Figure 5-59: Fluid Flow Produced by the RCE at 25rpm and 25°C in Water

The critical Reynolds number ($Re = \omega * d^2/2\nu$) at 25°C is 200[43]. The Reynolds number for the copper electrolyte at 45°C and 25rpm is 204.

The experimental conditions for the CV tests are summarized in Table 5-22. These tests were conducted to determine the polarization behaviour of Guar and APAM on 316L stainless steel and on copper pre-plated onto 316L stainless steel at 10mA/cm^2 for 225 seconds.

The EIS tests were conducted in potentiostatic mode. The EIS tests were always conducted on pre-plated copper[8] formed as follows: chronopotentiometry for 360 seconds at 10mA/cm^2 current density to pre-plate copper, followed by automatic stabilization for 15 seconds at the potential to be applied during the EIS experiment followed by the EIS test itself. The EIS tests were run using 6mV AC over the

frequency range from 30kHz to 0.2Hz using the RCE and 50kHz – 0.2Hz using the RDE. Preliminary tests were run using 8mV AC and the impedance data obtained were similar to those observed using 6mV AC. Therefore, it was confirmed that the system was linear[3].

Table 5-22: Experimental Conditions for CV and EIS Experiments

Copper, g/L	36
Sulfuric acid, g/L	160
Chloride ions, mg/L	25
Guar Preparation Media	Water at 25°C
APAM Preparation Media	16-fold DE
APAM Preparation Media Temperature, °C	50
Electrolyte Volume, mL	500
APAM Concentration in Electrolyte, mg/L	2
RCE rpm	10 and 25
Copper Pre-plating Time for CV and EIS, respectively, sec	225 and 360
Current Density during Pre-plating, mA/cm^2	10
Electrolyte Temperature, °C	45 and 65
Sweep rate, mV/sec	1
Diffusion Layer Thickness for ***CV*** using RCE, at ***10 rpm***, μm*	90 (110)
Diffusion Layer Thickness for ***EIS*** using RCE, at ***25rpm***, μm*	87 (99)
Outer Cylinder Diameter, cm	7.6
Inner (rotating) Cylinder Diameter, cm	1.2
WE (316L Stainless Steel) surface area for CV, cm^2 [Set up: Potential 0 = -370 mV, Potentials 1 and 2 = -725mV vs. MSE]	2
WE surface area for EIS using RCE and RDE, respectively, cm^2	1.5 and 0.178
Schmidt Number (ν/D) for EIS at 45°C and 65°C, respectively	1005 and 435

*Diffusion layer thickness at 45°C and 65°C in brackets.

The pre-plating process of copper onto the stainless steel at 10mA/cm^2 was done to obtain a smooth deposit and to plateau the surface overpotential. The potential of the working electrode was fixed at -470 mV vs. MSE or 300 A/m^2 (30mA/cm^2) and -490mV vs. MSE 340 A/m^2 (34mA/cm^2) current density at steady-state conditions in the absence of APAM and Guar. All tests were replicated at least twice. The reference electrode was located about 1.5cm away from the WE to maintain a uniform velocity of the electrolyte around the electrode. This experimental configuration was similar to that reported by Kelly[8].

5.3 Cyclic Voltammetry in the Presence of Guar at 45°C

These tests were conducted to determine the polarization behaviour of Guar during copper electrodeposition on bare 316L stainless steel and on pre-plated copper at 10mA/cm^2 for 225 seconds. The pre-plating process achieves a constant overpotential over this period. These tests determined how the polarization behaviour varied when Guar was aged in the electrolyte heated at 45°C over a 5-hour period.

The initial cathodic scan of the cyclic voltammetry curves are presented in Figure 5-60. The left and right-sets of curves were obtained on stainless steel (SS) and on pre-plated copper (Cu), respectively. Each curve was sequentially obtained every hour starting with the bare stainless steel electrode after about 20minutes once Guar was dosed and followed with the pre-plated copper electrode and so on up to five hours. Therefore, CVs on stainless steel were conducted at 0.3, 2, and 4-hours and on pre-plated copper at 1, 3, and 5-hours.

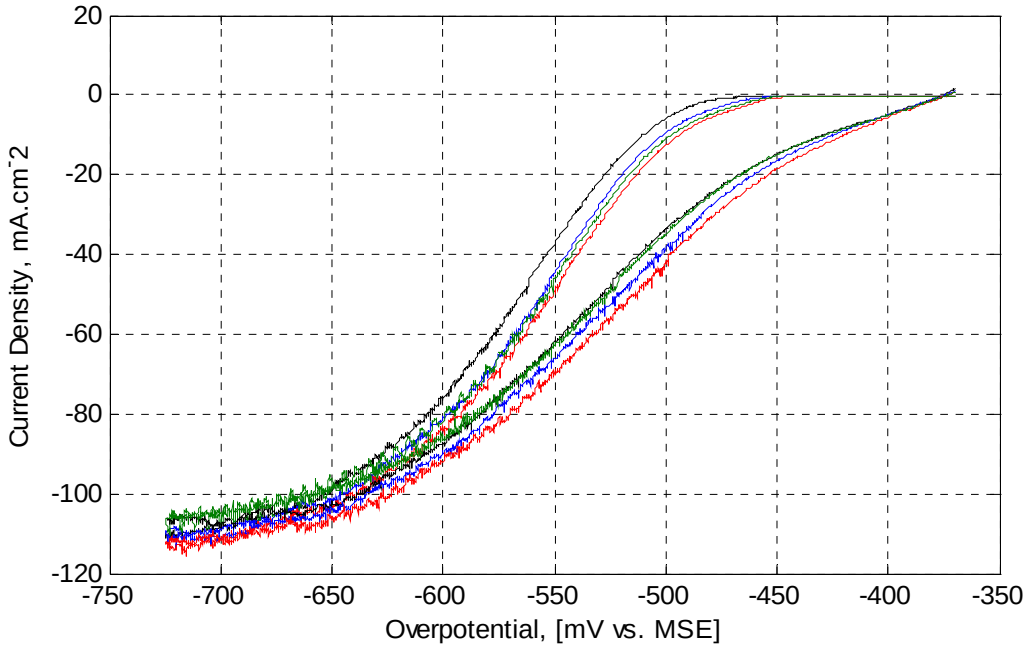

Figure 5-60: Effect of Guar Residence Time on Depolarization at 45°C.

Legend: Left-Set of Curves on Stainless Steel and Right-Set of Curves on Pre-plated Copper: Control (without Guar) – Black; 0.3 (SS) and 1Hr (Cu) – Blue; 2 (SS) and 3Hrs (Cu). – Red; and 4 (SS) and 5Hrs (Cu) – Green.

It can be seen that Guar de-polarized the electrode on both stainless steel and pre-plated-copper. This is based on the observation that the electrode potential in the presence of an additive is less negative than the potential without the additive at a determined current density. It can also be seen that there is a trend in the depolarization behaviour. Polarization increases from the 0.3-1hr to a maximum in 2-3hours and then its depolarizing activity decayed such that within 4-5hours an insignificant effect can be observed on pre-plated copper.

The limiting current density remains about constant in the presence and absence of Guar as others have observed in the presence of PEG and chloride ions[9, 11]. Figure 5-60 also indicates that less energy is required to plate on fresh copper-metal formed than on the stainless steel substrate. The same preferential deposition was obtained with PEG and chloride ions when the working electrode was made of copper metal[9]. This preferential deposition is probably due to the reduced activation energy required to nucleate on fresh copper-metal and the growth may also follow the Stranski-Krastanov mode where 3D copper metal islands form on top of the pre-deposited 2D copper overlayers[45] described in Chapter 2 – Section 2.5.1.

CV and EIS tests were found to be more reproducible on pre-plated stainless steel than on bare-stainless steel. Kelly et al.[8] also reported that EIS tests on pre-plated copper metal WE for 3minutes were more reproducible than on unpre-plated WE. This effect is probably due to the crystallographic misfit between 316L stainless steel and the freshly plated copper metal. This pre-plating process would simulate commercial electrowinning and electrorefining operations on 316L stainless steel since traces of copper are always left behind after the copper plate is stripped off.

Table 5-23 presents the depolarization data at 30mA/cm^2 (300Amp/m^2) current density extracted from Figure 5-60. Figure 5-61 depicts the extracted data and indicates that a maximum depolarization of approximately 14mV was obtained at 2-3 hours residence time whether on stainless steel or copper metal.

The polarization curves in the presence and absence of Guar were also used to calculate the potential at zero current (Ei=0), the (cathodic) Tafel slope (b) and the transfer coefficient (α). These values are shown in Table 5-24 for pre-plated copper

only. It can be seen that the potential at zero current appears to follow the overall polarization pattern of the aging of Guar in the electrolyte. The most important result in Table 5-24 is the transfer coefficient value of 0.50 in the absence of Guar. This agrees with that given by Wu and Barkey[46] and Mattson and Bockris[47].

Table 5-23: De-polarization Behaviour of Guar at 45°C

On Stainless Steel		On Pre-plated Copper	
Residence Time, Hrs	Potential, mV vs. MSE at 30 mA/cm^2 Current Density,	Residence Time, Hrs	Potential, mV vs. MSE at 30 mA/cm^2 Current Density,
0(Nil Guar)	-541	0(Nil Guar)	-493
0.3	-533	1	-484
2	-527	3	-478
4	-530	5	-491

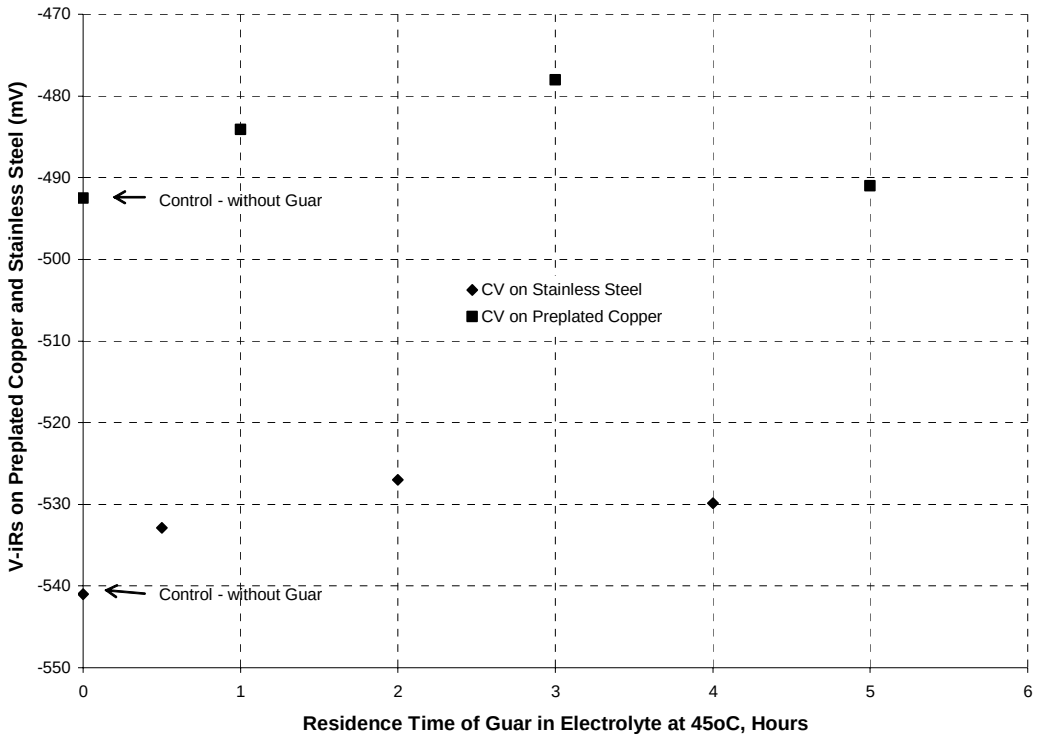

Figure 5-61: Effect of Time on the De-polarization Behaviour of Guar at 45°C at 300A/m^2 Current Density.

Table 5-24: Kinetic Parameters for Copper Deposition in the Presence of Guar at 45°C

Residence Time, Hours	E(i=0) mV vs. MSE	Tafel Slope, mV b	Transfer Coefficient α [=2.3R*T/(b*F)]
0 (Nil Guar)	-375.3	-127.1	0.50
1	-374.4	-122.6	0.52
3	-373.0	-123.6	0.51
5	-373.2	-125.9	0.50
Wu and Barkey[46]		-122	0.5 ± 0.05

5.4 Cyclic Voltammetry in the Presence of Activated Polyacrylamide at 45°C

These tests were conducted to determine the polarization behaviour of APAM during copper electrodeposition on bare 316L stainless steel and on pre-plated copper at 10mA/cm^2 for 225 seconds.

Figure 5-62 shows the results obtained at 45°C in the presence and absence of APAM. It indicates that APAM polarizes or inhibits the working electrode whether it is stainless steel or pre-plated copper. It can also be seen that APAM appears to confer higher adsorption on pre-plated copper electrode than on stainless steel since the polarization values are higher for pre-plated copper than that for the stainless steel electrode. This result contrasts with those of Vereecken and Winand[48] who found that polyacrylamide did not polarize the electrode when it was prepared in water and in full-strength electrolyte. It is therefore concluded that the preparation of APAM, i.e., the formation of block copolymers, confers an increase of the adsorption and therefore the polarization of the working electrode.

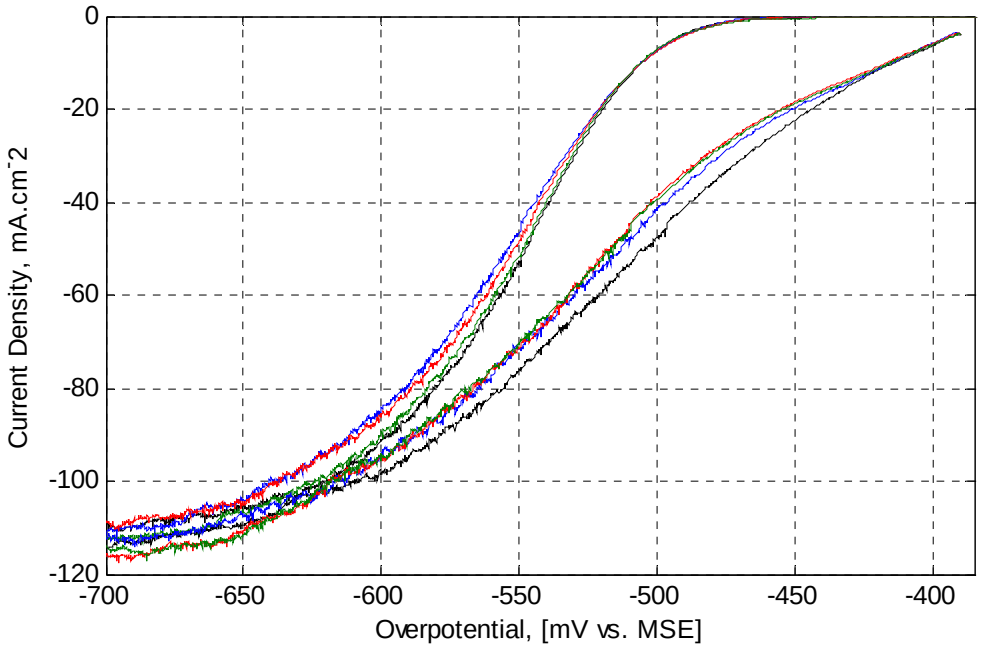

Figure 5-62: Effect APAM Residence Time on Polarization at 45°C.

Legend: Left-Set of Curves on Stainless Steel and Right-Set of Curves on Pre-plated Copper: Control (without APAM) – Black; 0.3 (SS) and 1 Hr. (Cu) – Blue; 2 (SS) and 3 Hrs. (Cu) – Red; and 4 (SS) and 5 Hrs. (Cu) – Green.

Table 5-25 shows the data extracted from Figure 5-62 for stainless steel and pre-plated copper at 300 and 400A/m^2. Figure 5-63 depicts the data from Table 5-25 for pre-plated copper only since it closely reflects a commercial application as discussed previously. A maximum polarization of 14mV is observed at 3 hours residence time.

Table 5-25: Polarization in the Presence of APAM at 45°C

On Stainless Steel			On Pre-plated Copper		
Residence Time, Hours	Potential, mV vs. MSE Current Density, mA/cm^2		Residence Time, Hours	Potential, mV vs. MSE Current Density, mA/cm^2	
	30	**40**		**30**	**40**
0 (No APAM)	-529	-538	0 (No APAM)	-468	-489
0.3	-533	-544	1	-477	-497
2	-532	-543	3	-482	-503
4	-531	-540	5	-481	-502

Figure 5-63 shows that the presence of APAM results in a significant polarization of the electrode over the 5-hour experimental period. These results are consistent with APAM acting as a surfactant/levelling agent and doing so for extended

period of time, which is consistent with the results described in Chapters 3 where 1mg/L APAM was dosed once for 6 hours electrowinning time.

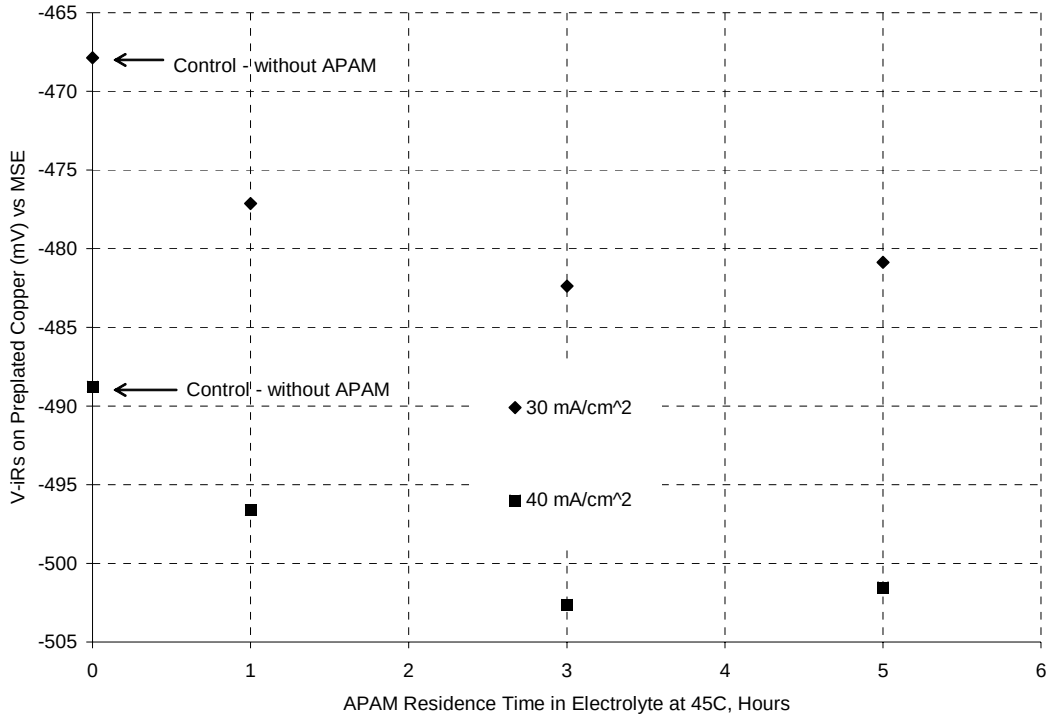

Figure 5-63: Effect of APAM Ageing on Polarization on Pre-plated Copper at 45^{o}C

5.5 Cyclic Voltammetry in the Presence of Activated Polyacrylamide at 65^{o}C

These tests were conducted at the temperature used in copper electrorefining[49]. Figure 5-64 shows the results in the presence of APAM at 65^{o}C. It can be seen clearly that the polarization behaviour of APAM increases with time giving a maximum polarization in the first hour (blue colour). Table 5-26 shows the potentials at 300 and 400 A/m^2 extracted from Figure 5-64. Figure 5-65 depicts these values.

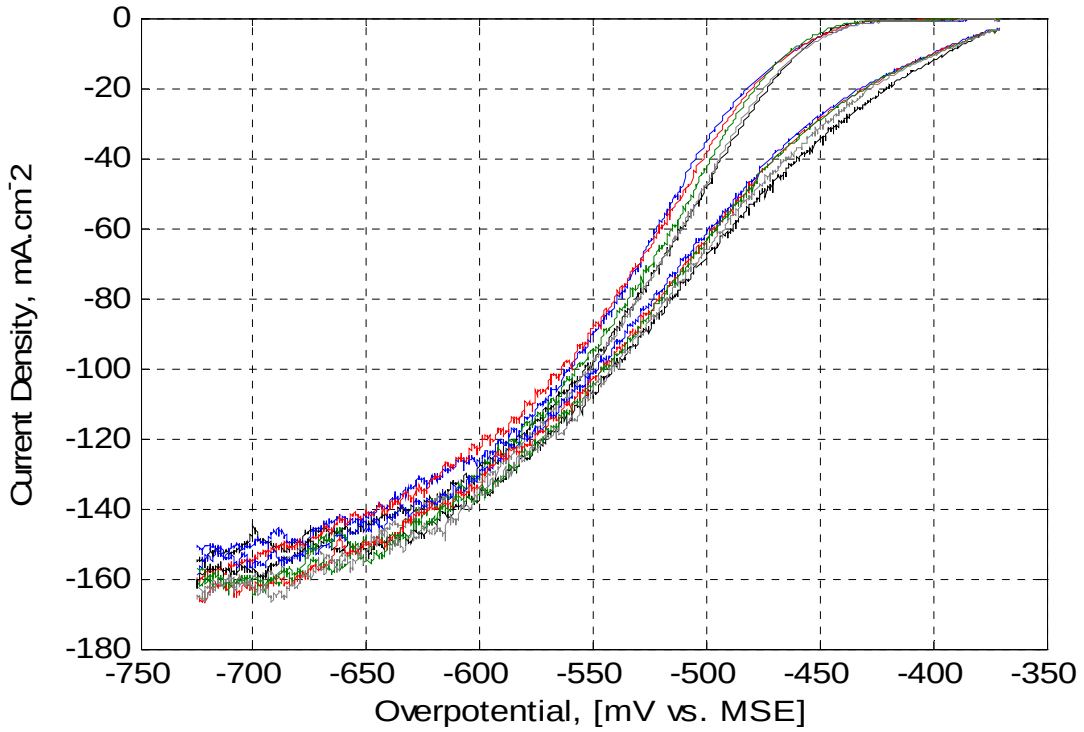

Figure 5-64: Effect of APAM Residence Time on Polarization at 65°C and 10rpm.

Legend: Left Set of Curves on Stainless Steel and Right Set of Curves on Pre-plated Copper: Control (without APAM) – Black; 0.3 (SS) and 1 Hr (Cu) – Blue; 2 (SS) and 3 Hrs.(Cu) – Red; 4 (SS) and 5 Hrs.(Cu) – Green; 6 (SS) and 7 Hrs.(Cu) – Grey.

Figure 5-64 shows that the presence of APAM results in a significant polarization of the electrode over a 7-hour period, with the polarization reaching a maximum of 13mV at 1hr residence time at 300A/m^2. It can also be noted that APAM appears to confer higher adsorption on pre-plated copper than on stainless steel since the net polarization values are higher for pre-plated copper than for stainless steel. This preferential adsorption on pre-plated copper was also observed at 45°C. Once again, these results indicate that APAM acts as a levelling agent for extended periods of time. The effectiveness of APAM is also dependent on the temperature. It has been shown in Sections 4.3.1 and 4.3.2 that APAM in the temperature range of 45°C- 65°C had the highest significant effect on reducing surface roughness than in the temperature range of 45°C-55°C. This result is also consistent with those described in Chapter 4 where APAM was dosed once for 6 hours electrowinning time and produced smoother copper deposits than Guar.

Table 5-26: Polarization in the Presence of APAM at 65°C

On Stainless Steel			On Pre-plated Copper		
Residence Time, Hours	Potential, mV vs. MSE Current Density, mA/cm2		Residence Time, Hours	Potential, mV vs. MSE Current Density, mA/cm2	
	30	40		30	40
(0) No APAM	-484	-493	(0) No APAM	-441	-459
0.3	-494	-505	1	-454	-472
2	-492	-501	3	-453	-470
4	-489	-499	5	-452	-470
6	-485	-494	7	-448	-464

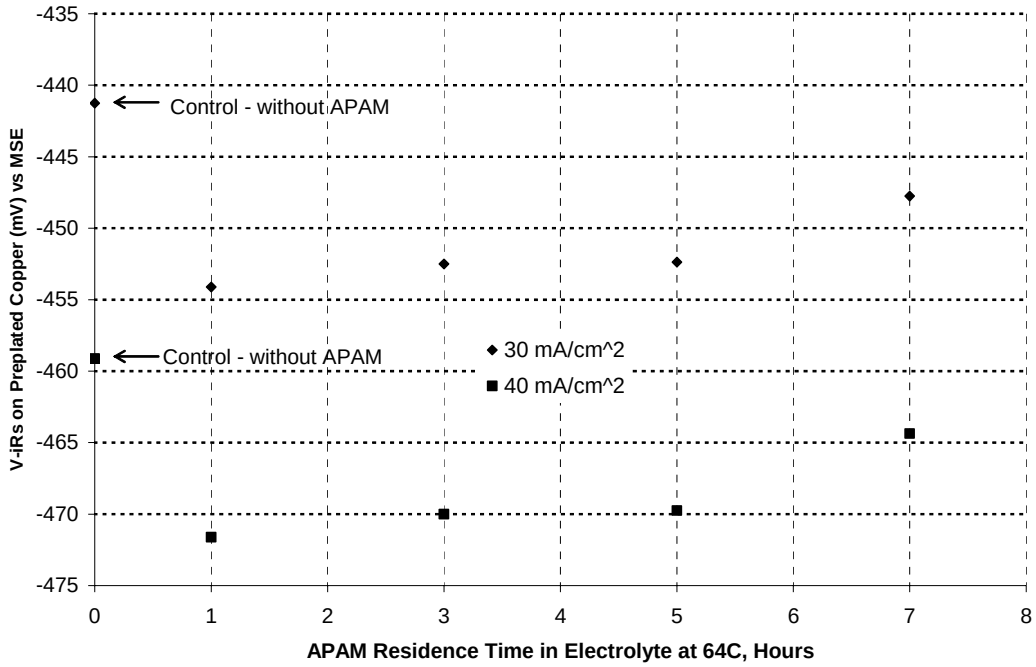

Figure 5-65: Polarization of APAM on Pre-plated Copper at 65°C

The maximum polarization at 45°C and 65°C is approximately 14mV but the time to attain this maximum value is about 3.5 hours at 45°C and 1.5 hours at 65°C as shown in Figure 5-66.

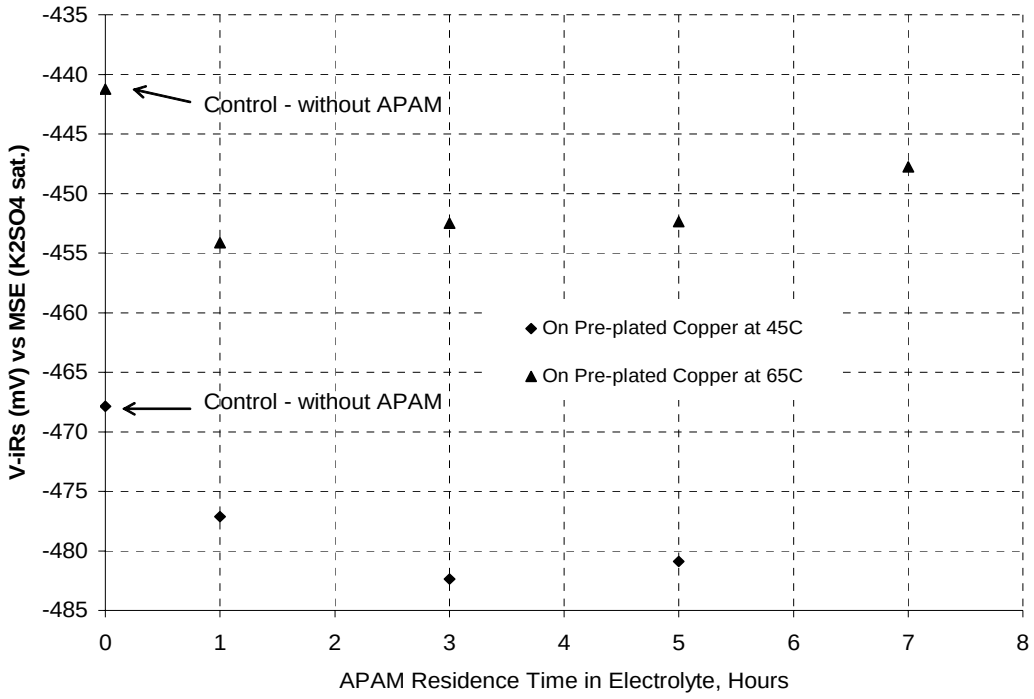

Figure 5-66: Effect of Temperature on APAM Polarization at 300 A/m^2 and 45^{o}C and 65^{o}C

5.6 Electrochemical Impedance Spectroscopy Results in the Absence of Additives

Preliminary tests were conducted to compare the results of this work with those presented in the literature in the absence of organic additives[8]. Figure 5-67 shows experimental data at two potentials (-470 and -490mV versus MSE) as open symbols and data fitted to the equivalent circuit shown in Figure 5-56 produced by LEVM as solid lines.

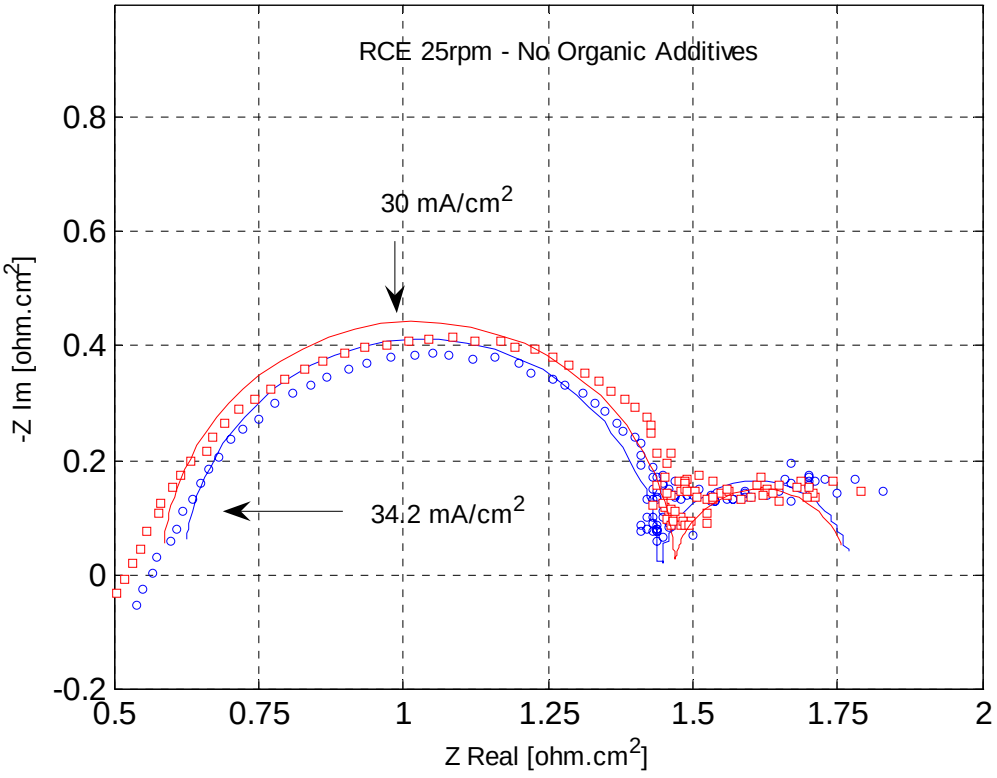

Figure 5-67: Complex-Plane Plot of Experimental and Simulated EIS data at -470 (30mA/cm^2 - red) and -490mV (34.2mA/cm^2 - blue) vs. MSE and 45^{o}C in the Absence of Organic Additives. Charge-Transfer Resistance, R_{ct} in the High Frequency loop, at 25 rpm and 30mA/cm^2 = 1.45ohm.cm^2 and at 25rpm and 34.2mA.cm^2 = 1.4ohm.cm^2.

It can be seen that the data can be reasonably interpreted in terms of an equivalent circuit as shown in Figure 5-56 which results in the prediction of two loops. The predicted two loops are the results of resistors and capacitors in parallel.

The results shown in Figure 5-67 are in agreement with studies of adsorbed species undergoing a single electron transfer step. Such reaction have been shown to have equivalent circuits that consist only of capacitors and resistors and exclude inductive behaviour[21]. This conclusion is valid for the Langmuir isotherm[21] and possibly for the Frumkin isotherm. The capacitor is often known as the constant phase element (CPE) to describe different electrochemical phenomena such as double-layer capacitance, adsorption and surface coverage[21]. The adsorption of polyacrylamide in acid solutions follows the Frumkin isotherm slightly better than the Langmuir isotherm according to Grchev et al.[50].

Figure 5-67 correlates with the experimental work in the published literature[8, 14, 17, 51-53] where RDEs were used in terms of the electrolyte resistance and the charge-transfer resistance, Rct, in the high frequency loop. However, measurement modelling or regression analysis was absent from the above published literature, except from the work of Fabricus et al.[17]and Chassaing et al.[52]. It has been recently stated that the inherent non-uniform primary current distribution of the rotating disc electrode precludes measurement modelling[40].

The results presented in Figure 5-67 will be compared with those in the literature to confirm the validity of EIS spectra recorded with the RCE. However, since there are no RCE data in the literature except the data from Nava et al.[25] who used 15.7mM cupric ions in 1M H_2SO_4; this comparison will be made with data recorded with RDE's in the literature.

It can be seen in Figure 5-67 that the electrolyte (0.567M $CuSO_4$, 1.6M H_2SO_4 and 25mg/L chloride ions at 45^oC) resistance is about 0.6ohm.cm^2 where the curve crosses the imaginary impedance (See Figure 5-57). This result correlates well with that of Kelly et al.[8] who reported 0.5ohm.cm^2 for 0.25M $CuSO_4$, 1.8M H_2SO_4 and 50mg/L chloride ions using a RDE at 25^oC.

Figure 5-67 indicates that at 45^oC the R_{ct} from the simulated data at 25 rpm and 30mA/cm^2 is equal to 1.45ohm.cm^2 and at 25rpm and 34.2mA/cm^2 is equal to 1.4ohm.cm^2. It would be expected that the R_{ct} would decrease at the higher current density, as is observed.

The charge-transfer resistance, Rct, for the high frequency loop can also be obtained from the studies of Kelly et al.[8] and Gabrielli et al.[14] Kelly et al.[8] obtained R_{ct} values of about 1.97ohm.cm^2 at 400rpm and 36mA/cm^2 and 1.47ohm.cm^2 at 2500 rpm and 43mA/cm^2. These values do not exactly correlate with the data produced by Gabrielli et al.[14] who obtained 1.7ohm.cm^2 at 100 rpm and 25mA/cm^2 using also a RDE at 25^{o}C for the same cupric ions and sulfuric acid concentrations as used by Kelly et al.[8] but with a concentration of chloride ions of 35mg/L.

The R_{ct} results presented in this section with the RCE broadly correlate with the Rct data reported in the preceding paragraph where RDEs were used. The RCE results at 25rpm (laminar flow with 2-3 vortexes)[54] and with 0.567M $CuS0_4$ in 1.6M H_2SO_4 at 45^{o}C gave faster copper deposition kinetics (lower R_{ct} value) than the RDE (laminar flow) data obtained from 0.25M $CuSO_4$ in 1.8M H_2SO_4 at 25^{o}C as would be expected given the lower concentration of cupric ions and temperature in the latter study.

The low frequency loop is more complex and less understood in terms of the number and nature of the parameter values. It depends on the surface preparation of the substrate, growth mode[55] of the deposit including its crystallographic orientation, hydrodynamic conditions and current density[56]. The cylindrical diffusion produced by the rotating cylinder electrode results in the relatively constant imaginary impedance component[3, 41] and therefore the RCE appears highly sensitive to surface roughness in the low frequency range as will be shown in the next Sections. It is stated by Macdonald[4] that the roughness of an electrode may lead to a frequency dispersion of the interface, the lines of electric force do not converge evenly on that surface and therefore the double-layer will be charged unevenly.

The simulated data of the low frequency range in Figure 5-67 also shows the difference between the diffusion of cupric ions across the concentration boundary layer: more cupric ions at 30mA/cm^2 yields a reduced amount of charge-transfer resistance than that at 34.2 mA/cm^2. This observation is similar to that presented by Kelly[8].

It is therefore concluded that EIS data presented in this thesis using the RCE are valid. The results are in agreement with mechanistic studies for single electron transfer

steps that have equivalent circuits that consist only of capacitors and resistors and exclude an inductive loop. The charge-transfer resistance values for the high frequency loop are consistent with the rate of copper deposition at different current densities.

The noise level predominantly observed in the low frequency region in the present study appears be inherent to deposition processes since the nucleation and growth of the deposit is different in the presence and absence of organic additives. This hypothesis will be shown in the following Sections where the presence and absence of both Guar and APAM are evaluated.

5.7 Electrochemical Impedance Spectroscopy Results in the Presence of Activated Polyacrylamide at -470mV vs. MSE and 45°C

These tests were conducted to determine the effect of APAM ageing on the kinetics of copper deposition. The EIS tests on freshly plated copper were carried out every hour for 7-hours.

Figure 5-68 presents the EIS response over the 7-hour period and shows a sequential increase of the charge-transfer resistance in the high frequency ranges. The monotonic increase in the high frequency range is possibly due to the ageing process of APAM in the cupric ion-sulfuric acid electrolyte at 45°C, i.e., additional hydrolysis of the block copolymer backbone and reduction of its molecular weight. Grchev et al.[50] found the surface coverage at 2-3ppm polyacrylamide concentration decreased from about 0.52, 0.3, 0.2 to 0.02 as the polyacrylamide molecular weight increased from $5x10^3$, $2.2x10^4$, $2.25x10^5$ and $1.5x10^6$, respectively. (see also Section 2.6.3 – Polyacrylamide Adsorption Mechanism). It was also found by Radeva et al.[57] that the adsorbed layer thickness of 4% and 12% hydrolysed polyacrylamide has a *flatter* conformation than that of nonionic or neutral polyacrylamide.

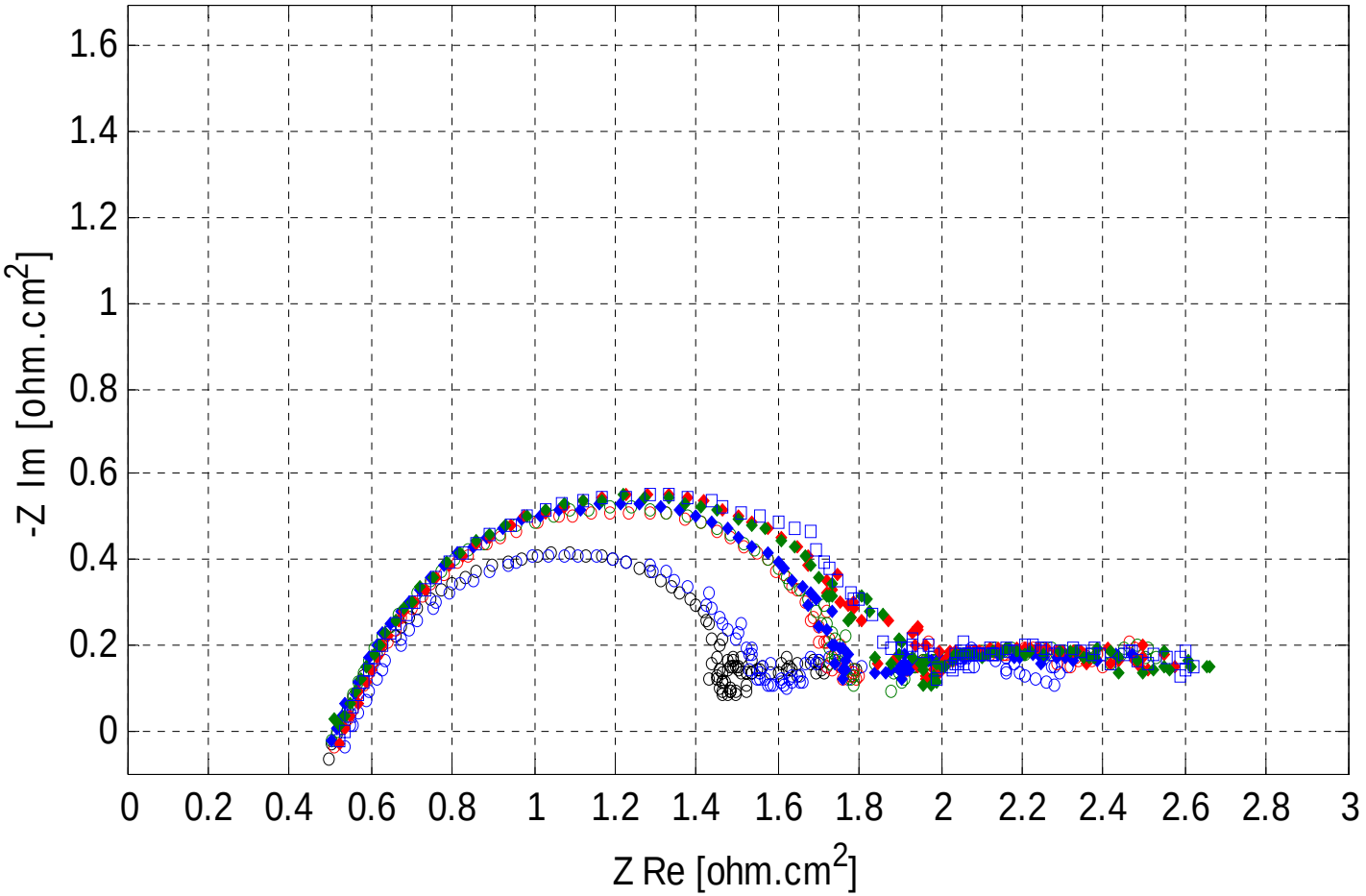

Figure 5-68: Complex-Plane Plots of Experimental EIS in the Presence and Absence of APAM at -470mV vs. MSE and 45°C
Legend: o - Black – Control – without APAM; o blue, 0.5 Hrs; o red, 1Hr; o green, 2Hrs; ♦ blue, 3Hrs; ♦ red, 5 Hrs; ♦ green, 6 Hrs and □ blue, 7 Hrs Residence Time of APAM in Electrolyte at 45oC. Overpotential: 93mV vs. SHE.

Figure 5-68 also shows that in the low frequency range, Z_{Im} is approximately constant or changes very slowly. This is consistent with the work of Lasia[3] and Jacobsen[41] who solved the cylindrical diffusion equations and concluded that cylindrical diffusion gives an almost constant imaginary impedance component in the low frequency range.

Figure 5-69 shows a subset of the experimental data (dots) from Figure 5-69 and simulated data (line) at -470mV versus SME (93mV vs. SHE) which corresponds to about 30mA/cm^2 in the absence of APAM. Two data sets are presented; one in the absence of APAM and the other is for the experiment after 2 hours residence time of APAM in the electrolyte.

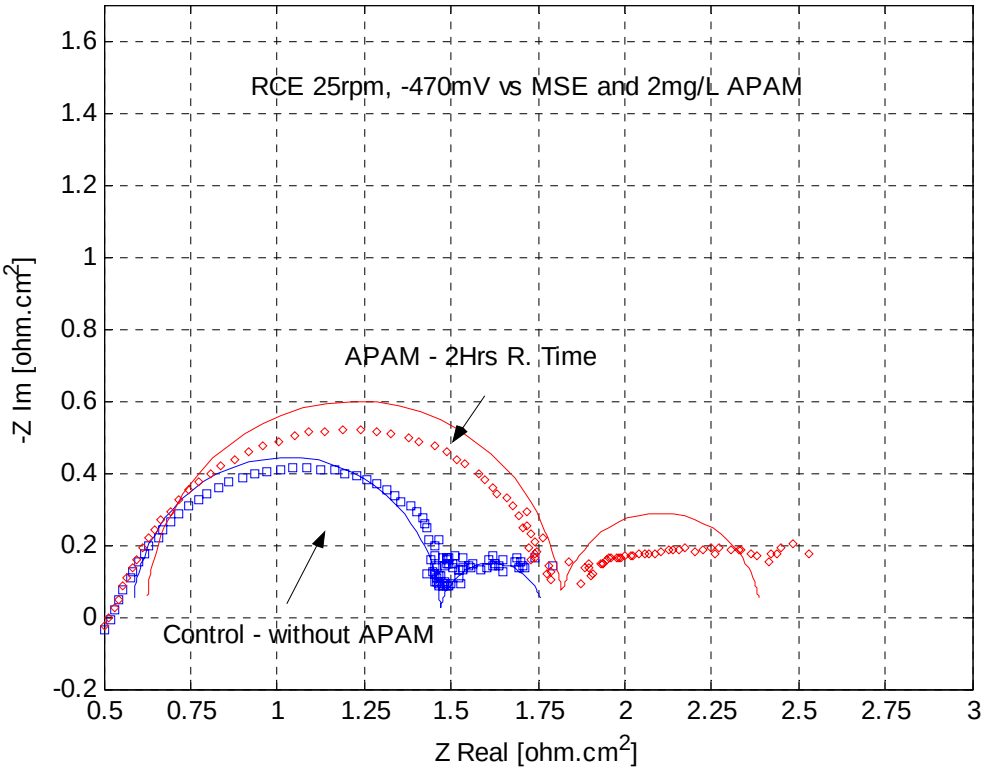

Figure 5-69: Complex-Plane Plot of Experimental and Simulated Impedance Spectra in the Presence and Absence of APAM at -470mV versus MSE and 45°C. Overpotential: 93mV vs. SHE.

Table 5-27 shows the variation of the calculated charge-transfer resistance, double-layer capacitance and current density in the presence and absence of APAM for

periods up to seven hours residence time of APAM in the electrolyte. Table 5-27 also shows that the current density decreased in the presence of APAM. Figures 5-70 and 5-71 depict the effect of time on the value of these parameters. LEVM[28], ZSipmWin™[36] and Voltamaster4[58] give approximately the same parameter values for the high frequency loop. The low frequency loop is more complex and less understood since the fitting process fails to simulate the cylindrical diffusion produced by the rotating cylinder electrode. However the difference between the presence and absence of APAM can be assessed qualitatively in the low frequency loop: APAM also increases diffusion impedance, "the kind of resistance to mass transfer"[1].

Table 5-27: Results for APAM at 45°C and -470mV CD versus MSE

	Charge-Transfer Resistance (P4)		Double-Layer Capacitance (P5)		C. Density
Hours	Ohm.cm^2	Std. Dev.	μF/cm^2	Std. Dev.	mA/cm^2
0(Nil)	0.89	1.43E-02	1.04E-04	3.80E-07	30
0.5	0.96	1.98E-02	1.01E-04	5.23E-07	27
1	1.16	1.47E-02	9.57E-05	3.87E-07	27
2	1.20	1.46E-02	9.57E-05	3.84E-07	25
3	1.20	1.39E-02	8.98E-05	3.64E-07	26
5	1.26	1.41E-02	9.52E-05	3.74E-07	25
6	1.27	1.44E-02	9.37E-05	3.80E-07	25
7	1.31	1.35E-02	9.51E-05	3.56E-07	25

The main elementary phenomena which take place at the electrode interface are the heterogeneous kinetics of the two one-electron steps reactions, mass transport and above all diffusion. It is not clear whether species adsorbed on the surface including APAM are located on macroscopic areas where the reactant species diffuse through the Nernst layer or that the species including APAM are adsorbed on active sites, i.e., the protruding sites.

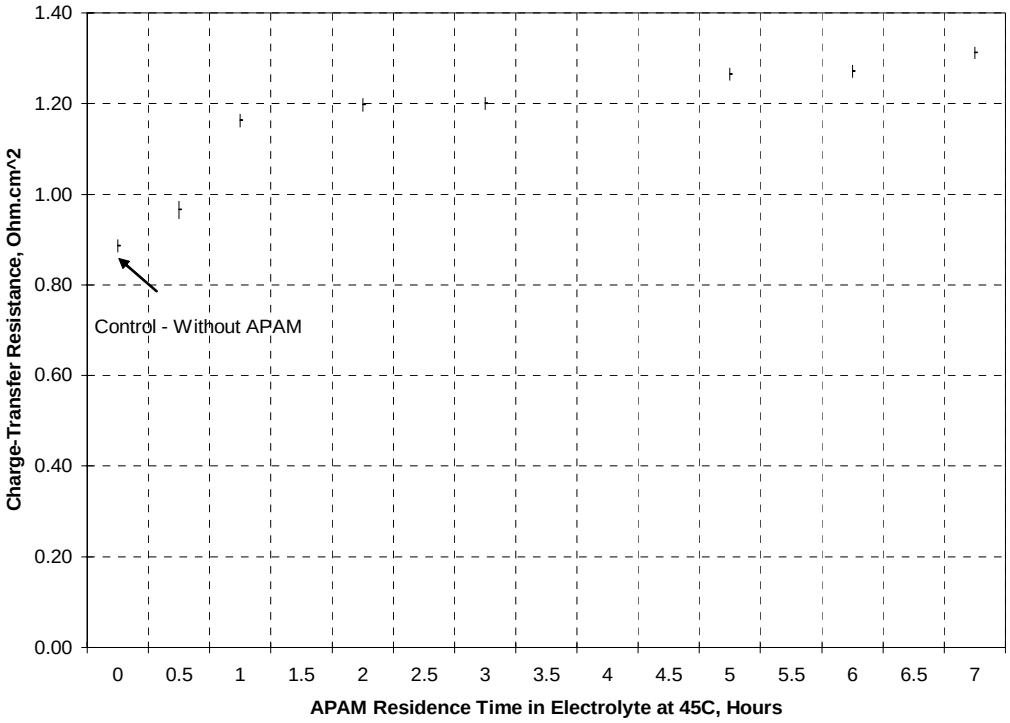

Figure 5-70: Effect of Time on Simulated Charge-Transfer Resistance (P4) in the Presence of APAM at -470mV DC versus MSE at 45°C.

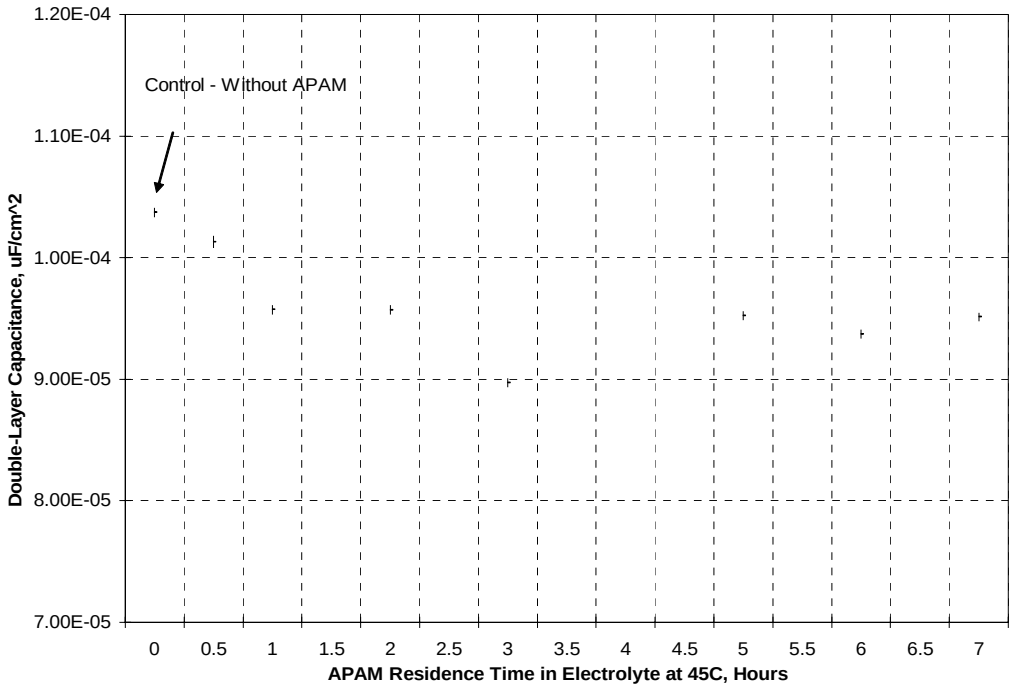

Figure 5-71: Effect of Time on the Simulated Double-Layer Capacitance (P5) in the Presence of APAM at -470mV DC vs. MSE and 45°C

The ageing trend clearly indicates that APAM increased charge-transfer resistance and decreased the double-layer capacitance and that this effect persisted over 7 hours at 45°C. This result is consistent with electrowinning results where 1mg/L APAM was dosed once for 6 and 12 hours at 45°C where smoother deposits were obtained with APAM than with Guar (Chapter 4).

The results presented above with APAM will be compared with similar studies recently published in the literature. These studies often refer to the effect of polyethylene glycol (PEG), an inhibitor/surfactant, on copper deposition for the damascene process. Gabrielli et al.[14] studied the effect of PEG and chloride ions on the deposition of copper using a RDE and obtained about 1.7ohm.cm^2 as the charge-transfer resistance in the high frequency loop at 100rpm, at a current density of 25mA/cm^2 at 25°C using 0.25M $CuSO_4$, 1.8M H_2SO_4 and 60mg/L chloride ions in the absence of PEG. When 300mg/L PEG was added to the system, this charge-transfer resistance decreased from 1.7 to about 1.2ohm.cm^2. These EIS results are inconsistent with Cyclic Voltammetry tests that indicate that PEG polarizes the elecrode[10-12, 24, 59, 60] and hence the reduction of the R_{ct}.

In contrast, Figure 5-68 shows the increase in the charge-transfer resistance in the high frequency loop on addition of 2mg/L APAM. It is widely known that the high frequency loop represents the region of kinetic control[1] and PEG did not show this inhibition/levelling behaviour in this loop. It is thought that EIS tests with PEG at an RDE should also indicate an increase in the charge-transfer resistance in the high frequency loop.

The effect of PEG and APAM on the low frequency loop is similar. The charge-transfer resistance may also be deduced from the low frequency loops (2 loops) as described qualitatively by Gabrielli et al.[14]. Their induction loop[14] is not considered since theoretical studies of two single-electron transfer steps do not include its presence[21]. Gabrielli et al.[14] showed that the charge-transfer resistance increased from about 1.2ohm.cm^2 in the absence of PEG to 2ohm.cm^2 in its presence. This increase of the charge-transfer resistance in the low frequency loops is consistent with the results for APAM described above.

5.8 Electrochemical Impedance Spectroscopy Results in the Presence of Guar at -490mV vs. MSE and 45°C

In this Section, the effect of the ageing process of Guar in the electrolyte at 45°C on the parameter values of the equivalent circuit is presented. Appendix C shows all the experimental data and measurement models for the ageing process of Guar in the electrolyte determined every hour for up to 5hours. Figure 5-72 shows the complex-plane plot after 2-hours residence time of Guar in the electrolyte and in its absence.

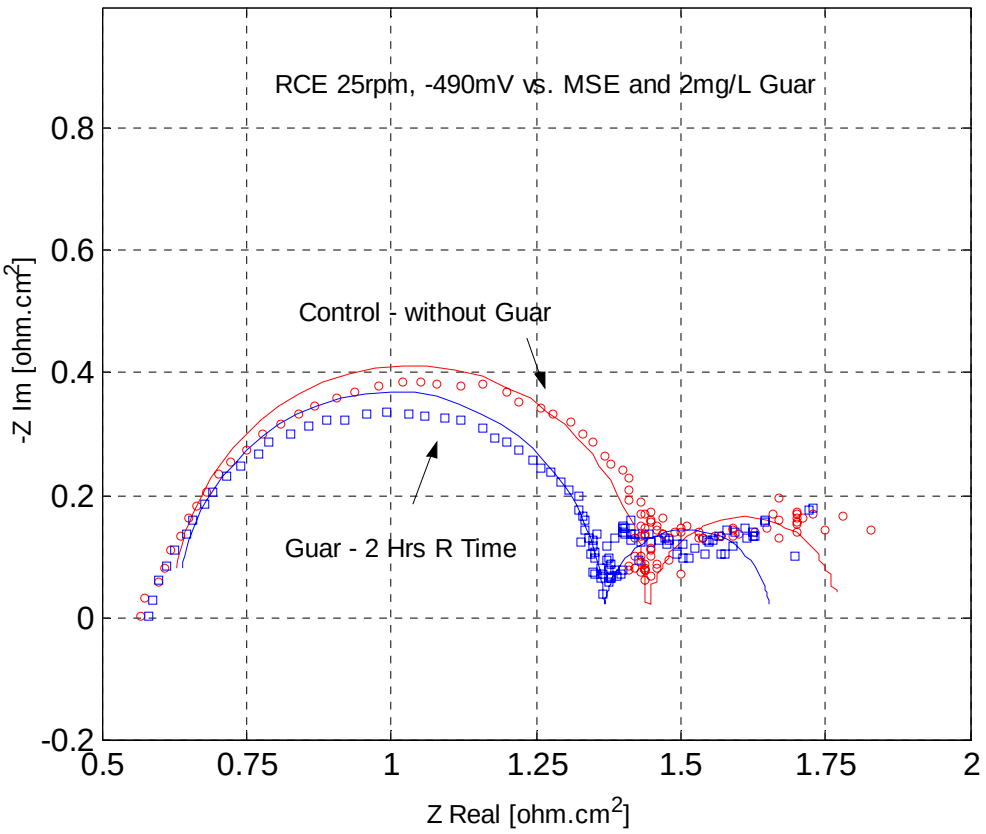

Figure 5-72: Complex-Plane Plot of Experimental and Simulated Impedance Spectra at 45°C in the Presence and Absence of Guar. Overpotential: 113mV vs. SHE

Table 5-28 shows the charge-transfer resistance (P4) and double-layer capacitance (P5) values and their relative standard deviation for the *high frequency loop only* calculated by LEVM[28].

The EIS experiments were measured potentiostatically and therefore the current density varied slightly between tests. Table 5-28 also shows that the current density (34mA/cm^2) obtained in the absence of Guar slightly increased in its presence. The

mechanism for this increase is not understood but it indicates that Guar does not behave as a levelling agent since a levelling agent polarizes the electrode and therefore at constant potential should decrease the current density. This result is consistent with the de-polarization behaviour of Guar observed from Cyclic Voltammetry tests.

Figures 5-73, 5-74 and Table 5-28 summarize the effect of the ageing process of Guar in the electrolyte in terms of its change on charge-transfer resistance and double-layer capacitance over 5-hours.

Table 5-28: Simulation Results for Guar at 45°C and -490 mV DC versus MSE

	Charge-Transfer Resistance (P4)		Double-Layer Capacitance (P5)		C. Density
Hours	Ohm.cm^2	Std. Dev	µF/cm2	Std. Dev.	mA/cm^2
Nil	0.83	0.50E-02	8.93E-05	2.05E-07	34
0.5	0.83	1.59E-02	8.47E-05	4.21E-07	35
1	0.75	1.67E-02	8.59E-05	4.34E-07	39
2	0.74	1.66E-02	8.62E-05	4.35E-07	40
3	0.75	2.03E-02	8.74E-05	5.36E-07	40
4	0.79	1.67E-02	8.79E-05	4.41E-07	38
5	0.79	1.66E-02	8.78E-05	4.38E-07	38

Figure 5-73 shows that the effect of Guar on charge-transfer resistance is relatively small, but a reduction in charge-transfer resistance is apparent after 1-hour. Therefore Guar confers little or no effect on the charge-transfer resistance. The scale used for the charge-transfer resistance shown in Figure 5-73 is the same as used for APAM to allow a direct comparison.

Figure 5-74 shows that Guar reduces the double-layer capacitance. As the residence time increases, this effect becomes progressively less pronounced. The reduction of the double-layer capacitance in the presence of additives is consistent with the literature[61, 62].

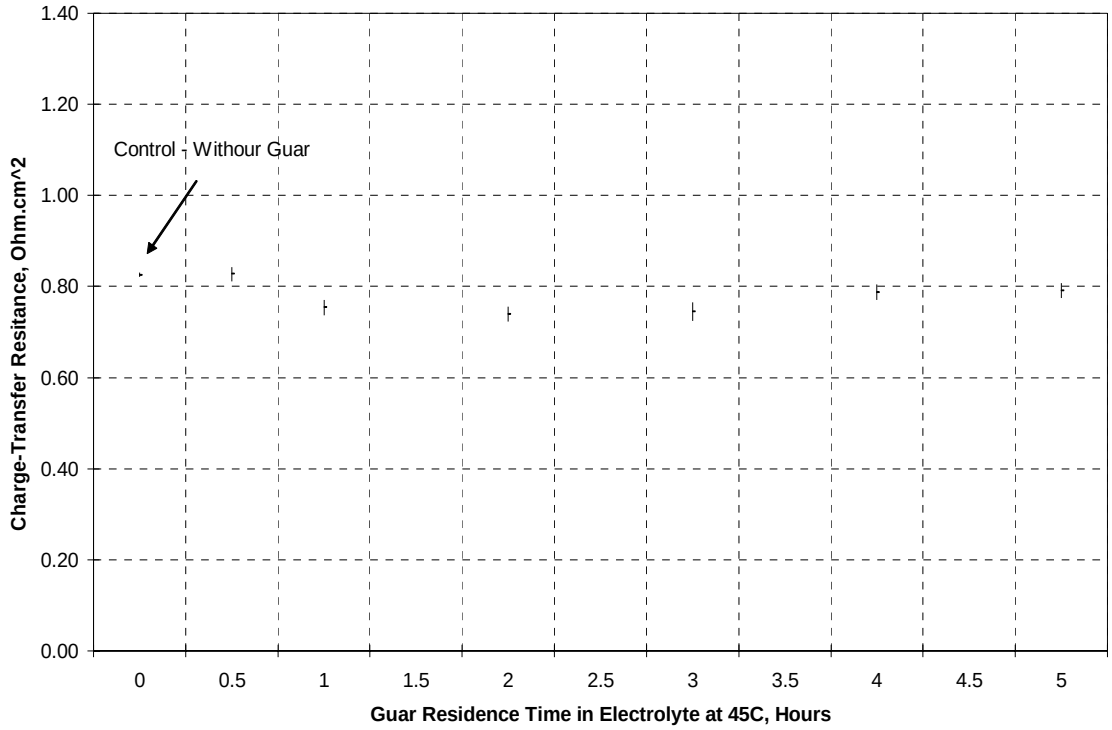

Figure 5-73: Effect of Time on Charge-Transfer Resistance in the Presence of Guar at 45^{o}C

It has been shown from CV tests (Section 5.3) that Guar depolarizes the electrode and from EIS tests it slightly decreases the charge-transfer resistance or polarization resistance. This result will be discussed by comparison with the effect of chloride ions on copper deposition. Sulfate ions, SO_4^{2-} rather than bisulfate ions, HSO_4^- are adsorbed on copper even though the latter is the predominant species in a cupric ion-sulfuric acid electrolyte[63, 64]. However, chloride ions are more strongly adsorbed on the surface of the cathode than sulfate ions causing the reduction of Cu^+ to Cu to become the rate limiting step instead of Cu^{2+} to Cu^{+}[46, 56] and therefore sulfate ions are displaced by chloride ions[63]. Gabrielli et al.[53] in a very recent study also indicated that chloride ion is a depolarizer. It is then concluded from the literature that chloride ions depolarize the electrode.

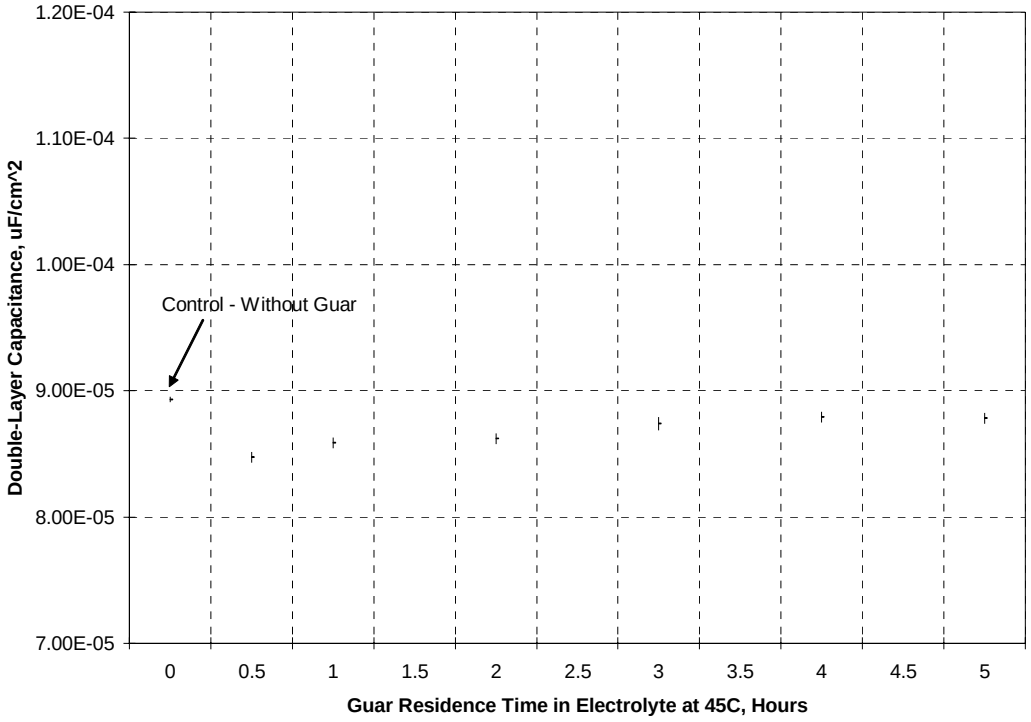

Figure 5-74: Effect of Time on the Double-Layer Capacitance in the Presence of Guar

It was shown in Chapter 4 that Guar increases surface roughness and Ilgar and O'Keefe[65] also have shown that chloride ions also increases surface roughness. It is widely known that the competition between nucleation and growth controls the smoothness of the deposit: the higher the nucleation rate; the finer the crystal size[45]. It can be therefore concluded that the presence of Guar and chloride ions increase the growth rate of copper rather the nucleation rate. In contrast, the form of the growing crystals determines the physical appearance and structure: for a higher growth rate of the crystal size normal to the substrate, a more *fibrous* structure is obtained. It will be shown in Chapter 6 that the cross-section of a copper deposit produced with Guar possesses a porous structure. The experimental Cyclic Voltammetry and EIS results correlate and indicate that Guar further depolarizes the electrode beyond that caused by chloride ions.

5.9 Electrochemical Impedance Spectroscopy Results in the Presence of Activated Polyacrylamide at -490mV vs. MSE and 45°C

These tests were conducted to determine the effect of APAM on the kinetics of copper deposition at potentials more cathodic than -470mV versus MSE (93mV vs.

SHE). This testwork at -490mV vs. MSE was conducted to compare APAM with Guar under the same experimental conditions. Separate EIS testwork was also conducted using a rotating disc electrode (RDE) to determine the behaviour of the charge-transfer resistance in the high frequency loop.

Figure 5-75 shows the complex-plane plot at -490mV versus MSE (113mV vs. SHE) which corresponds to about 34mA/cm^2 with and without APAM using the RCE. The EIS results obtained every hour are shown in Appendix B. Figure 5-75 also shows a constant imaginary impedance component at low frequencies as described in Section 5.7. The gap observed in the low frequency range was attributed to 50Hz mains power noise. Table 5-29 presents the values of the charge-transfer resistance and the double-layer capacitance up to four hours. Figures 6-76 and 6-77 depict the effect of time on the value of these parameters.

Table 5-29: Results for APAM at -490mV CD versus MSE and 45^{o}C

	Charge-Transfer Resistance (P4)		Double-Layer Capacitance (P5)		C. Density
Hours	Ohm.cm^2	Std. Dev.	Hours	μF/cm^2	mA/cm^2
0(Nil)	0.79	1.64E-02	1.046E-04	4.35E-07	34
0.5	0.96	1.98E-02	1.01E-04	5.23E-06	31
1	0.96	1.92E-02	9.78E-05	5.09E-07	30
2	0.99	1.76E-02	9.55E-05	4.66E-07	30
3	1.02	1.62E-02	9.30E-05	4.29E-07	29
4	1.01	1.63E-02	9.29E-05	4.28E-07	29

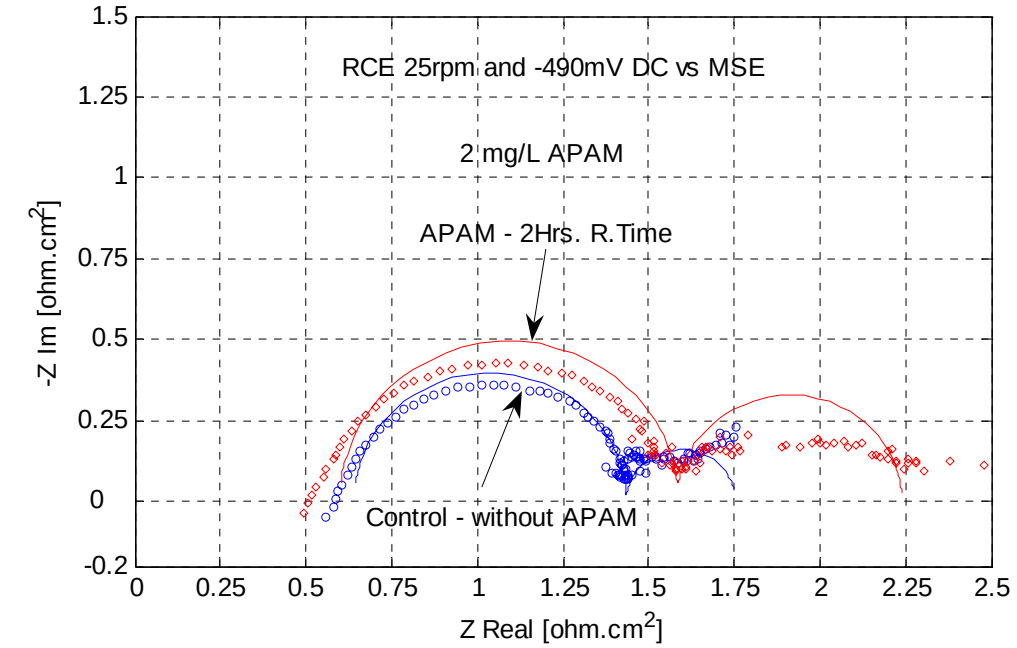

Figure 5-75: Complex-Plane Plot of Experimental and CNLS Simulated Impedance Spectra in the Presence and Absence of APAM at -490mV versus MSE and 45°C. Overpotential: 113 vs. SHE.

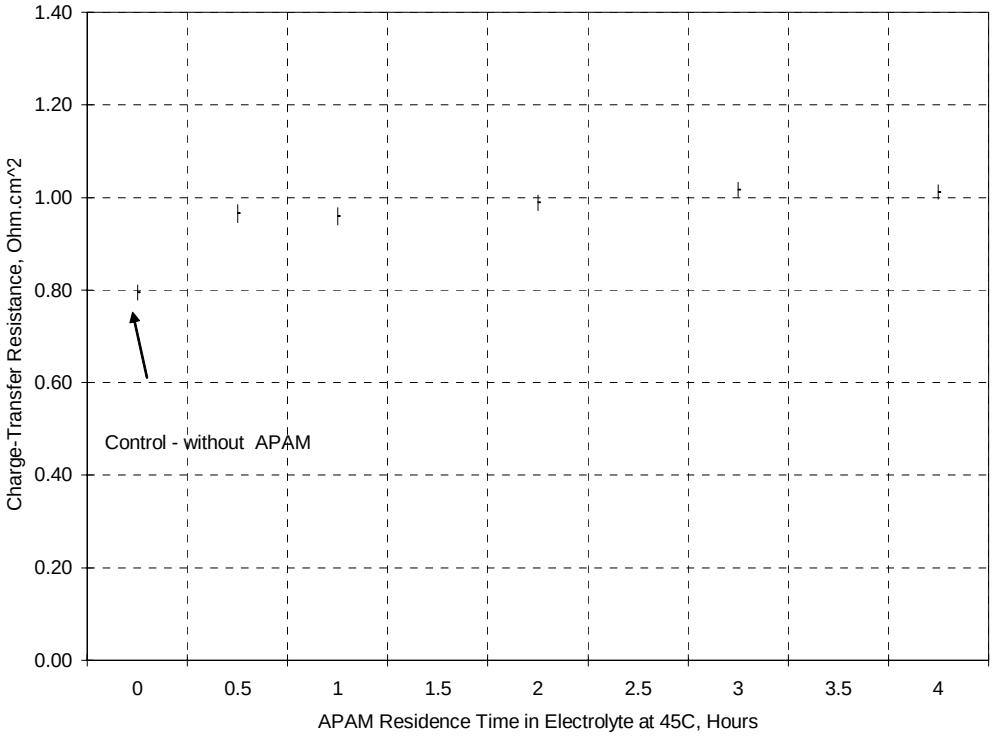

Figure 5-76: Effect of Time on the Simulated Charge-Transfer Resistance in the Presence of APAM at -490mV DC versus MSE and 45°C.

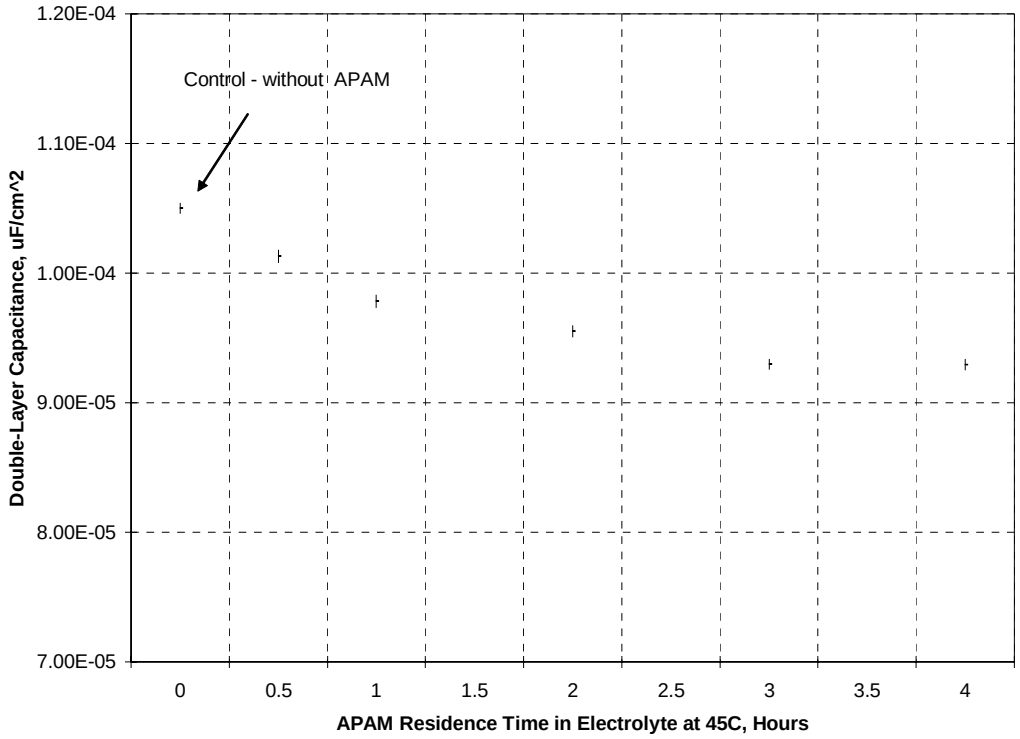

Figure 5-77: Simulated Double-Layer Capacitance versus Time in the Presence of APAM at -490mV DC versus MSE and 45^{o}C.

The increase in the charge-transfer resistance in the high frequency range is possibly due to the ageing process of APAM in the cupric ion-sulfuric acid electrolyte at 45^{o}C through additional hydrolysis of the block copolymer backbone and reduction of its molecular weight. Figure 5-77 indicates also that the double-layer capacitance steadily decreases up to 3 hours then it levels off at about 4 hours. This trend was also observed at -470mV vs. MSE overpotential where tests where conducted up to 7 hours and fully described in Section 5-7.

Figure 5-78 compares the complex-plane plots for 2-hours aged APAM and 2-hours aged Guar, and Nil additives at -490 mV vs. MSE at 45^{o}C using the RCE. It can be seen that the charge-transfer resistance is greatest in the presence of APAM and least in the presence of Guar.

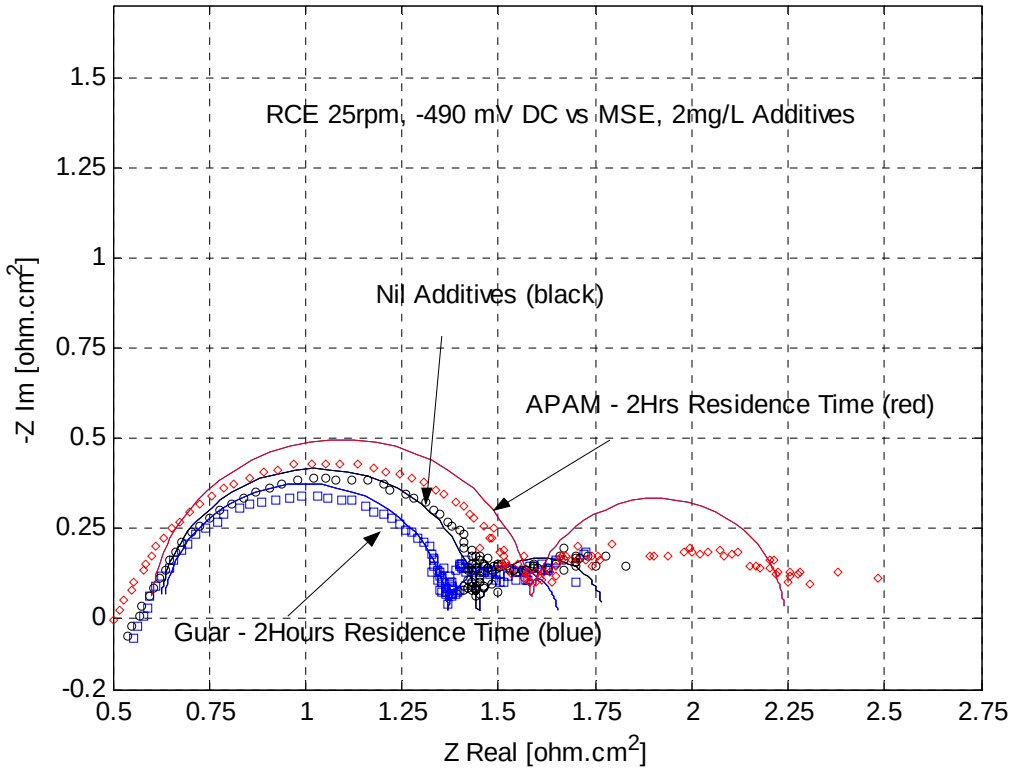

Figure 5-78: Comparison of Complex-Plane Plot of Experimental and Simulated Impedance Spectra in the Presence of both APAM and Guar at -490mV DC and at 45°C.
Legend: Black – 340A/m^2 CD in the Absence of APAM and Guar. APAM (red dots and line) increases the charge-transfer resistance and Guar (blue dots and line) decreases the charge-transfer resistance.

A short set of EIS experiments were undertaken on an RDE to compare with the results on a RCE. The rationale for doing this was the fact that no published EIS data have been collected on both electrodes.

Figure 5-79 shows the EIS results using the rotating disc electrode (RDE). The EIS testwork with the RDE started at 50kHz as in the experiments conducted by Kelly et al.[8] and with the RCE at 30kHz.

Figure 5-79 shows the ageing of APAM in the electrolyte also increases the charge-transfer resistance in the high frequency loop up to six hours. The other important findings from Figure 5-79 are: (i) the electrolyte resistance, Rs, is constant with and without the presence of APAM and (ii) The Rs value with the RDE is about one-half of that obtained with the RCE (Figure 5-76). The reasons for this difference are unclear but the electrolyte/electrode interface must be at steady-state during the

presence and absence of additive. Therefore, a difference can be expected in the presence and presence of additives due to inhibition (surface coverage). However, there is a clear difference for the RDE with APAM at 45°C and with PEG at 25°C. The presence of PEG at 25°C reduced the charge-transfer resistance as discussed in Section 5.7 but the presence of APAM at 45°C increased the charge-transfer resistance at the RDE and RCE.

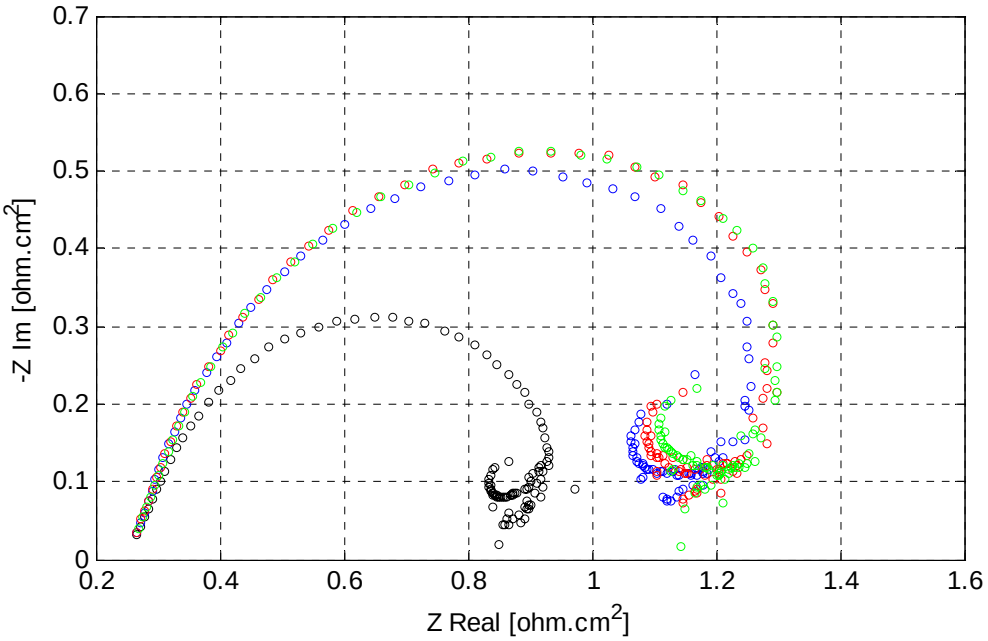

Figure 5-79: Complex-Plane Plot using RDE at -490mV vs. MSE, 25rpm and 45°C (50^3Hz-0.2Hz).
Legend: Black – Control without APAM, Blue – 1 Hrs, Red – 3Hrs. and Green – 6Hrs.

The EIS response presented in Figure 5-79 cannot be simulated using the equivalent circuit presented in Figure 5-56 possibly due to convection and low stirring affecting the diffusion in the low frequency range. Moreover, the non-uniform current distribution inherent to the RDE may also influence the formation of the inductive type EIS data in the low frequency loop. The Ohmic resistance in solution determines the primary current distribution, which then becomes a unique function of cell geometry[38]. It has been also observed in Sections 5.4 and 5.5 that the electrode kinetics of copper electrodeposition is faster on pre-plated copper than on bare stainless steel. Therefore, the problem of the non-uniform primary current distribution inherent to the RDE may have become more serious due to the faster reaction, large current density and large disc ($0.178cm^2$)[38]. In contrast, the motivation to use the RCE was to achieve a uniform

metal distribution during the electrodeposition process. Nevertheless, it has been shown that APAM increased the charge-transfer resistance in the high frequency loop whether RCE or RDE was used.

5.10 Electrochemical Impedance Spectroscopy Results in the Presence of Activated Polyacrylamide at -445mV vs. MSE at 65°C

These EIS tests were run using RCE and RDE at 65°C, the copper electrorefining electrolyte temperature. The RCE was used for nil APAM and at 0.5, 2 and 5hours APAM residence time in the electrolyte. The RDE was used for nil APAM and at 1, 3 and 6hours APAM residence time in the electrolyte. The speed of rotation of both electrodes were 25rpm. These runs were carried out by simply replacing the RCE shown in Figure 5-59 by an RDE of the same height. Figure 5-80 shows the complex-plane plot at -445mV vs. SME which corresponds to about 50mA/cm^2 in the absence of APAM at 65°C for the RCE. The EIS spectra obtained for 0.5 and 5 hours are also presented in Appendix B.

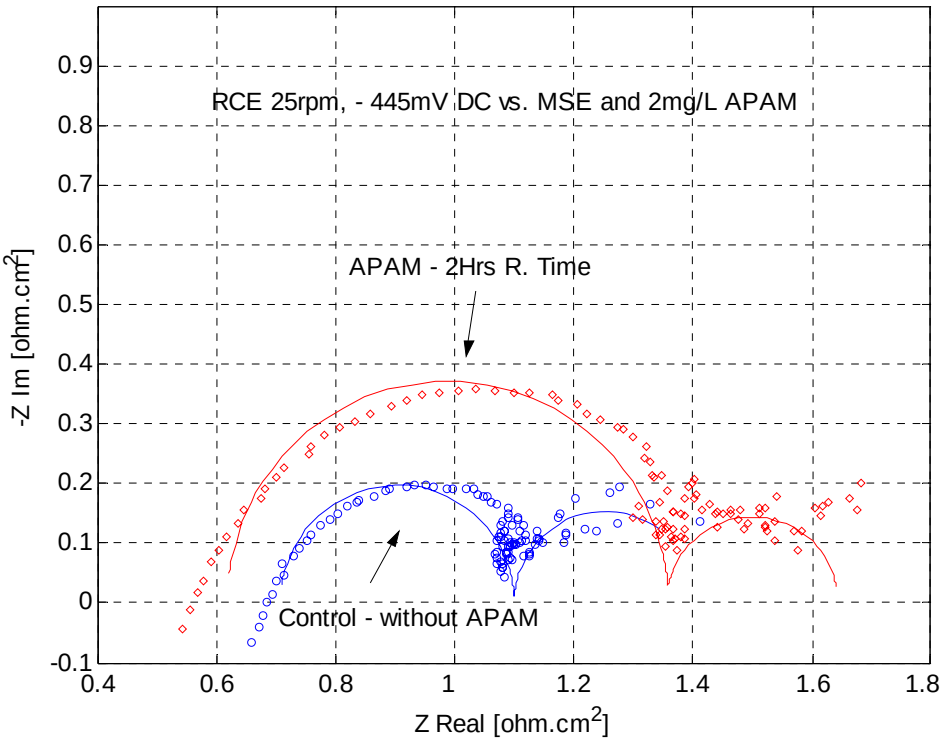

Figure 5-80: Complex-Plane Plot of Experimental and CNLS Simulated Impedance Spectra in the Presence and Absence of APAM at -445mV versus MSE and 65°C. Overpotential: 90mV vs. SHE.

Figure 5-80 clearly shows that the presence of APAM at 2-hours residence time in the electrolyte increases the charge-transfer resistance in the high frequency loop as also found in Sections 5.7 and 5.9. Table 5-30 presents the charge-transfer resistance and double-layer capacitance for this testwork. Figures 5-81 and 5-82 depict the data presented in Table 5-30.

Table 5-30: Results for APAM at 65°C and -445mV CD versus MSE

	Charge-Transfer Resistance (P4)		Double-Layer Capacitance (P5)		C. Density
Hours	Ohm.cm^2	Std. Dev.	μF/cm^2	Std. Dev.	mA/cm^2
Nil APAM	0.39	2.91E-02	1.84E-04	7.76E-06	50
0.5	0.73	2.08E-02	1.16E-04	5.53E-06	34
2	0.74	2.02E-02	1.13E-04	5.32E-06	33
5	0.69	2.12E-02	1.16E-04	5.60E-06	34

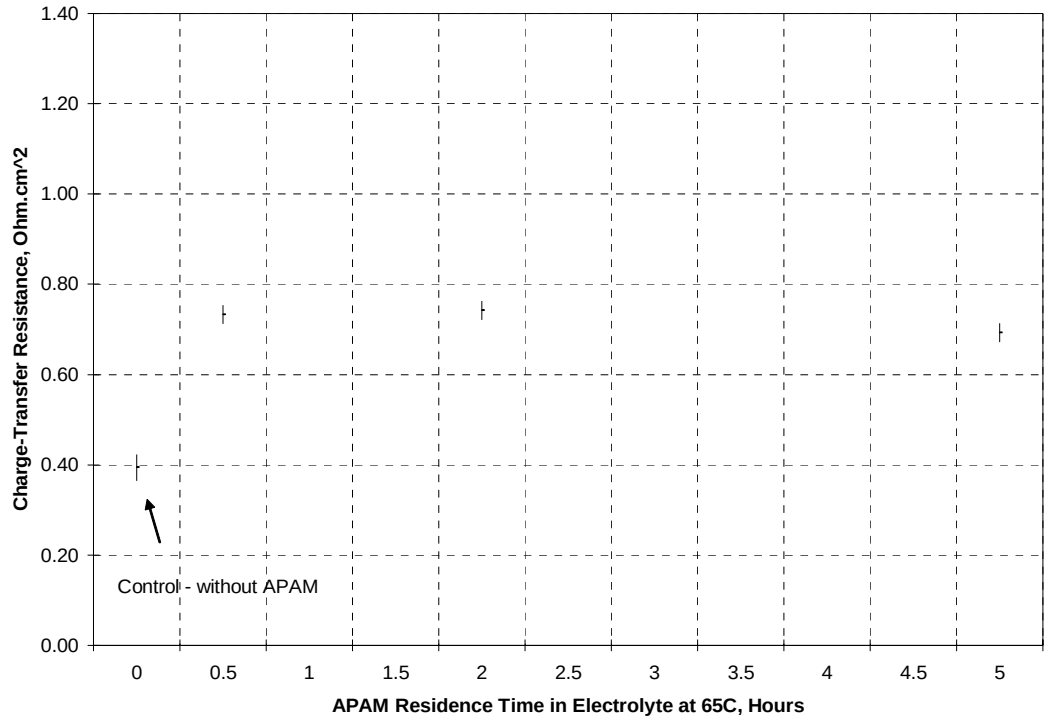

Figure 5-81: Effect of Time on the Simulated Charge-Transfer Resistance (P4) in the Presence of 2mg/L APAM at 65°C and -445mV DC vs. MSE

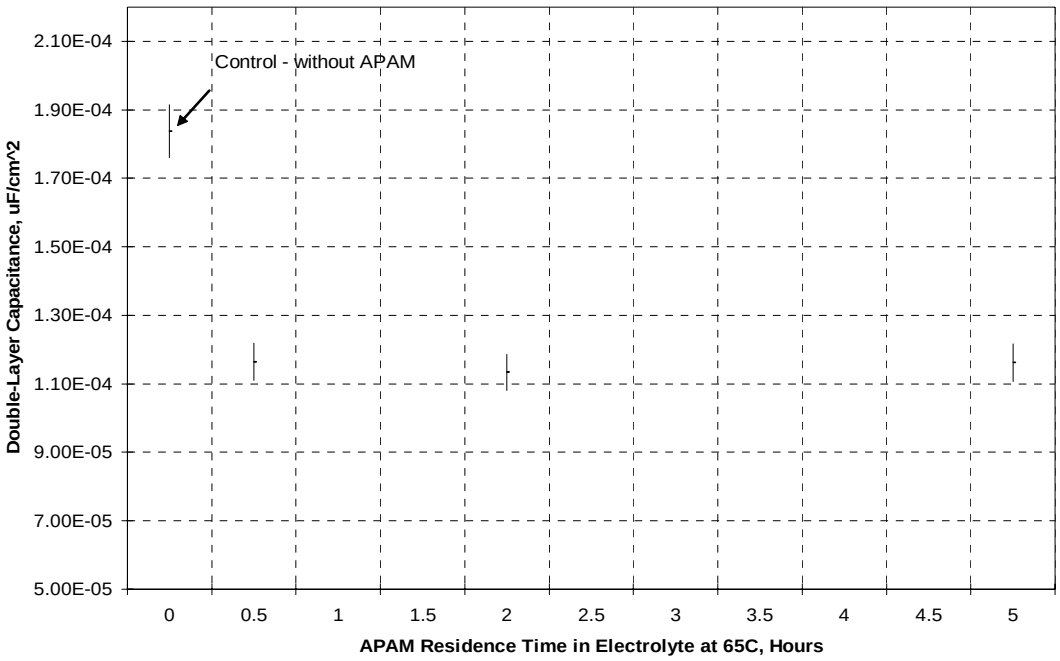

Figure 5-82: Effect of Time of the Simulated Double-Layer Capacitance (P5) in the Presence of 2mg/L APAM at 65°C and -445mV DC vs. MSE.

The noise in the low frequency loop is not clearly understood. It may be due to non-steady state conditions of the electrochemical crystal growth process and surface topography[45] and to the fluid flow of the system. Different impedance features can be observed on single crystals with and without screw dislocations[45]. It will be recalled (Sections 3.2.3 and 3.2.4) that at Reynolds number of approximately 200, a transition from laminar to laminar with vortexes occurs. Accordingly, since Reynolds number increases from 204 at 45°C to 293 at 65°C, a significant change in the fluid flow is likely which may account for the increased noise at 65°C due to the unstable and superimposed Taylor vortices.

Figure 5-83 shows the EIS results using the rotating disc electrode (RDE). It can be seen than the ageing of APAM in the electrolyte occurs more rapidly and increased the charge-transfer resistance in the high frequency loop from the first hour to 3-4hours and then decreases at 6-hours residence time. This trend of APAM was also observed from the CV results at 65°C, Figure 5-65 and the EIS results using the RCE at 65°C, Figure 5-81. However, these curves also cannot be simulated using the equivalent circuit presented in Figure 5-56. However, Figure 5-83 shows that APAM

increases the charge-transfer resistance in the high frequency loop whether RCE or RDE is used at 45°C and 65°C and the electrolyte resistance, Rs is constant with and without APAM.

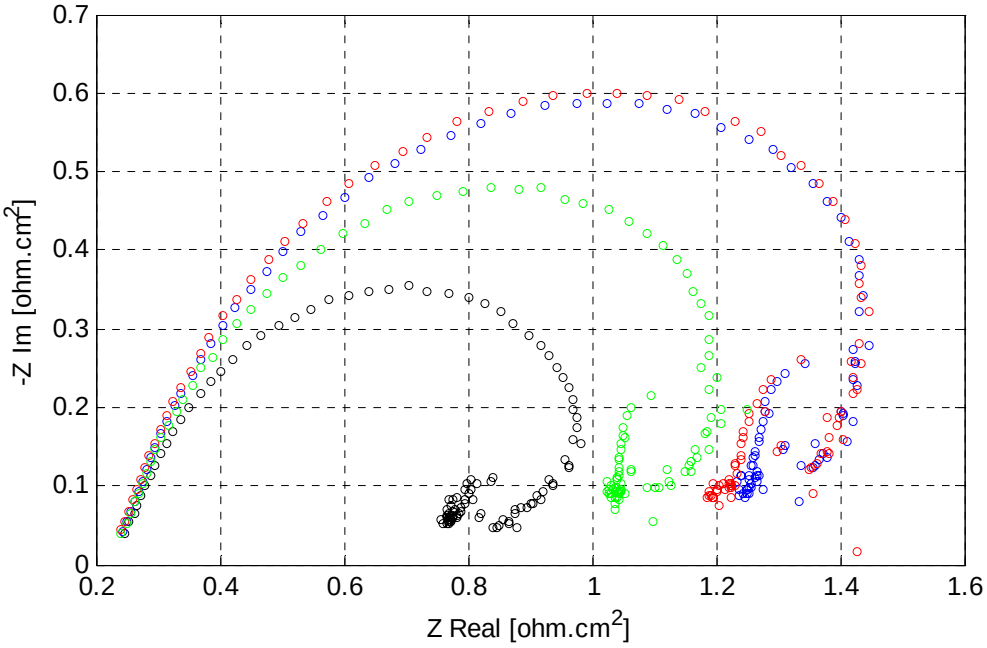

Figure 5-83: Complex-Plane Plot using RDE at -445mV vs. MSE, 25 rpm and 65°C (50^3 Hz-0.2Hz).
Black – Control without APAM, Blue – 1 Hrs, Red – 3Hrs. and Green – 6Hrs.

5.11 Discussion and Conclusions

It was seen by Cyclic Voltammetry that Guar de-polarized the electrode on both stainless steel and pre-plated-copper (Section 6-3). It was also seen that there was a trend in depolarization behaviour as measured by Cyclic Voltammetry. It increases from 0.3-1hour to a maximum at 2-3hours and then its depolarizing activity decayed such that within 4-5hours an insignificant effect was observed on pre-plated copper. The transfer coefficient value of 0.50 in the absence of Guar agrees with that given by Wu and Barkey[46] and Mattson and Bockris[47]. The charge-transfer resistance determined by EIS for Guar also follows the overall trend of the *depolarization* behaviour of Guar from Cyclic Voltammetry tests.

In contrast, cyclic voltammetry tests indicate that APAM *polarizes* the electrode. The maximum polarization at 45°C and 65°C was approximately 14mV but the time to attain this maximum value was about 3.5 hours at 45°C and 1.5 hours at 65°C as shown in Figure 5-66. These results correlate with the fractional factorial experimental results in which it was demonstrated that APAM had a more significant effect on reducing surface roughness at 65°C than at 45°C (See Chapter 4). These results indicate that APAM at 45°C requires about 3.5 hours ageing to produce the smoothest deposit while at 65°C it requires about 1hour.

APAM also appeared to confer higher adsorption on pre-plated copper than on stainless steel since the net polarization values are higher for pre-plated copper than for stainless steel at 45° and 65°C. These results are consistent with both APAM acting as a surfactant/levelling agent and doing so for extended periods of time, which is consistent with the results described in Chapter 3 where APAM was dosed once for 6 hours electrowinning time.

The complex-plane plots presented in this thesis using a RCE agree with the theoretical work for single-electron step reactions requiring only the presence of resistors and capacitors in the equivalent circuit[21]. It also agrees with experimental work in the published literature[8, 14, 17, 51-53] where RDEs were used in terms of the electrolyte resistance and the charge-transfer resistance, Rct, in the high frequency loop. However, measurement modelling or regression analysis were absent from the above published literature, except from the work of Fabricius et al.[17]and Chassaing et al.[52]. It has been recently stated that the inherent non-uniform primary current distribution of the rotating disc electrode precludes measurement modelling[40]. In contrast, the uniform current distribution produced by the RCE is widely documented[38].

The low frequency loop is more complex and less understood in terms of the number and nature of the parameter values. It depends on the surface preparation of the substrate, growth mode[55] of the deposit including its crystallographic orientation, hydrodynamic conditions and current density[56]. The cylindrical diffusion produced by the rotating cylinder electrode results in the relatively constant imaginary impedance component[3, 41]. Comparison of Figures 5-69 (-470mV vs. MSE, 30mA/cm^2 and 45°C), 5-75 (-490mV, 34mA/cm^2, 45°C) and 5-80 (-445mV, 50mA/cm^2, 65°C) show that the

noise level in the low frequency loop increases as the current density increases. This indicates that the RCE is highly sensitive to surface roughness in the low frequency range. It is known that the roughness of an electrode may lead to a frequency dispersion of the interfacial impedance[4] and the lines of electric force do not converge evenly on the surface. The double layer will therefore be charged unevenly[4]. This behaviour was more apparent in the presence and absence of Guar than in the presence of APAM.

Table 5-31 summarizes the maximum change in the charge-transfer resistance and double-layer capacitance produced by APAM and Guar at 45°C and 65°C. APAM increased the charge-transfer resistance throughout the testwork while Guar reduced it. APAM reduced the double-layer capacitance more than Guar at 45°C. This reduction of the double-layer capacitance increased when the temperature was increased from 45°C to 65°C. These results indicate that *APAM is more specifically* adsorbed than Guar.

Table 5-31: Maximum Change in Charge-Transfer Resistance and Double-Layer Capacitance Relative to the Presence and Absence of Guar and APAM

Additive	mV vs. MSE	Max. Change in C-T Resistance, R_{ct}, ohm.cm^2	Max. Change in D-L Capacitance, x 10^{-5}, C_{dl}, µF/cm^2	Guar/APAM Residence Time in Electrolyte, Hrs.*
Guar	-490mV and 45°C	-0.086	-0.46	2-3
APAM	-470 mV and 45°C	+0.42	-1.2	3-5
APAM	-490mV and 45°C	+0.23	-1.2	3-5
APAM	-445mV and 65°C	+0.34	-6.8	2

*Maximum change determined at these residence times.

It was also shown that the effect of temperature on the ageing sequence is consistent with reaction kinetics for polyacrylamide hydrolysis and cleavage, i.e., it is faster at 65°C than at 45°C as would be expected. The EIS data at 65°C and 45°C are consistent with the CV data whether the RCE or RDE was used but the EIS data with the RDE was not amenable to be modelled using the equivalent circuit presented in Figure 5-56.

The CV results at 45°C area consistent with the EIS results at 45°C in that Guar depolarizes the electrode or decreases the charge-transfer resistance. In other terms Guar increases the rate of growth rather than the rate of nucleation. In contrast, APAM polarizes the electrode or increases the charge-transfer resistence, promotes nucleation

rate rather than growth rate. These results for APAM were replicated at 65^{o}C. Overall electrowinning tests, crystallite size measurements, Cyclic Voltammetry and Electrochemical Impedance Spectroscopy indicated that Guar depolarises the electrode and, in contrast, APAM polarizes the electrode. Therefore, APAM behaves as a true levelling agent and does so for extended periods of time, which is consistent with the results described in Chapter 3 where APAM was dosed 1mg/L once for 6 hours electrowinning time.

5.12 References

1. Bard AJ, Faulkner L. *Electrochemical Methods, Fundamentals and Applications*. Second ed. Brisbane: John Wiley & Sons, Inc.; 2001.

2. Calvo EJ. The Current-Potential Relationship. In: Bard AJ, Stratmann M, editors. *Encyclopedia of Electrochemistry, Volume 2: Interfacial Kinetics and Mass Transport*: Wiley-VCH; 2003. p. 3-30.

3. Lasia A. Electrochemical Impedance Spectroscopy and Its Applications. In: Conway B, Bockris J, White R, editors. *Modern Aspects of Electrochemistry*: Kluwer Academic / Plenum; 1999. p. 143-245.

4. Macdonald JR, editor. *Impedance Spectroscopy Emphasizing Solid Materials and Systems*. Brisbane: John Wiley & Sons; 1987.

5. Conway B, Bockris J, White R, editors. *Electrochemical Impedance Spectroscopy and Its Applications in Modern Aspects of Electrochemistry*: Kluwer Academic / Plenum; 1999.

6. Macdonald D. *Transient Techniques in Electrochemistry*: Plenum Press; 1977.

7. Grafov BM, Damaskin BB. *Theory of Electrochemical Faradaic Impedance for Mixed Electrolyte Solutions*. Electrochimica Acta 1996;41(17):2707-2714.

8. Kelly J. Copper Deposition in the Presence of Mixed Surfactants [PhD]: Columbia University; 1999.

9. Bonou L, Eyraud M, Denoyel R, Massiani Y. *Influence of Additives on Cu Electrodeposition Mechanisms in Acid Solution: Direct Current Study*

Supported by Non-Electrochemical Measurements. Electrochimica Acta 2002;47(26):4139-4148.

10. Moffat T, Bonevich J, Huber W, Stanishevsky A, Kelly D, Stafford G, Josell D. *Superconformal Electrodeposition of Copper in 500-90 Nm Features*. J. Electrochem. Soc. 2000;147(12):4524-4535.

11. Moffat TP, Wheeler D, Josell D. *Electrodeposition of Copper in the Sps-Peg-Cl Additive System*. Journal of the Electrochemical Society 2004;151(4):C262-C271.

12. Moffat T, Baker B, Wheeler D, Josell D. *Accelerator Aging Effects During Copper Electrodeposition*. Electrochemical and Solid-State Letters 2003;6(4):C59-C62.

13. Feng ZV, Li X, Gewirth A. *Inhibition Due to the Interaction of Polyethylene Glycol , Chloride and Copper in Plating Baths: A Surface-Enhanced Raman Study*. J. Phys. Chem. B 2003;107:9415-9423.

14. Gabrielli C, Kittel J, Mocoteguy P, Perrot H, Zdunek A, Bouard P, Haddix M, Doyen L, Clech MC. *A Model of Copper Deposition for the Damascene Process*. Proceedings - Electrochemical Society 2003;2003-13(Thin Film Materials, Processes, and Reliability):100-109.

15. Vereecken PM, Binstead RA, Deligianni H, Andricacos PC. *The Chemistry of Additives in Damascene Copper Plating*. IBM Journal of Research and Development 2005;49(1):3-19.

16. Fabricius G, Sundholm G. *The Effect of Additives on the Electrodeposition of Copper Studied by the Impedance Technique*. Journal of Applied Electrochemistry 1984;14:797-801.

17. Fabricius G. The Electrochemistry of Copper in Sulfuric Acid in the Presence of Additives [Doctor of Technology Thesis]. Espoo: Helsinki University of Technology; 1995.

18. Onicio L, Muresan L. *Some Fundamental Aspects of Levelling and Brightening in Metal Electrodeposition*. Journal of Applied Electrochemistry 1991;21:565-574.

19. Jordan K, Tobias C. *The Effect of Inhibitor Transport on Leveling in Electrodeposition*. J. Electrochem. Soc. 1991;138(5):1251-1259.

20. Chung D. Localized Adsorption of Organic Additives During Copper Electrodeposition [Ph.D.]. Urbana-Champaign: University of Illinois; 1996.

21. Harrington DA, van den Driessche P. *Equivalent Circuits for Some Surface Electrochemical Mechanisms*. Journal of Electroanalytical Chemistry 2004;567(2):153-166.

22. Franceschetti DR, Macdonald JR. *Diffusion of Neutral and Charged Species under Small-Signal A.C. Conditions*. J. Electroanal. Chem. 1979;101:307-316.

23. Mansfeld F, Shih H, Greene H, Tsai C. Analysis of Eis Data for Common Corrosion Processes. In: Scully JR, Silverman DC, Kending MW, editors. *Electrochemical Impedance: Analysis and Interpretation*; 1993; 1993. p. 37-53.

24. Jovic VD, Jovic BM. *Copper Electrodepositon from Copper Acid Baths in the Presence of Polyethylene Glycol and Sodium Chloride*. J. Serb. Chem. Soc. 2001;66(11-12):935-952.

25. Nava de Oca J, Sosa E, Ponce de Leon C, Oropeza M. *Effectiveness Factors in an Electrochemical Reactor with Rotating Cylinder Electrode for the Acid-Cupric/Copper Cathode Interface Process*. Chemical Engineering Science 2001;56(8):2695-2702.

26. Diard JP, Montella C. *Diffusion-Trapping Impedance under Restricted Linear Diffusion Conditions*. Journal of Electroanalytical Chemistry 2003;557:19-36.

27. Brett CMA, Brett AMO. *Electrochemistry, Principles, Methods and Applications*. New York; 1993.

28. Macdonald J. Levm Manual - Complex Nonlinear Least Squares (Cnls). In. 8.0 ed; 2003.

29. Gabrielli C. Electrochemcial Impedance Spectroscopy: Principles, Instrumentation and Applications. In: Rubinstein I, editor. *Physical Electrochemistry*. New York: Marcel Dekker, Inc; 1995. p. 243-292.

30. Madore C, Agarwal P, Landolt D. *Blocking Inhibitors in Cathodic Leveling Iii. Electrochemical Impedance Spectroscopy Study*. J. Electrochem. Soc. 1998;145(5):1561-1565.

31. Agarwal P, Orazem ME, Garcia-Rubio L. *Measurement Models for Electrochemical Impedance Spectroscopy I. Demonstration and Applicability*. J. Electrochem. Soc. 1992;139(7):1917-1927.

32. Agarwal P, Moghissi O, Orazem M, Garcia-Rubio L. *Application of Measurement Models for Analysis of Impedance Spectra*. Corrosion 1993;49(4):278-89.

33. Agarwal P, Orazem ME, Garcia-Rubio LH. *Application of Measurement Models to Impedance Spectroscopy. Iii. Evaluation of Consistency with the Kramers-Kronig Relations*. Journal of the Electrochemical Society 1995;142(12):4159-68.

34. Orazem ME, Wojcik PT, Durbha M, Frateur I, Garcia-Rubio LH. *Application of Measurement Models for Interpretation of Impedance Spectra for Corrosion*. Materials Science Forum 1998;289-292(Pt. 2):813-828.

35. Boukamp BA. *A Package for Impedance/Admittance Data Analysis*. Solid State Ionics 1986;18-19(1):136-40.

36. Princeton-Applied-Research. Zsimpwin Electrochemical Spectroscopy Analysis Software V3.1. In; 2003.

37. Orazem ME, Agarwal P, Jansen AN, Wojcik PT, Garcia-Rubio LH. *Development of Physico-Chemical Models for Electrochemical Impedance Spectroscopy*. Electrochimica Acta 1993;38(14):1903-11.

38. Newman J, Thomas-Alyea KE. *Electrochemical Systems*. Third ed. Hoboken, New Jersey: John Wiley & Sons, Inc.; 2004.

39. Durbha M, Orazem ME, Tribollet B. *A Mathematical Model for the Radially Dependent Impedance of a Rotating Disk Electrode*. J. Electrochem. Soc. 1999;146(6):2199-2208.

40. Shukla PV, Orazem ME. *Hydrodynamics and Mass-Transfer-Limited Current Distribution for a Submerged Stationary Hemispherical Electrode under Jet Impingement*. Electrochimica Acta 2004;49:2901-2908.

41. Jacobsen T, West K. *Diffusion Impedance in Planar, Cylindrical and Spherical Symmetry*. Electrochimica Acta 1995;40(2):255-262.

42. Filzwieser A, Hein K, Hanko G. Application of Two Phase Hydrodynamic Modeling to an Electrowinning Cell. In: Dutrizac JE, Ji J, Ramachandran V, editors. *Copper 99 - Cobre 99 International Conference*; 1999: The Minerals, Metals & Materials Society; 1999.

43. Gabe D. *Rotating Electrodes for Use in Electrodeposition Process Control*. Plating & Surface Finishing 1995;9:69-76.

44. Schlichting H. *Boundary-Layer Theory*. Sydney: McGraw-Hill; 1968.

45. Budevski E, Staikov G, Lorenz W. *Electrochemical Phase Formation and Growth, an Introduction to the Initial Stages of Metal Deposition*. New York: VCH; 1996.

46. Wu Q, Barkey D. *Faceting and Roughening Transitions on Copper Single Crystals in Acid Sulfate Plating Baths with Chloride*. Journal of the Electrochemical Society 2000 Mar;147(3):1038-1045.

47. Mattsson E, Bockris JOM. *Galvanostatic Studies of the Kinetics of Deposition and Dissolution in the Copper+Copper Sulphate System*. Transaction Faraday Soc. 1959;55:1586-1601.

48. Vereecken J, Winand R. *Influence of Polyacrylamides on the Quality of Copper Deposits from Acidic Copper Sulphate Solutions*. Surface Technology 1976; 4:227-235.

49. Robinson T, Davenport WG, Quinn J, Karkas G. Electrolytic Copper Refining - 2003 World Tankhouse Operating Data. In: Dutrizac JE, Clement CG, editors. *Copper 2003 - Cobre 2003*; 2003; Santiago, Chile: Canadian Institute of Mining, Metallurgy and Petroleum; 2003. p. 3-66.

50. Grchev T, Cvetkovska M, Stafilov T, Schultze J. *Adsorption of Polyacrylamide on Gold and Iron from Acidic Aqueous Solutions*. Electrochimica Acta 1991;36(8):1315-1323.

51. Reid J, David A. *Effects of Polyethylene Glycol on the Electrochemical Characteristics of Copper Cathodes in an Acid Copper Medium*. Plating & Surface Finishing 1987;74(1):66-70.

52. Chassaing E. *Effect of Organic Additives on the Electrocrystallization and the Magnetoresistance of Cu-Co Multilayers*. Journal of the Electrochemical Society 2001;148(10):C690-C694.

53. Gabrielli C, Mocoteguy P, Perrot H, Wiart R. *Mechanism of Copper Deposition in a Sulfate Bath Containing Chlorides*. Journal of Electroanalytical Chemistry 2004;572(2):367-375.

54. Mandin P, Fabian C, Lincot D, Ridd M. *In Preparation*.

55. Gabrielli C, Mocoteguy P, Perrot H, Zdunek A, Bouard P, Haddix M. *Electrochemical Impedance Spectroscopy Investigation of Bath Ageing in Damascene Process Chemistries*. Electrochemical & Solid-State Letters 2004;7(3):C31-C34.

56. Chassaing E, Wiart R. *Epitaxial Growth and Electrode Impedance of Copper Electrodeposits*. Electrochimica Acta 1984;29(5):649-660.

57. Radeva T, Petkanchin I. *Electro-Optic Study of Oxide Particles in Hydrolyzed Polyacrylamide Solutions*. Journal of Colloid and Interface Science 1995;182:1-5.

58. Radiometer-Analytical. Voltamaster 4.0. In; 2003.

59. Kelly J, Tian C, West A. *Leveling and Microstructural Effects of Additives for Copper Electrodeposition*. Journal of the Electrochemical Society 1999;146(7):2540-2545.

60. Moffat T, Wheeler D, Huber W, Josell D. *Superconformal Electrodeposition of Copper*. Electrochemical & Solid-State Letters 2001;4(4):C26-C29.

61. Tsai W-C, Wan C-C, Wang Y-Y. *Pulsed Current and Potential Response of Acid Copper System with Additives and the Double Layer Effect*. J. Electrochem. Soc. 2002;149(5):C229-C236.

62. Petri M, Kolb D, Memmert U, Meyer H. *Adsorption of Polyethylene Glycol on Au(111) Single-Crystal Electrodes and Its Influence on Copper Deposition*. J. Electrochem. Soc. 2004;151(12):C793-C797.

63. Hope GA, Woods R. *Transient Adsorption of Sulfate Ions During Copper Electrodeposition*. J. Electrochem. Soc. 2004;151(9):C550-553.

64. Lipkowski J. *1998 Alcan Award Lecture - Surface Electrochemistry - Surface Science with a Joy Stick*. Canadian Journal of Chemistry 1999;77(7):1163-1176.

65. Ilgar E, O'Keefe T. Surface Roughening of Electrowon Copper in the Presence of Chloride Ions. In: Dreisinger D, editor. *Aqueous Electrotechnologies: Progress in Theory and Practice*; 1997: The Minerals Metals and Materials Society; 1997. p. 51-62.

CHAPTER 6

BENCH SCALE COPPER ELECTROWINNING TESTS

6.1 Introduction

This testwork was aimed at investigating the effectiveness of Guarfloc 66 (Guar) and activated polyacrylamide (APAM) in controlling dendrite growth in a *continuous* copper electrowinning system using *parallel plate* electrodes. These tests were also conducted for longer EW times than previously described.

In metal deposition, nucleation is a very important process. The first step of metal deposition is the formation of nuclei of the depositing metal on a foreign substrate and on a substrate of the same metal. The competition between nucleation and growth determines the smoothness of the deposit: the higher the nucleation rate; the finer the crystal size[1]. Moreover, the forms of the growing crystals determine the physical appearance and structure. A higher crystal size growth rate normal to the substrate leads to a more fibrous structure. A brightening effect can be achieved when large developed crystal faces grow parallel to the substrate.

The formation of coherent deposit can take place by a layer growth mechanism or 3D crystallite growth (or nucleation-coalescence growth)[2]. The layer growth mechanism is indicated by lateral spreading of discrete layers, one after another across

the surface. The 3D crystallite growth mechanism forms a coherent deposit by coalescence of these crystallites. Three-dimensional (3D) epitaxial crystallites have been observed in the first stages of copper electrodeposition[2]. The coherent deposit was formed by growth and coalescence of the three dimensional epitaxial crystallites.

6.2 Experimental

The comparison between Guar and APAM was carried out using the current-industry standard copper electrowinning operating conditions except for current density which was increased to 340A/m^2 from the industry standard[3] of 280-300 A/m^2. Additionally, Guar and APAM concentrations were also increased from about 175 grams/tonne copper cathode or 0.25-0.50 mg/L in the electrolyte as it was dosed at Mount Gordon Operations to 200grams/tonne or 0.68 mg/L.

The electrolyte was prepared using AR grade copper sulphate and AR grade sulphuric acid. Figure 6-84 shows the EW cell design in detail and Figure 6-85 shows the overall bench scale design. Figure 6-86 shows a photograph of the equipment.

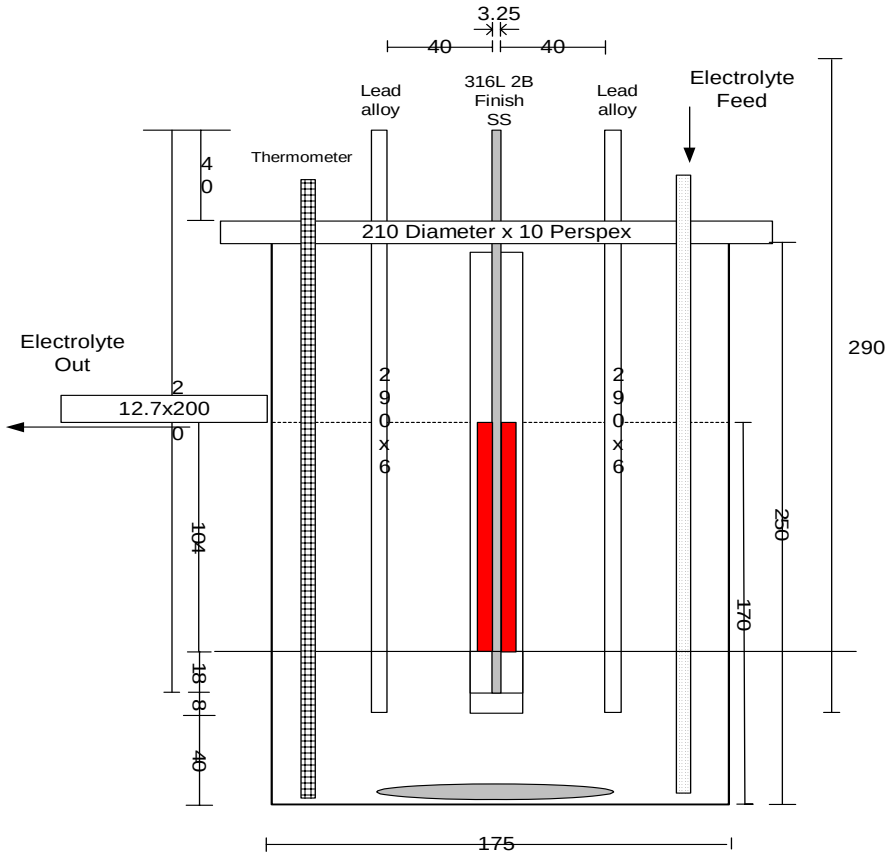

Figure 6-84: EW cell design – parallel plate electrodes

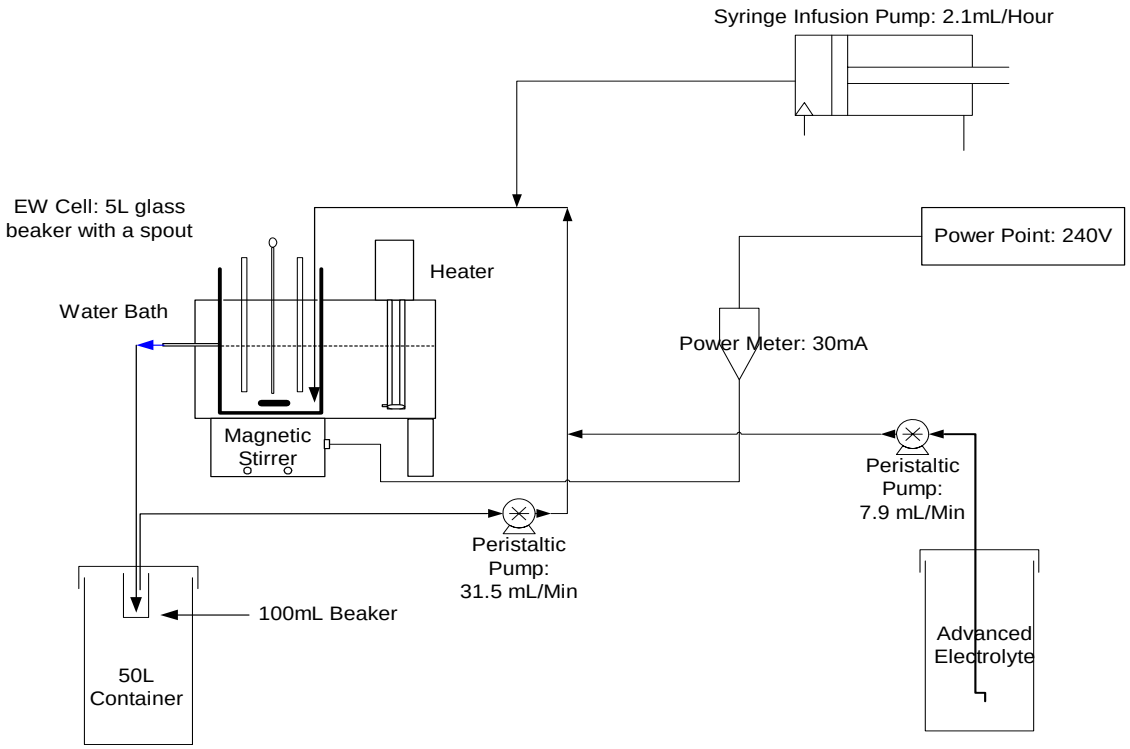

Figure 6-85: Bench Scale Process

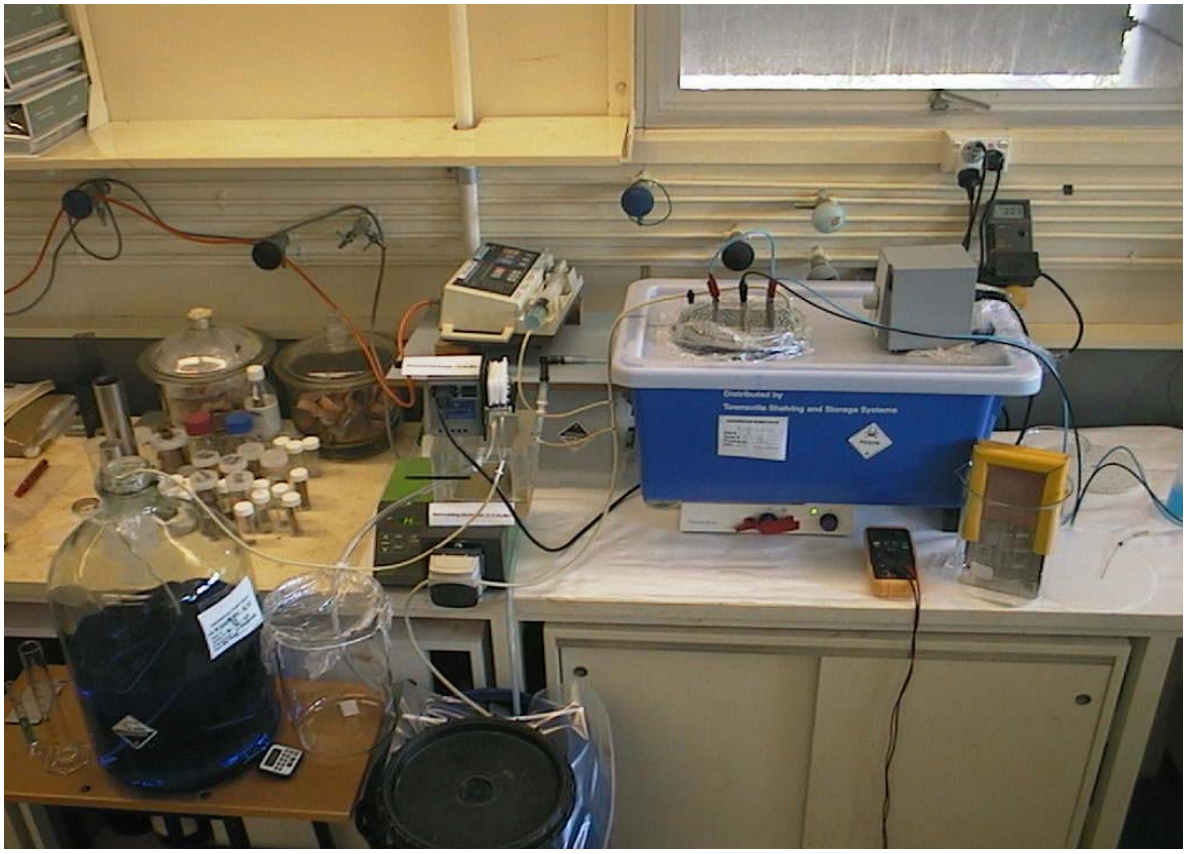

Figure 6-86: Photograph of Bench Scale Equipment

Table 6-32 shows the details of the operating conditions. The net electrolyte volume in the EW cell was 3.9L (without electrodes) and the flow rates of the re-circulating and advanced electrolyte were maintained constant at 31.5 and 7.9 mL/Min, respectively. Eighty percent of the total electrolyte flow rate was re-circulated to the EW cell using a Watson Marlow 505S peristaltic pump to simulate the commercial operation at Mt. Gordon. This recirculation maintains the activity of Guar or APAM constant in the EW cell and also possibly controls their ageing process. The organic additives were dosed constantly at 2.1 mL/hour using a syringe infusion pump. The concentration of the organic additive in the aliquot was 0.68 mg/mL. The electrolyte in the EW cell was stirred using a magnetic stirrer at 30 mA measured with a power meter. This low current induced a minimum agitation to improve the diffusion of the organic additive. The electrolyte temperature was kept at 50.5±0.5^{o}C in a water bath.

Table 6-32: Experimental Conditions

Current Density, A/m^2	340
Voltage Drop, V	2.15
EW Time	44 hours 35 Minutes
Deposition Area (85.5x103.5mm), cm^2	88.5
Average Copper Concentration, g/L	35±1
Sulphuric Acid Concentration, g/L	160
Chloride ions Concentration mg/L	25
Electrolyte Net Volume, L	3.9
Electrolyte Temperature, ^{o}C	50.5 ± 0.5
Guar or APAM, g/tonne Copper Cathode	200
Guar or APAM Conc. in Electrolyte, mg/L	0.68
Advanced Electrolyte, mL/Min	31.5
Recirculating Electrolyte, mL/Min	7.9
Syringe Pump - Dosing Guar or APAM, mL/Hour	2.1
Power to Stir Solution, (30 mA), Watts	7-8
Copper Conc. in Advanced Electrolyte, g/L	50
Sulphuric Conc. in Advanced Electrolyte, g/L	142
Chloride Conc. in Advanced Electrolyte, mg/L	30

The cathode substrate was a 316L 2B finish stainless steel procured from Townsville Refinery Operations, Xstrata and the anodes were prepared from a lead alloy anode received from Mt. Gordon. Current industry-standard ABS edge strips were inserted on the stainless steel and the corners were joined at 45^{o} with Araldite

K138 and hardener K138 Part B, an acid resistant and thermally stable epoxy resin. The stainless steel substrates (3 cathodes) were thoroughly washed with acetone and water, soaked in an electrolyte solution for 24 hours and washed again with distilled water. The distance between the electrodes was 40mm which is similar to the industry standard of copper electrowinning.

Guar was dissolved in water at room temperature, under stirring, for two hours and APAM in 16-fold diluted electrolyte at 50^{o}C also under stirring for two hours.

X-Ray diffraction data was collected using a Siemens/Bruker General Area Detector Diffraction Solution, GADDS diffractometer at the Advanced Analytical Center of James Cook University. The instrumental parameters such as collimator size, detector resolution and beam divergence critically affect the determination of peak broadening[4]. The description of the instrumental parameters used to determine the peak broadening and the electrowinning conditions are presented elsewhere[5] as Appendix C. The GADDS diffractometer was set up to automatically map out a 2cm^2 surface area from the 88.5 cm^2 copper deposits obtained from these electrowinning tests. Preparation of the copper cathode samples for SEM analysis was described in Section 4.2.

6.3 Experimental Results

Three EW tests were conducted (i) with nil additives for 10 hours; (ii) with Guar 44 hours 35 minutes and (iii) and with APAM 44 hours 35 minutes. The copper deposits obtained from the three tests showed no dendrites greater than 1-2mm. The surface roughness of the copper deposits was unable to be measured since it surpassed the specifications of the M1 Perthometer (10nm-100μm). Photographs of the electrowon copper deposits in the presence of Guar are shown in Figures 6-87 and 6-88 and in the presence of APAM are shown in Figures 6-89 and 6-90. It can be seen that the physical appearance of copper deposit obtained with Guar was rougher than that obtained with APAM. Both sides of the deposit produced with Guar have a needle-like, granular appearance throughout the plate. In contrast, the deposit produced with APAM is smoother, brighter and more compact than the copper deposit produced with Guar. Moreover, the copper deposits obtained with Guar possess three areas where copper

deposition has not taken place. This is described as “lacy copper” and was also reported by Sun and O’Keefe[6] in the absence of additives. This kind of deposit is often found at commercial scale electrowinning operations but not at electrorefining operations where animal glue and thiourea are used as organic additives.

These results are consistent with previous EW tests conducted with a rotating cylinder electrode and with CV and EIS tests on the RCE. CV tests indicate that Guar predominantly behaves as a depolarizer on bare stainless steel and on pre-plated copper stainless steel substrates. EIS on pre-plated copper also indicates that Guar reduces the charge-transfer resistance which is consistent with depolarization behaviour. The stainless steel substrate with pre-plated copper at 10 mA/cm^2 for 6 minutes simulates a stainless steel mother plate *in-use* since copper is always present after a stripping operation. In contrast, CV with APAM indicates that under the same conditions it polarizes the electrode and EIS with APAM indicates that it increases the charge-transfer resistance. The polarization behaviour of APAM is similar to a typical levelling agent/surfactant, i.e., glue and polyethylene glycol (PEG).

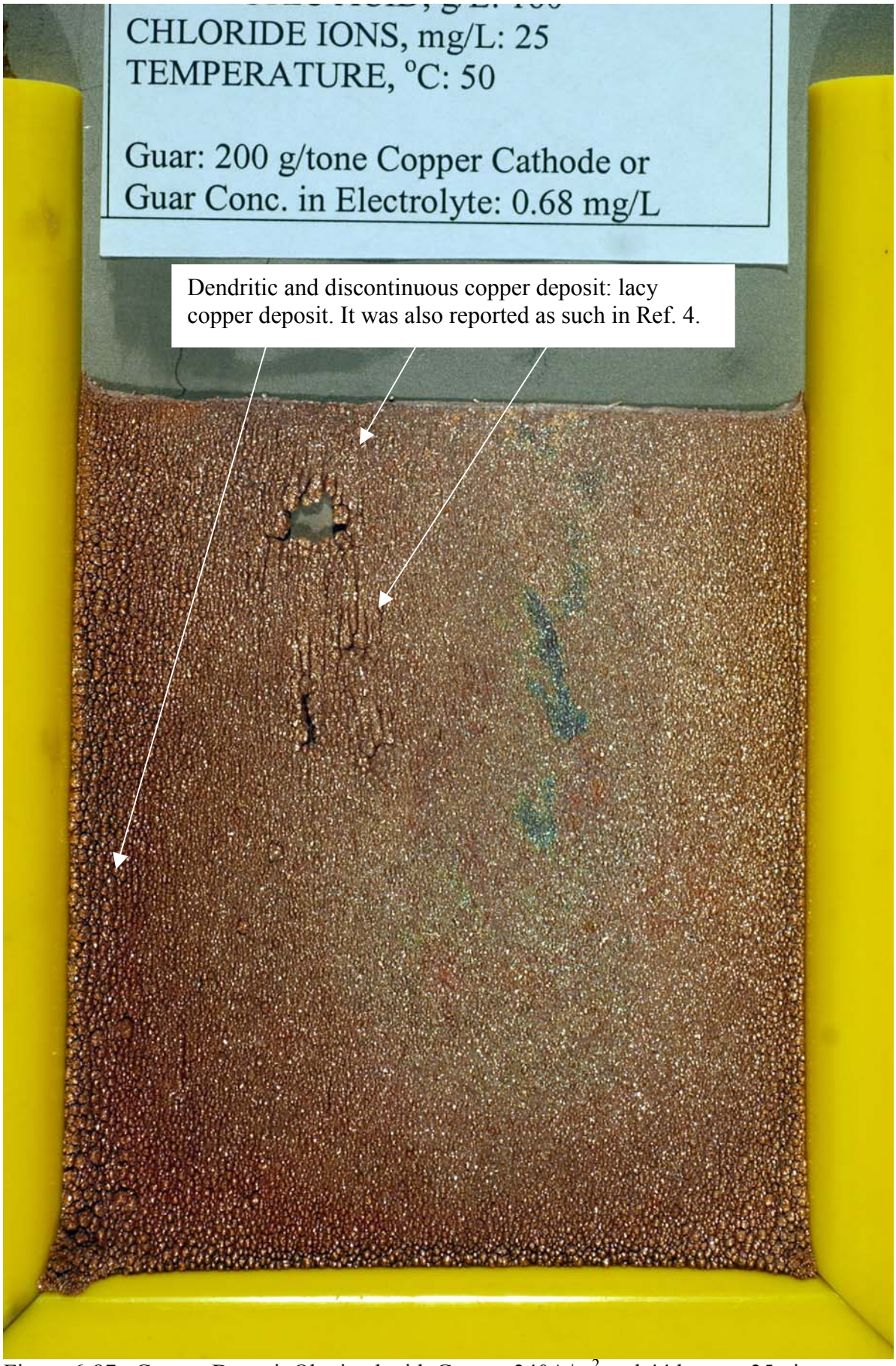

Figure 6-87: Copper Deposit Obtained with Guar at 340A/m^2 and 44 hours - 35minutes

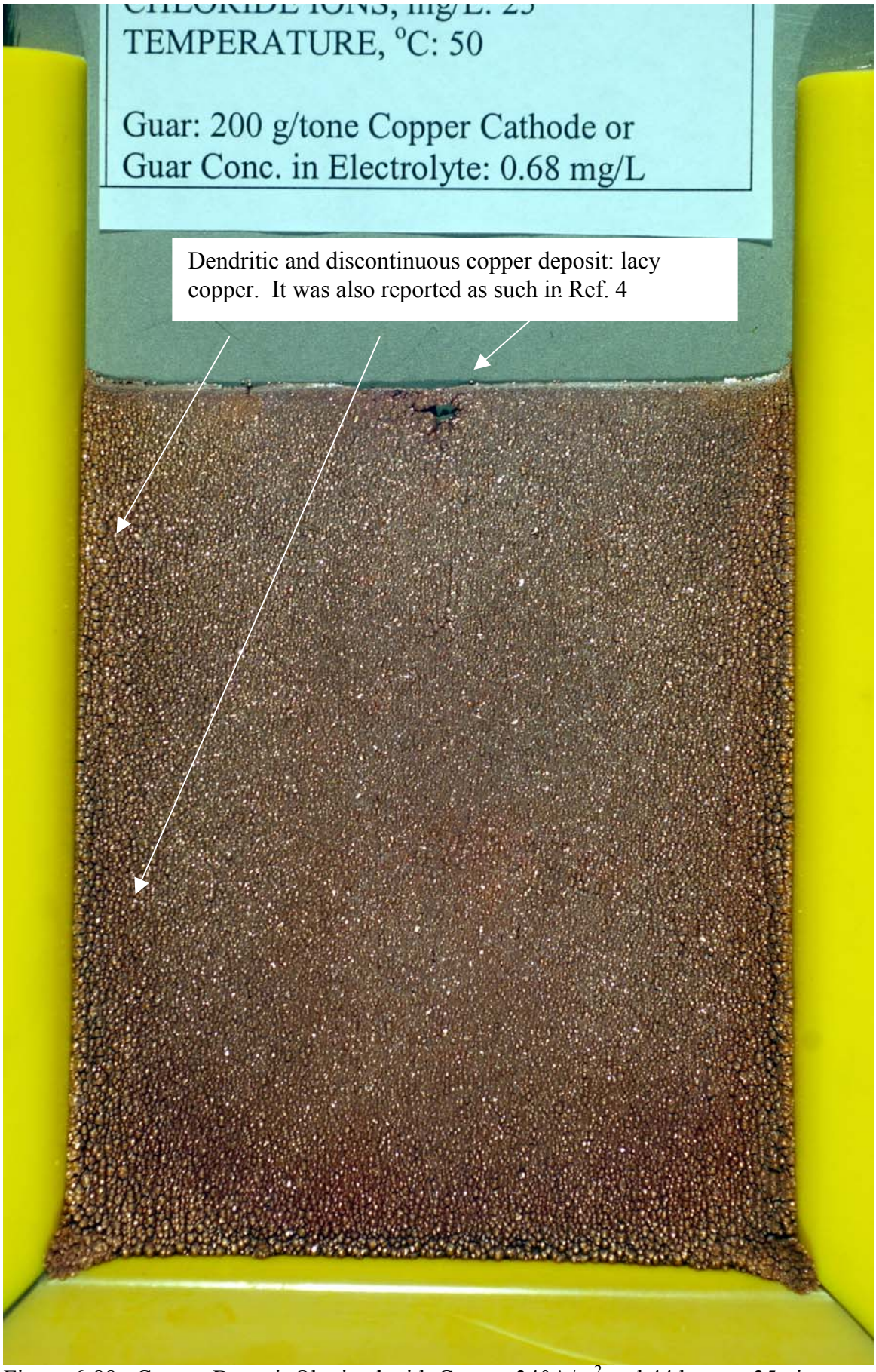

Figure 6-88: Copper Deposit Obtained with Guar at 340A/m^2 and 44 hours - 35minutes

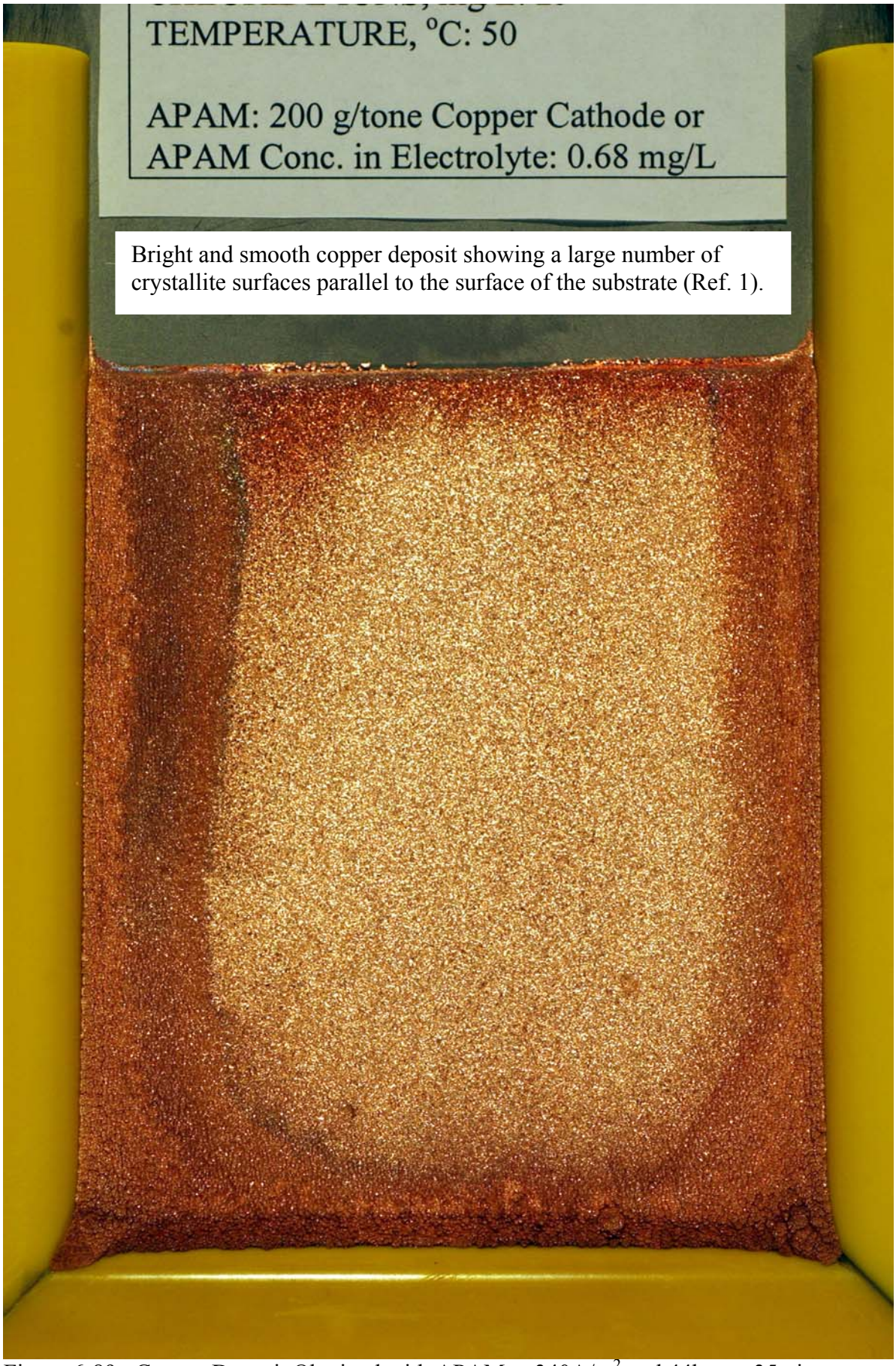

Figure 6-89: Copper Deposit Obtained with APAM at 340A/m^2 and 44hours-35minutes

Figure 6-90: Copper Deposit Obtained with APAM at 340A/m^2 and 44hours-35minutes

6.4 Scanning Electron Microscopy of Copper Cathode Cross-Sections

Figures 6-91 and 6-92 show the scanning electron microscopy (SEM) micrographs of the cross-sectioned copper cathodes obtained from this test work. It can be seen in Figure 6-91 that the cross section of the copper cathode obtained with APAM is slightly columnar growth. It has been reported that this type of growth may be improved into an equiaxial microstructure by adding a sulfur bearing organic additive into the electrolyte bath[7].

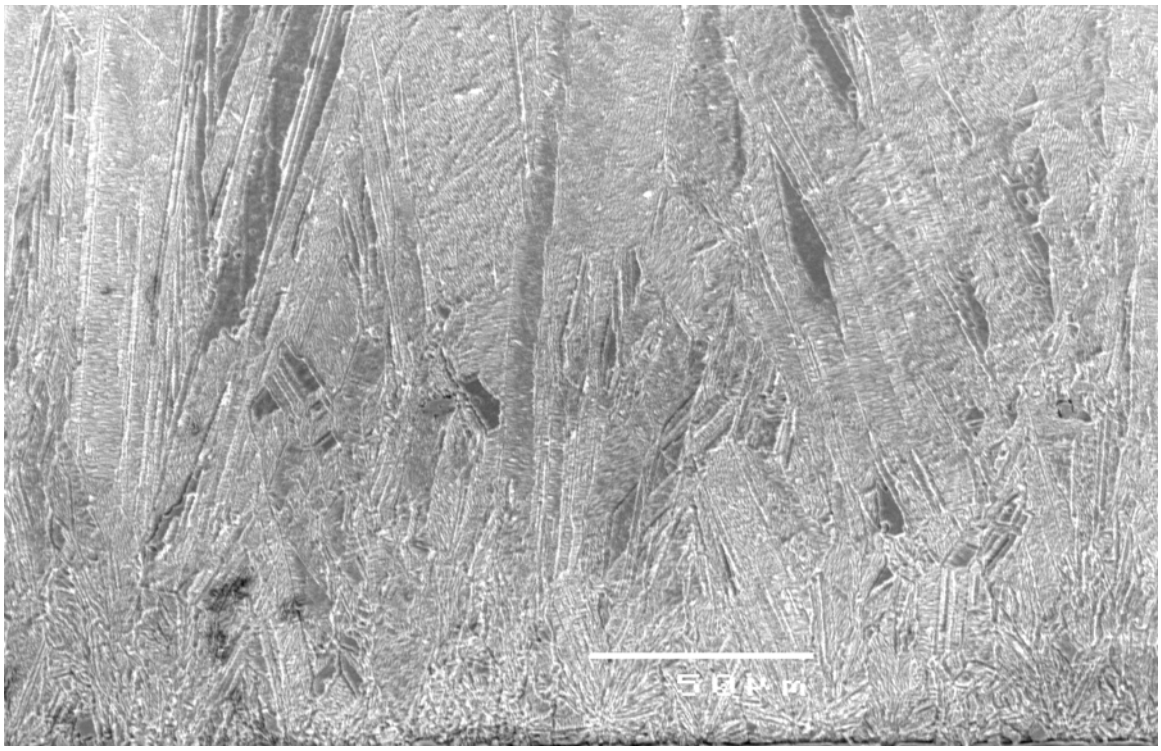

Figure 6-91: SEM micrograph of the copper deposit obtained using 0.68mg/L APAM (200 g/tonne Copper Cathode) at 340 A/m^2 current density. Note the slightly fibrous or columnar structure.

In the presence of Guar (Figure 6-92) the microstructure of the copper deposit is *porous*. This porosity appears to be consistent with the reduction in the charge-transfer resistance that Guar imparts during the deposition process and the inferred predominance of crystal growth over crystal nucleation as discussed in Section 5.8.

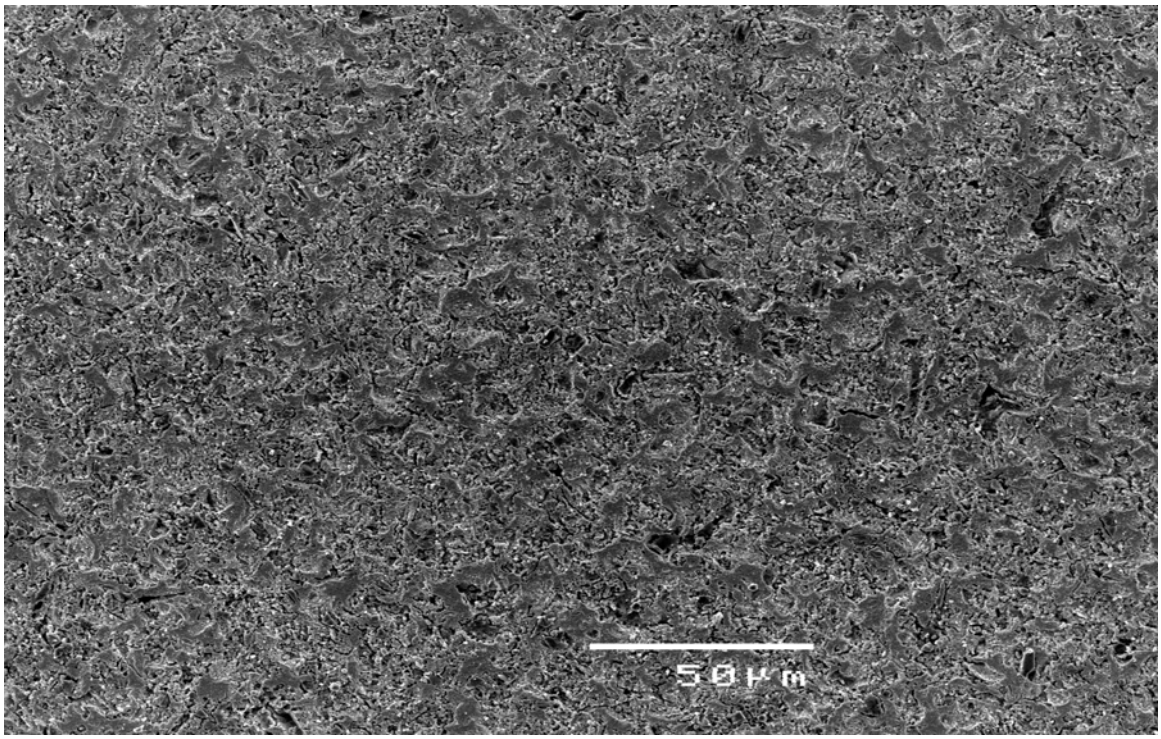

Figure 6-92: SEM micrograph of the copper deposit obtained using 0.68mg/L Guar (200 g/tonne Copper Cathode) at 340 A/m^2 current density. *Note a porous copper cathode.*

6.5 Determination of Crystallite Size

Crystallite size was measured using the General Area Diffraction Detector Solution (GADDS) as described in the paper Fabian et al[5] and reproduced in Appendix C. In summary, GADDS is an x-ray diffraction technique by which the breadth β of the pure diffraction profile commonly also known as the full-width at half-maximum (FWHM) is determined. The crystallite size can then be estimated using the Sherrer Equation as described in Equation 6-27[4,8]:

$$L = \frac{K.\lambda}{\beta.\cos\theta} \qquad (6\text{-}27)$$

where θ and λ are the Bragg angle and x-ray diffraction wavelength in Ansgtroms (Å), respectively. β is the line breadth intensity of the peak in radians. The line breadth is corrected using a Gaussian profile fit ($\beta^2 = U^2\text{-}S^2$; U= copper cathode sample, S= standard). K, λ and θ are 0.9, 1.54184 and 15 degrees, respectively. Lanthanum hexaboride (LaB_6, 660a) procured from National Institute of Standards and

Technology (NIST) was the standard reference material. The GADDS Diffractometer Parameters are shown in Table 6-33.

Table 6-33: GADDS Diffractometer Parameters

Radiation	Cu
Sample-detector distance, cm	30
Collimator, μm	500
kV, mA	40,52
Data Collection time/reading, sec	60
2θ, ω	70, 30
Step size, mm	0.5
Copper plate mapped area, cm^2	~2

The crystallite size was determined to assess whether the presence of APAM or Guar results in different have higher nucleation rates during EW under otherwise constant conditions. These tests may also be important to determine coalescence of small crystallite sizes to form larger crystal sizes according to the mechanism of 3D crystallite size growth.

Table 6-34 and Figure 6-93, reproduced from Fabian et al[5], presented as Appendix C, show the Kruskal-Wallis test results for the effect of the ageing of APAM on crystallite size. The typical preferred orientation profile was [110]>>[111]>[100] for all samples. The copper cathode samples for this analysis were obtained using the *RCE* described in Section 3.2.1. The data was analysed using SPSS program version 11. It indicates that the mean crystallite size differs significantly between the four tests at the 99% confidence level. It can be concluded that at least one of the four samples differs from the others. Inspection of Table 6-34 shows that the crystallite size mean rank and the median crystallite size decreased in the presence of fresh APAM (364 Å) and degraded APAM (398 Å). These values increase in old APAM (438 Å) when APAM had undergone further degradation at 50^oC from 18 to 22 hours by which time it had possibly become inactive. The crystallite size with old APAM (436 Å) is similar to nil APAM (426 Å). Thus:

$$FreshAPAM < DegradedAPAM < OLDAPAM \cong NILAPAM$$

Table 6-34 also shows that the proportion of crystallites larger than 4500Å varied between the 4 Tests. Fresh APAM produced the lowest proportion of crystallite size greater than 4500 Å (15%). Degraded APAM produced greater proportion of crystallites greater than 4500 Å (38%) compared with old APAM (26%) and nil organic additive (27%). Test 3 shows a maximum number of large crystallites and an intermediate median crystallite size. This must mean that there are large numbers of smaller crystallites as well as large crystallites. This is consistent with the formation of a relatively large proportion of small crystallites formed on top of large crystals and their subsequent 3D coalescence.

Table 6-34: Kruskal-Wallis Test Results for APAM Crystallite Size

Test No.	1	2	3	4
Presence/Age of APAM	Nil	Fresh	Degraded	Old
Electrowinning Time, Hours	4	4	4	4
APAM Ageing in Electrolyte at 50°C, Hours		0-4	8-12	18-22
FWHM* Number of Readings, N	1428	156	1479	1493
Crystallite Size Data Processed, N	1040	133	913	1102
Crystallites Size > 4500 Å, %	27	15	38	26
Kruskal-Wallis Crystallite Size Mean Rank	1657	1333	1414	1716
Asymptotic. Sig., Monte Carlo Sig., 99% CI, lower and upper bounds	p = .0000			
Median Crystallite Size, Å	426	364	398	438

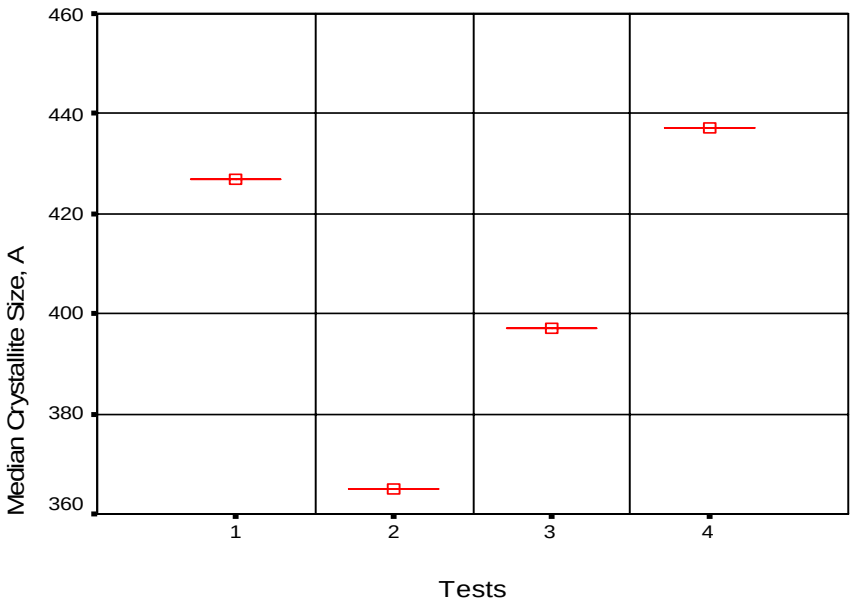

Figure 6-93: Median of Crystallite Size

Table 6-35 shows the Kruskal-Wallis test results for APAM and Guar crystallite size obtained from the bench scale testwork using *parallel plate electrode*. Due to the experimental design, fresh, degraded and old APAM are simultaneously present in the electrowinning cell as would be the case in commercial plants for any additive. It can be seen that the median crystallite size for APAM is smaller than that for Guar. Therefore, APAM appears to favour a higher nucleation rate than Guar. The other important results are the percentage of crystallite size greater than 1800 Å: 41% and 24% for APAM and Guar, respectively. It appears that 3D crystallite growth and coalescence is higher with APAM than that with Guar. This behaviour is probably acceptable as long as the copper deposit is smooth as it is the case with APAM compared with the copper deposit produced with Guar.

Finally, Table 6-34 shows that for degraded APAM (Test 3) 38% of crystallites were larger than 4500Å and 41% (Table 6-35) were larger than 1800Å. It appears from both results that fresh and degraded APAM, also produced in the continuous electrowinning process, favours smoother, brighter with greater proportions of large and small crystallite sizes. The median crystallite size with APAM (405Å) is smaller than with Guar (427Å). Therefore must be a larger number of smaller crystallites with APAM than Guar.

Table 6-35: Kruskal-Wallis Test Results for APAM and Guar Crystallite Size

Test No.	APAM	Guar
Electrowinning Time, Hrs	44.60	44.60
FWHM Number of Readings, N	338	440
Crystallite Size Data Processed, N	198	335
Crystallites Size > 1800 Å, %	41	24
Kruskal-Wallis Crystallite Size Mean Rank	220	295
Asymptotic Significance	0.000	
Median Crystallite Size, Å	405	427

6.6 Conclusions

The rate of nucleation and growth play a dominant role in determining the overall deposition kinetics, as well as the appearance, structure and properties of the

deposit. The copper deposit with APAM is brighter and does have greater amounts of smaller and larger crystallite sizes than those with Guar. It can therefore be inferred that the presence of APAM favours higher nucleation rates and greater 3D crystallite growth and coalescence than those in the presence of Guar (see Table 6-35). APAM is a levelling agent and therefore polarizes the electrode and thus assists the nucleation rate which in turn produces purer copper deposits since voids and porosity are reduced by smaller crystallites. APAM possibly covers the active surface areas (peaks) and therefore deposition has to restart from less active areas (valleys) by forming new nucleates. The brightening effect of the copper deposit in the presence of APAM was probably achieved through large crystal faces that are parallel to the substrate[1].

The quality of the copper deposits in terms of smoothness obtained with APAM are greater than those with Guar. This result is consistent with previous EW tests conducted on a rotating cylinder electrode and CV and EIS tests.

6.7 References

1. Budevski E, Staikov G, Lorenz W. *Electrochemical Phase Formation and Growth, an Introduction to the Initial Stages of Metal Deposition*. New York: VCH; 1996.

2. Paunovic M, Schlesinger M. *Fundamentals of Electrochemical Deposition*: John Wiley & Sons, Inc.; 1998.

3. Robinson T, Rasmussen S, Davenport WG, Jenkings J, King M. Copper Electrowinning - 2003 World Tankhouse Operating Data. In: Dutrizac JE, Clement CG, editors. *Copper 2003 - Cobre 2003 Copper Electrorefining and Electrowinning*; 2003; Santiago, Chile; 2003. p. 421-472.

4. Klug H, Alexander L. *X-Ray Diffraction Procedures for Polycrystalline and Amorphous Materials*. Second ed. Sydney: John Willey & Sons; 1974.

5. Fabian C, Ridd M, Ness S, Lancaster T, Griffin G. Determination of Crystallite Size and Surface Roughness of Copper Deposits for Electrowinning in the Presence of an Organic Additive. In: CA Young AA, CG Anderson, DB Dreisinger, B Harris and A James, editor. *Hydrometallurgy 2003*; 2003; Vancouver, BC Canada: TMS; 2003. p. 1233-1245.

6. Sun M, O'Keefe T. *The Effect of Additives on the Nucleation and Growth onto Stainless Steel Cathodes*. Metallurgical Transaction B 1992;23B:591-599.

7. Plieth W. *Additives in the Electrocrystallization Process*. Electrochimica Acta 1992;37(12):2115-2121.

8. Siemens, Bruker. GADDS Introduction Manual; 2001.

CHAPTER 7

SUMMARY AND CONCLUSIONS

7.1 Introduction

The aim of this thesis was to investigate the role of polyacrylamide as an organic additive in copper electrodeposition. Despite the variety of mechanisms proposed for the smoothening effect of additives[1], a consensus exists that adsorption of the additive on the substrate plays the determining role[2, 3]. The polarizer/inhibitor/leveller controls the vertical growth to produce smooth deposits by conferring preferential adsorption on the peaks or active sites. The grain refiner/accelerator may predominantly control the nucleation process by promoting the formation of new nuclei to form new crystallites at the recesses. There is a synergy between the action of the inhibitor that reduces the rate of vertical growth and the grain refiner that accelerates the formation of nuclei in the recesses of the surface. This synergistic process between the leveller/inhibitor and grain refiner is aimed at improving the overall quality of the copper deposit in terms of purity, smoothness and plant productivity by for example elimination/reduction of short-circuits caused by dendrites in copper electrometallurgy and superconformal growth in the damascene process.

The mechanism and electrochemical action of both Guar and chloride ions have been poorly documented in the literature for copper electrowinning compared with those of glue, thiourea and chloride ions for copper electrorefining.

A better understanding of the role of polyacrylamide and Guar, alone and combined, on copper deposition is particularly important since Mount Gordon Operations of Western Metals Copper Limited, Australia occasionally produced the smoothest copper cathode ever known in the industry. At the commencement of the work described in this thesis, it was not known whether polyacrylamide behaved as a levelling agent or grain refiner or both. The industry-standard additives for copper deposition are shown in Table 7-36. While a levelling agent, grain refiner and chloride ions are dosed in copper electrorefining and in the microelectronics industry, only Guarfloc (Guar) and chloride ions are dosed for copper electrowinning. Guar in copper electrowinning is known as "weak levelling/polarizer" but it has been found throughout this study that Guar is a depolarizer.

Table 7-36: Industry-Standard Additives Used in Copper Electrodeposition

Role of the Additive	Electrorefining		Electrowinning		Microelectronics, PCB and IC	
	Additive	mg/L	Additive	mg/L	Additive	mg/L
Leveller	glue	1	Nil	Nil	PEG*	100-300
Brightener**			Guar	0.25-5		
Grain refiner	thiourea	2	Nil	Nil	SPS&JGB/MPSA*	1&1/1,respectively
Depolarizer	Cl^-	50-60	Cl^-	20-25	Chloride ions	40-60

*PEG, polyethylene glycol; SPS, bis(3-sulfo-propyl) disulfide; JGB, Janus Green B (safranine dye); MPSA, 3-mercapto-1-propanesulfinate. Cl^- = chloride ions, **Guar is also known as weak polarizer in the industry.

It is widely known in the copper deposition industry that chloride ions depolarize the electrode or in other words increases the rate of charge-transfer and consequently increases surface roughness since it enhances growth rate rather than nucleation rate[4-6].

7.2 Hydrolysis and Adsorption of Polyacrylamide

(v)

(vi) Polyacrylamide hydrolysis increases the number of carboxyl functional groups in the polymer chain and the initial hydrolysis reaction is faster than the remainder. Hydrolysis in water at room temperature is

negligible (<2 percent)[7]. Hydrolysis of non-anionic polyacrylamide in strong acid solutions can also lead to the formation polyacrylimide.

(vii)

(viii) It is stated by Halverson et al.[8] and Panzer et al.[9, 10] that hydrolysis at pH 2 predominantly produced *blocks of continuous acrylic acid* or acrylamide segments, i.e., AAA (acrylamide segments) and BBB (acrylic acid segments) functional groups but alkaline hydrolysis contains ABB, BAB, ABA triads. The B-segments from alkaline hydrolysis indicate that it are well distributed along the polymer chain or recently known as *random copolymer*. This average sequence length of carboxyl groups from pH 2 acid hydrolysis was about ten-fold greater[10] than that from alkaline hydrolysis at 110°C after 24-hours. The presence of polyacrylimide was insignificant at pH 2 and alkaline hydrolysis.

(ix)

(x) Literature on the adsorption of PAM on copper metal and 316L stainless steel appears to be nonexistent. The adsorption of polyacrylamide depends on the solution pH, chemical nature of the surface, the presence of solutes and functional groups in the polymer chain. The reaction pathway and therefore product from alkaline hydrolysis is different to that from acid hydrolysis. In general, polyacrylamide adsorption onto solid surfaces may involve both chemical and physical adsorption. Nonionic polyacrylamide in a strong acid medium is attached to the surface through hydrogen bonding as shown in Figure 7-94.

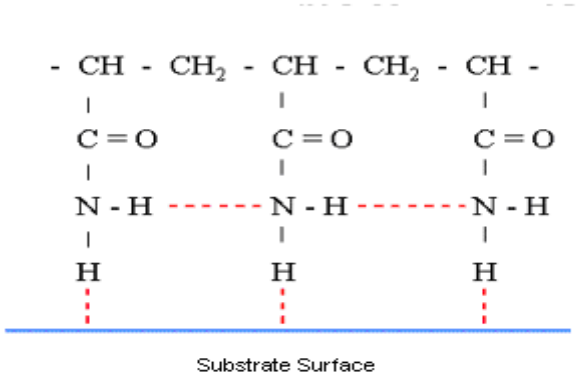

Figure 7-94: Hydrogen Bonding of Non-ionic Polyacrylamide

B*lock copolymers*, Figure 7-95, obtained at pH 2 acid hydrolysis appear to exhibit adsorption by covalent bonding or "salt linkage" where electrons are transferred from the acrylate group to multivalent cations like calcium and iron present in or on the mineral surface[8, 10]. Moreover, light scattering data indicates that under slightly acidic conditions the molecular weight of the polymer remained relatively "static" during the hydrolysis process[11].

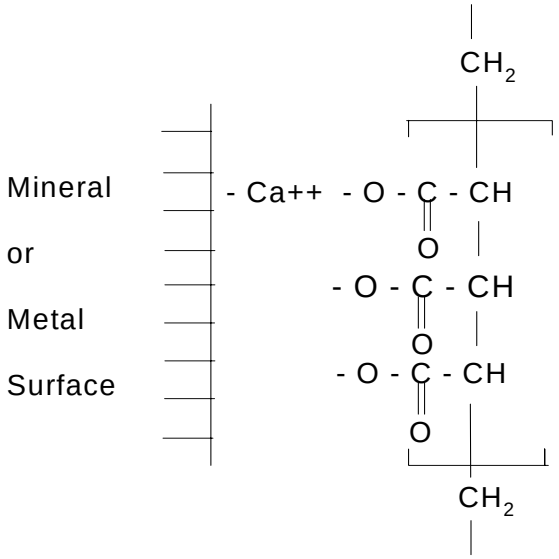

Figure 7-95: Blocky polyacrylamide may exhibit covalent bonding with divalent ions such as calcium and iron [64]

Grchev et al.[12] showed that the surface coverage of 2-3ppm polyacrylamide concentration under strong acid conditions decreased from about 0.52 to 0.02 as the polyacrylamide molecular weight increased from $5x10^3$ to $1.5x10^6$.

7.3 Rotating Cylinder Electrodes

Two rotating cylinder electrodes were built as part of the investigations for this thesis. The diffusion layer thickness (δ) obtained by using the equation developed by Arvia et al.[13] more closely replicate the experimental data than those obtained by using the equation developed by Eisenberg et al.[14]. Moreover, the equation developed by Arvia et al.[13] gives similar δ for the small and large RCE used in this thesis. Therefore diffusion layer thicknesses obtained using Arvia et al.'s[14] equation were compared with

the experimental data produced for this thesis. The results were shown in Chapter 3-Section 3.2.3.

It was shown that the average of surface roughness measurements obtained in this testwork is consistent with those results obtained with Ilgar and O'Keefe[4] who used parallel plate electrodes. However, the δ of 175μm (30°C-40°C) reported by Ilgar and O'Keefe[4] for natural convection, is higher than 97μm at 45°C and 115μm at 65°C δ obtained for this thesis at 0rpm. Nevertheless, these experimental δ values obtained for natural convection for this thesis more closely agrees to 78μm at 25°C which was recently used by Drews et al.[15] but reported elsewhere[16] to conduct Monte Carlo simulation for an electrolyte composition of 18g/L cupric ions and 180g/L sulfuric acid. It has been therefore shown that the fluid flow produced for the RCE built for this thesis is within the published data[4 16] and therefore the fluid flow data produced by the RCE build for this thesis are validated. Moreover, the fluid flow shown produced by the small RCE is *laminar with vortices* and by the large RCE is turbulent with vortices according to Reynolds and Taylor numbers.

7.4 Effect of Polyacrylamide Preparation Media on Surface Roughness

It was shown that when 15 million Dalton Ciba Magnafloc® 800HP nonionic polyacrylamide was prepared in 16-fold diluted electrolyte (sulfuric acid, 10 g/L; copper, 2.25g/L; pH 1.5) at 50°C for 2 hours the under stirring produced a surface with a statistically significantly lower roughness than PAM prepared in water, full-strength electrolyte and alkaline hydrolysis (3hours preparation time). In acid solutions, the surface roughness decreases as the concentration of sulfuric acid decreases indicating its effect on the hydrolysis of polyacrylamide and hence on surface roughness. Based on the material presented in Section 7.2 that showed the formation of block copolymers due to acid hydrolysis of PAM, it is inferred that the reaction product from the 16-fold DE at 50°C for 2 hours under stirring is a block copolymer[8], depicted below, which may also confer covalent bonding with divalent metals as stated by Halverson et al.[8] and Panzer et al.[9, 10]. This reaction product from 16-fold diluted electrolyte is named activated polyacrylamide (APAM) throughout the thesis.

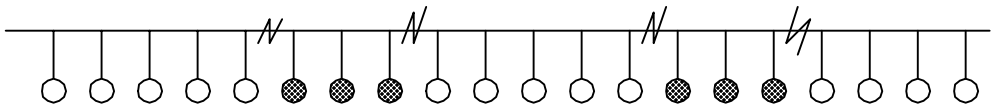

OR

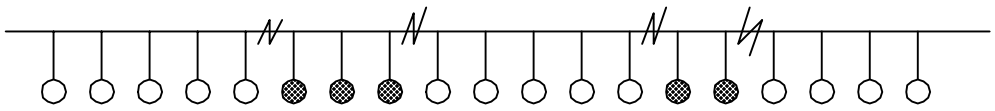

In contrast, it has also been shown that a random copolymer, depicted below, produced from alkaline hydrolysis[8-10], is less effective in controlling the surface roughness than APAM. Based on these results it is also inferred that the adsorption of a random copolymer is less effective than that produced by a block copolymer during copper deposition.

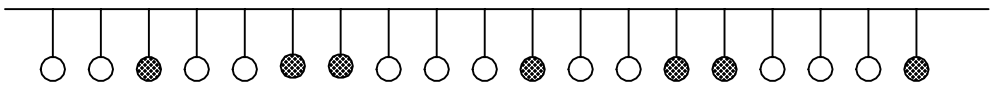

Nonionic polyacrylamide prepared in water, where hydrolysis is insignificant, and in full-strength electrolyte produces similar hydrolysis reactions and products. These hydrolysis products may also adsorb statistically significantly less possibly due to polyacrylimide formation discussed in Chapter 3.

Light scattering data indicated that under slightly acidic condition the molecular weight of the polymer remained relatively "static" during the hydrolysis process[17]. The structure of APAM was confirmed using ^{13}C NMR analysis which indicates the predominance of amide carbonyl carbon with less than 10% hydrolysis. This result is consistent with the experimental hydrolysis of 57% obtained at pH 2, 110^{o}C after 24-hours[8].

APAM is more effective at eliminating dendrite formations than polyacrylic acid up to 12-hours electrowinning. APAM can be maintained in 16-fold diluted electrolyte for about 24 hours without significantly affecting surface roughness.

The APAM degradation process consists of cleavage of the polyacrylamide backbone and this process may enhance the surface coverage and appears to be most likely beneficial to the reduction of surface roughness. This process correlates with the studies of Grchev et al.[12, 18, 19] on the adsorption of polyacrylamide on gold and mild steel in strongly acidified solutions. Polyacrylamide with low molecular weight confers higher surface coverage than polyacrylamide with high molecular weight.

The less optimal results obtained when polyacrylmide was prepared in water and full-strength electrolyte are similar to the experimental conditions conducted by of Pye and Schurz[23] and Vereecken ad Winand[24] who indicated that polyacrylamide controlled the surface roughness of electrowon copper less effectively than Guar. The results obtained with APAM are clearly the opposite than the findings of Pye et al.[23] and Vereecken et al.[24] and this difference is most probably due to the preparation media. APAM is a more effective organic additive to reduce surface roughness than Guar, the industry-standard additive.

7.5 Comparison of Activated Polyacrylamide with Guar

It is shown in the following Section that initially Guar and APAM were studied combined since at the beginning of this project it was not known whether their role were as levelling agent and/or grain refiner. As the results of the initial testwork indicate that APAM and Guar combined were unable to effectively control the surface roughness of the copper cathode due to the presence of Guar; the following testwork were conducted using Guar or APAM alone.

7.5.1 Effect of Guar and APAM on Surface Roughness of Copper Deposits

Two 2^{5-2} fractional factorial experimental designs were conducted as shown Table 7-37. The factors at low level are common for both designs and at high level differ in temperature only.

Table 7-37: Two 2^{5-2} Fractional Factorial Experimental Designs

Factors		Factor Level		
		Low	High	
A	T (Temperature, ^{o}C)	45	55	65
B	i (Current Density, A.m^{-2})	280	320	320
C	L (Guar, mg/L)	0.5	1	1
D	S (APAM, mg/L)	0.5	1	1
E	δ (Diffusion Layer Thickness, μm)	87 (25rpm)	108 (10rpm)	110 (10rpm)

At a 95% confidence interval the models derived from the fractional factorial experimental designs in the temperature range of 45^{o}C-55^{o}C was:

Surface Roughness (μm) =

$$+6.26+0.27*B-0.053*C-0.056*D+0.25*E-0.62*B*C-0.38*B*E \quad (7\text{-}28)$$

where A is temperature; B, current density; C, Guar; D, APAM and E, diffusion layer thickness (δ).

It can be seen from this model that the surface roughness is strongly influenced by an increment of the current density B, (α=0.0180) and diffusion layer thickness E, (α=0.0247). In addition, it is evident that there are two strong interacting terms involving B*C (Current Density*Guar, α<0.0001) and B*E (Current Density*Diffusion Layer Thickness, α=0.0009) which decreases the surface roughness. APAM (D, α=0.6098) and Guar (C, α=0.6316) have an insignificant effect on reducing surface roughness in this temperature range.

At a 95% confidence interval the model derived from the fractional factorial experimental designs in the temperature range of 45^{o}C-65^{o}C was:

Surface Roughness (μm) =

$$+6.16-0.051*A-0.089*B-0.075*C-0.41*D+0.23*E-0.17*B*C \quad (7\text{-}29)$$

It can be seen from this model that APAM D, (α=0.0041) has the most significant effect to reduce surface roughness and APAM is truly independent from Guar (C). Diffusion layer thickness E, (α=0.1004) has the next largest effect and it increases surface roughness as expected. The effect of current density (B) and Guar (C) are insignificant (B*C, α=0.2185). Current Density B (α=0.5192), Guar C, (α=0.5855) and Temperature A, (α=0.7129) follow the sequence and are also insignificant.

It can be seen that the aliased effect of current density (B)*Guar(C) decreases from significant (α<0.0001) in the first model at 45-55^{o}C to insignificant (α = 0.2120) in the second model at 45^{o}C-65^{o}C. This reduction in significance is probably due to the faster degradation of Guar at 65^{o}C than at 45^{o}C at the same current density. It was also shown that the effect of APAM on reducing surface roughness is greater in the 45^{o}C-65^{o}C range than in the 45^{o}C-55^{o}C. This may indicate that the rate of degradation of APAM at 65^{o}C is faster and more effective in reducing surface roughness from the start-up of the EW process than that at 45^{o}C. This is opposite to the effect of Guar.

An experimental design to investigate the effect of an optimal proportion of Guar to APAM on the reduction of surface roughness indicates that this ratio is nonexistent. Overall, Guar alone results in a surface roughness and standard deviation that is higher than for APAM alone or for APAM/Guar combination. This result indicates that Guar reacts faster and loses its levelling efficacy faster than APAM even when it was dosed twice for 6 hours EW time. As Guar quickly looses it levelling effect at 50^{o}C, its degradation process is probably faster at higher temperatures. Therefore, the role of Guar and APAM in copper deposition is independent.

The early stages of dendrite formation in copper electrodeposition occur simultaneously with lower surface roughness and higher number of Peaks-per-Centimeter in the absence of additives, i.e., 30mA/cm^2 and 4.64 hours deposition time. This result agrees with in-situ AFM studies[21, 22].

The peaks-per-Centimeter model for 6 hours electrowinning time accurately predicts that Guar produces higher Peaks-per-Centimeter than APAM. This correlation was clearly demonstrated when electrowinning was conducted for 12 hours where the surface roughness was unmeasurable from the copper cathode produced with Guar dosed for every three hours. In contrast, the surface roughness produced with one and two mg/L of APAM was still measurable (12.79 and 11.71μm) after 12-hours electrowinning time.

It appears that the use of surface roughness measurements to study the effect of organic additives under simulated commercial electrowinning and electrorefining conditions presented in this thesis is the first of its kind.

7.5.2 Physical Appearance, Scanning Electron Microscopy and General Area Detection Diffraction Solutions (GADDS) Results

The effect of the ageing of APAM in the electrolyte was examined using the crystallite size of copper cathodes produced from laboratory scale using a rotating cylinder electrode and bench scale using parallel plate electrodes where Guar or APAM were dosed continuously. An 80% of the spent electrolyte was recycled and mixed with the advanced electrolyte to simulate a commercial EW plant.

Inspection of the results indicate that the median crystallite size decreased in the presence of fresh APAM (364 Å) and degraded APAM (398 Å). These values increase in the presence of old APAM (438 Å) when fresh APAM had undergone further degradation at 50^{o}C from 18 to 22 hours by which time it had possibly become inactive. The crystallite size with old APAM (436 Å) is similar to nil APAM (426 Å).

It has also been shown that degraded APAM (8-12 hours in the electrolyte) has 38% of crystallite size greater than 4500Å and bench scale EW tests with parallel plate electrodes and continuous dosage of APAM shows 41% of crystallite size greater than 1800Å. Moreover, the bench scale copper deposits also indicate to have a median crystallite size of 405Å and 427Å with APAM and Guar, respectively. As the median

crystallite size with APAM is smaller than with Guar, there must be a larger number of smaller crystallites with APAM than Guar.

The rate of nucleation and growth play a dominant role in determining the overall deposition kinetics, as well as the appearance, structure and properties of the deposit. The copper deposit with APAM is brighter and does have greater amounts of smaller and larger crystallite sizes than those with Guar. It can therefore be inferred that the presence of APAM favours higher nucleation rates and greater 3D crystallite growth and coalescence than those in the presence of Guar. APAM possibly covers the active surface areas (peaks) and therefore deposition has to restart from less active areas (valleys) by forming new nucleates. The brightening effect of the copper deposit in the presence of APAM was probably achieved through large crystal faces that are parallel to the substrate[25].

7.5.3 Cyclic Voltammetry and Electrochemical Impedance Spectroscopy Results

Cyclic voltammetry and Electrochemical Impedance Spectroscopy experiments were conducted to investigate the effect of Guar and APAM on the metal electrode (stainless steel and pre-plated copper on stainless steel)/electrolyte interface.

Figure 7-96 depicts the depolarization behaviour of Guar extracted from CV testwork and indicates that about 15mV maximum depolarization was obtained at 2-3 hours residence time whether the metal electrode was stainless steel or copper metal.

In contrast, the maximum polarization on pre-plated copper at with APAM at 45^{o}C and 65^{o}C is approximately 13mV ± 1 but the time to attain this maximum value is about 3.5 hours at 45^{o}C and 1.5 hours at 65^{o}C as shown in Figure 7-97. These results correlate with the fractional factorial experimental results (Section 4.3.2) in which it was demonstrated that APAM had a more significant effect on reducing surface roughness at 65^{o}C than at 45^{o}C.

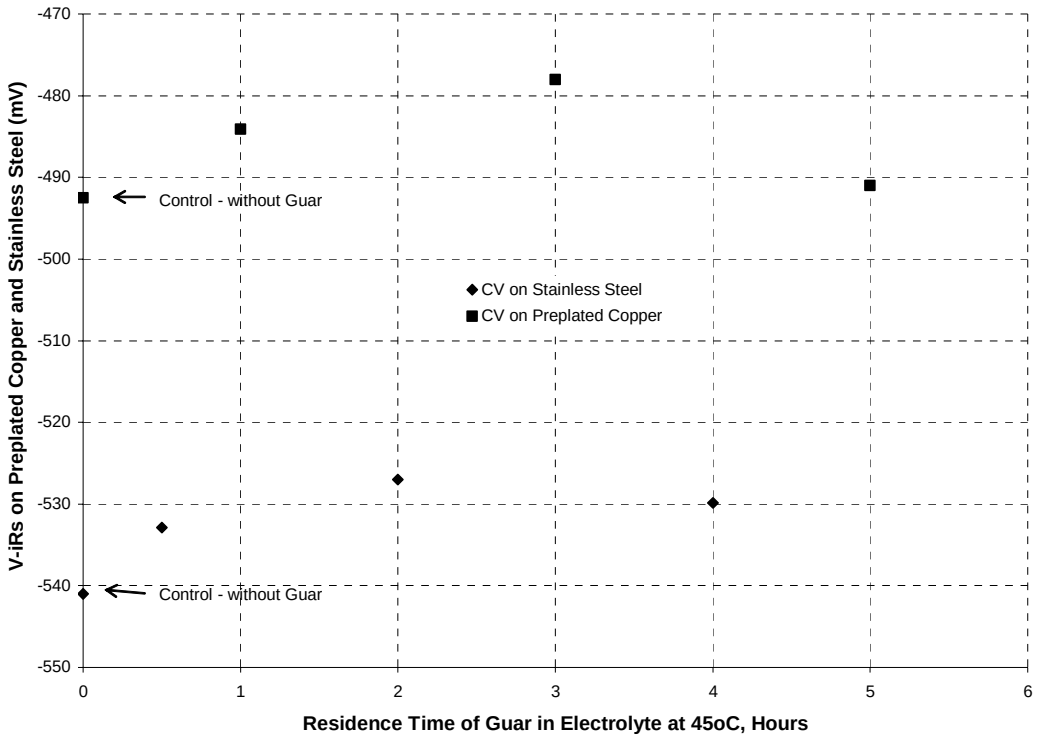

Figure 7-96: Effect of Time on the De-polarization Behaviour of Guar at 45°C at 300A/m^2 Current Density.

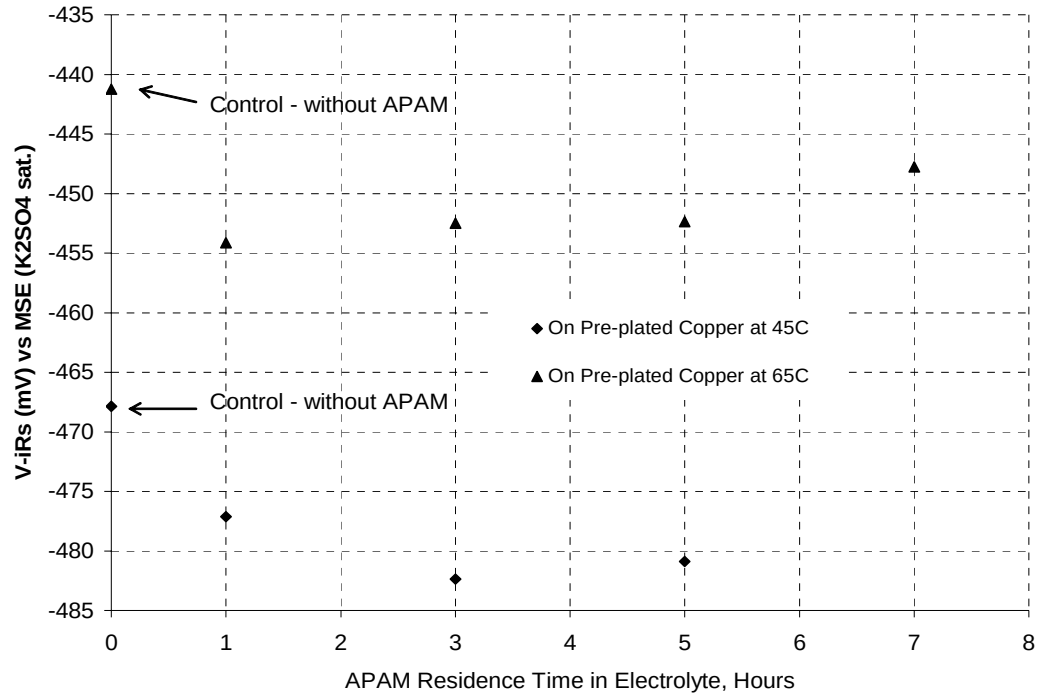

Figure 7-97: Effect of Temperature on APAM Polarization at 300 A/m^2 and 45°C and 65°C

The EIS experimental results were simulated using the equivalent circuit most often referred to in the literature for electrochemical interfaces as depicted in Figure 7-98[26-32] and the LEVM program[27, 33]. This equivalent circuit that consists *only* of resistors and capacitors is used to describe the two single-electron transfer steps[34]. This selection appears to be valid for Langmuir isotherms and other similar isotherms, i.e., Frumkin isotherm. This equivalent circuit was also used for copper deposition in the presence[29] and absence[30] of organic additives.

Table 7-38 summarizes the maximum change in the charge-transfer resistance and double-layer capacitance produced by Guar at 45°C and APAM at 45°C and 65°C. APAM increased the charge-transfer resistance throughout the testwork; in contrast, Guar reduced it. At 45°C, APAM reduced the double-layer capacitance more than Guar at 45°C. This reduction of the double-layer capacitance by APAM was increased when the temperature was increased from 45°C to 65°C. These results indicate that *APAM is more specifically* adsorbed than Guar.

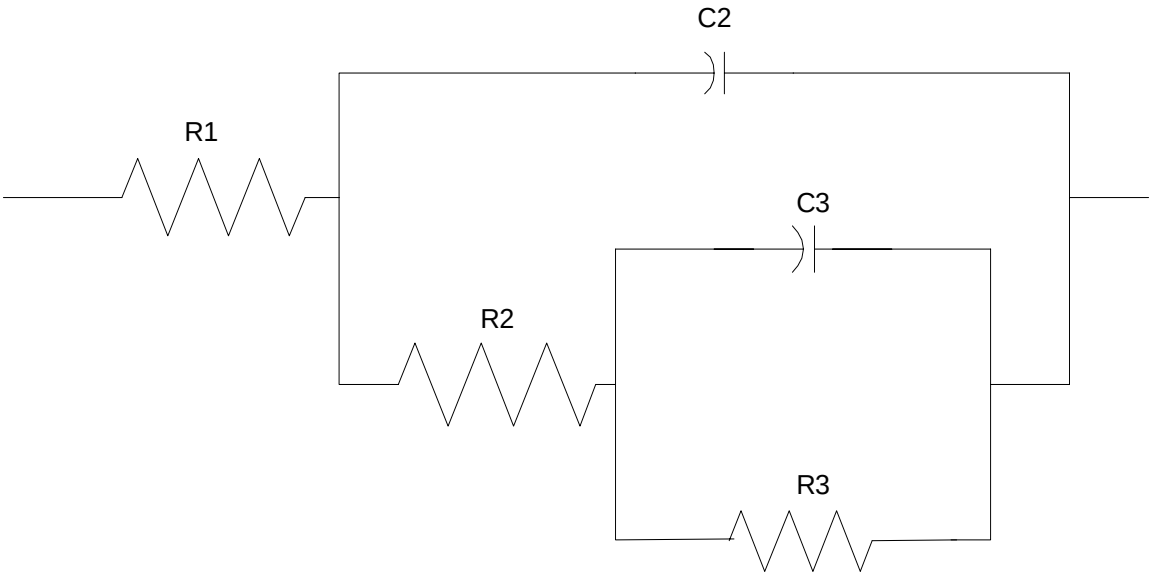

Figure 7-98: Parameters Definition in Equivalent Circuit B[33]

Table 7-38: Charge-Transfer Resistance and Double-Layer Capacitance Differences due to the Presence of Guar and APAM

Additive	EIS Conditions mV vs. MSE	Charge-Transfer Resistance, ohm.cm^2	D-L Capacitance, x 10^{-5}, μF/cm^2	Res. Time in Elec., Hrs.*
Guar	-490mV and 45^{o}C	-0.086	-0.46	2-3
APAM	-470 mV and 45^{o}C	+0.42	-1.2	3-5
APAM	-490mV and 45^{o}C	+0.23	-1.2	3-5
APAM	-445mV and 65^{o}C	+0.34	-6.8	2

*Maximum change determined at these residence times.

The CV results at 45^{o}C is consistent with the EIS results at 45^{o}C in terms that Guar depolarizes the electrode or decreases the charge-transfer resistance and APAM polarized the electrode or increases the charge-transfer resistance. These results for APAM were replicated at 65^{o}C. The EIS data were simulated using the most often referred to equivalent circuit for electrochemical interfaces depicted in Figure 7-98 and LEVM[27, 33]. Moreover, the EIS data with an RDE was not amenable to being modelled using the equivalent circuit presented in Figure 7-98. Overall Cyclic Voltammetry and Electrochemical Impedance Spectroscopy indicated that Guar depolarises the electrode and in contrast APAM polarizes the electrode. Therefore, APAM behaves as a true levelling agent and does so for extended periods of time.

The quality of the copper deposits in terms of smoothness obtained with APAM is greater than those with Guar. This result is consistent with previous EW tests conducted on a rotating cylinder electrode and CV and EIS tests. It is widely recognized in the copper electrometallurgy industry that a smoother copper deposit entrains less impurities. Therefore, APAM is a new levelling agent for copper deposition and may assist the production of copper cathodes with less than 10 ppm total impurities excluding oxygen and will attract a premium price since APAM produces more compacted copper deposits than Guar.

Further investigations to eliminate/reduce the slightly columnar copper deposit obtained with APAM needs to be undertaken. It has been shown that in copper electrorefining the additive system used for about 100 years consists of a levelling agent- glue; grain refiner-thiourea and chloride ions. Similarly, in copper deposition for the fabrication of printed circuit boards and interconnects the additive system consists of a levelling agent and an accelerator/grain refiner. It is therefore hypothesised that

APAM also requires the presence of an accelerator/grain refiner in the electrolyte bath to obtain further improvements of the copper deposits physical and chemical properties. The optimal concentrations of APAM and accelerator/grain in the electrolyte bath (tune up) could be determined using AFM.

(xi) The second research activity is the characterization of the chemical structure of APAM using surface –enhanced Raman spectroscopy (SERS). This study would assist to understand the adsorption mechanism of APAM at the electrode interface. It appears that two contiguous carboxyl oxygens in the block copolymer complex with cuprous or cupric ions. This hypothesis is drawn in accordance with a recently published SERS study on PEG[38].

7.6 References

1. Onicio L, Muresan L. *Some Fundamental Aspects of Levelling and Brightening in Metal Electrodeposition*. Journal of Applied Electrochemistry 1991;21:565-574.

2. Jordan K, Tobias C. *The Effect of Inhibitor Transport on Leveling in Electrodeposition*. J. Electrochem. Soc. 1991;138(5):1251-1259.

3. Chung D. Localized Adsorption of Organic Additives During Copper Electrodeposition [Ph.D.]. Urbana-Champaign: University of Illinois; 1996.

4. Ilgar E, O'Keefe T. Surface Roughening of Electrowon Copper in the Presence of Chloride Ions. In: Dreisinger D, editor. *Aqueous Electrotechnologies: Progress in Theory and Practice*; 1997: The Minerals Metals and Materials Society; 1997. p. 51-62.

5. Wu Q, Barkey D. *Faceting and Roughening Transitions on Copper Single Crystals in Acid Sulfate Plating Baths with Chloride*. Journal of the Electrochemical Society 2000 Mar;147(3):1038-1045.

6. Gabrielli C, Mocoteguy P, Perrot H, Wiart R. *Mechanism of Copper Deposition in a Sulfate Bath Containing Chlorides*. Journal of Electroanalytical Chemistry 2004;572(2):367-375.

7. Tackett J; inventor. Marathon Oil Company, assignee. A Method for Inhibiting Hydrolysis of Polyacrylamide patent WO 92/07881. 1992.

8. Halverson F, Lancaster J, O'Connor M. *Sequence Distribution of Carboxyl Groups in Hydrolyzed Polyacrylamide*. Macromolecules 1985;18(6):1139-44.

9. Panzer H, Halverson F, Lancaster J. *Carboxyl Sequence Distribution in Hydrolyzed Polyacrylamide*. Polymeric Materials Science and Engineering 1984;51:268-71.

10. Panzer H, Halverson F. Blockiness in Hydrolyzed Polyacrylamide. In: Moudgil B, Scheiner B, editors. *Flocculation Dewatering, Proc. Eng. Found. Conf.*; 1988; Palm Coast Florida, USA; 1988. p. 239-49.

11. Muller G, Fenyo J, Selegny E. *High Molecular Weight Hydrolyzed Polyacrylamides. Iii. Effect of Temperature on Chemical Stability*. Journal of Applied Polymer Science 1980;25:627.

12. Grchev T, Cvetkovska M, Stafilov T, Schultze J. *Adsorption of Polyacrylamide on Gold and Iron from Acidic Aqueous Solutions*. Electrochimica Acta 1991;36(8):1315-1323.

13. Arvia AJ, Carrozza JSW. *Mass Transfer in the Electrolysis of Cuso4-H2so4 in Aqueous Solutions under Limiting Current and Forced Convection Employing a Cylindrical Cell with Rotating Electrodes*. Electrochimica Acta 1962;7:65-78.

14. Eisenberg M, Tobias C, Wilke C. *Ionic Mass Transfer and Concentration Polarization at Rotating Electrodes*. Journal of the Electrochemical Society 1954;101(6):306-319.

15. Drews T, Ganley J, Alkire R. *Evolution of Surface Roughness During Copper Electrodepositon in the Presence of Additives*. J. Electrochem. Soc. 2003;150(5):C325-C334.

16. Wilke C, Eisenberg M, Tobias C. *Correlation of Limiting Currents under Free Convection Conditions*. J. Electrochem. Soc. 1953;100(11):513-523.

17. Radeva T, Petkanchin I. *Electro-Optic Study of Oxide Particles in Hydrolyzed Polyacrylamide Solutions*. Journal of Colloid and Interface Science 1995;182:1-5.

18. Grchev T, Cvetkovska M. *Electrochemically Initiated (Co)Polymerization of Acrylamide and Acrylonitrile on a Steel Cathode - Electrochemical and Impedance Study*. Journal of Applied Electrochemistry 1989;19(3):434-42.

19. Grchev T, Cvetkovska M, Schultze JW. *The Electrochemical Testing of Polyacrylic Acid and Its Derivatives as Inhibitors of Corrosion*. Corrosion Science 1991;32(1):103-12.

20. Haschke H, Miles MJ, Koutsos V. *Conformation of a Single Polyacrylamide Molecule Adsorbed onto a Mica Surface Studied with Atomic Force Microscopy*. Macromolecules 2004;37(10):3799-3803.

21. Szymanski G, Dymarska M, Zhao T, Lipkowski J. *Atomic Force Microscopy Study of the Morphology of Electrodeposited Nickel and Copper at Conditions Mimicking Industrial Nickel and Copper Electrorefining*. Electrometallurgy 2001, Proceedings of Annual Hydrometallurgy Meeting, 31st, Toronto, ON, Canada, Aug. 26-29, 2001 2001:375-387.

22. Schmidt W, Alkire R, Gewirth A. *Mechanic Study of Copper Deposition onto Gold Surfaces by Scaling and Spectral Analysis of in-Situ Atomic Force Microscopic Images*. J. Electrochem. Soc. 1996(10):3122-3132.

23. Pye D, Schurz G; inventors. The Dow Chemical Company, assignee. Electrowinning of Metals. United States patent 2,798,040. 1957 July 2, 1957.

24. Vereecken J, Winand R. *Influence of Polyacrylamides on the Quality of Copper Deposits from Acidic Copper Sulphate Solutions*. Surface Technology 1976; 4:227-235.

25. Budevski E, Staikov G, Lorenz W. *Electrochemical Phase Formation and Growth, an Introduction to the Initial Stages of Metal Deposition*. New York: VCH; 1996.

26. Franceschetti DR, Macdonald JR. *Diffusion of Neutral and Charged Species under Small-Signal A.C. Conditions*. J. Electroanal. Chem. 1979;101:307-316.

27. Macdonald JR, editor. *Impedance Spectroscopy Emphasizing Solid Materials and Systems*. Brisbane: John Wiley & Sons; 1987.

28. Mansfeld F, Shih H, Greene H, Tsai C. Analysis of Eis Data for Common Corrosion Processes. In: Scully JR, Silverman DC, Kending MW, editors. *Electrochemical Impedance: Analysis and Interpretation*; 1993; 1993. p. 37-53.

29. Jovic VD, Jovic BM. *Copper Electrodepositon from Copper Acid Baths in the Presence of Polyethylene Glycol and Sodium Chloride*. J. Serb. Chem. Soc. 2001;66(11-12):935-952.

30. Nava de Oca J, Sosa E, Ponce de Leon C, Oropeza M. *Effectiveness Factors in an Electrochemical Reactor with Rotating Cylinder Electrode for the Acid-Cupric/Copper Cathode Interface Process*. Chemical Engineering Science 2001;56(8):2695-2702.

31. Diard JP, Montella C. *Diffusion-Trapping Impedance under Restricted Linear Diffusion Conditions*. Journal of Electroanalytical Chemistry 2003;557:19-36.

32. Brett CMA, Brett AMO. *Electrochemistry, Principles, Methods and Applications*. New York; 1993.

33. Macdonald J. Levm Manual - Complex Nonlinear Least Squares (Cnls). In. 8.0 ed; 2003.

34. Harrington DA, van den Driessche P. *Equivalent Circuits for Some Surface Electrochemical Mechanisms*. Journal of Electroanalytical Chemistry 2004;567(2):153-166.

35. Chibowski S, Wisniewska M. *Study of Electrokinetic Properties and Structure of Adsorbed Layers of Polyacrylic Acid and Polyacrylamide at Ferric Oxide-Polymer Solution Interface*. Colloids and Surfaces A: Physicochemical and Engineering Aspects 2002;208(1-3):131-145.

36. Mark H, Gaylord N, Bikales N. *Encyclopedia of Polymer Science and Technology*; 1969.

37. Petri M, Kolb D, Memmert U, Meyer H. *Adsorption of Polyethylene Glycol on Au(111) Single-Crystal Electrodes and Its Influence on Copper Deposition*. J. Electrochem. Soc. 2004;151(12):C793-C797.

38. Feng ZV, Li X and Gewirth AA, *Inhibition due to the Interaction of Polyethylene Glycol, Chloride and Copper in Plating Baths: A Surface-Enhanced Raman Study*. J. Phys. Chem. B 107, 2003, 9415-9423.